

Publications (graphical abstracts) of

Thomas R. Knösche

Max Planck Institute for Human Cognitive and Brain Sciences, Leipzig

1 Computational Neuroscience

1.1 Neural mass modeling

2 Diffusion MRI & Tractography

2.1 Diffusion imaging & image processing

2.2 Local modeling & tracking

2.3 Validation of tractography

2.4 Connectivity based brain parcellation

3 EEG/MEG Analysis & Source Modeling

3.1 Source reconstruction algorithms

3.2 Volume conductor modeling

3.3 Spatial mapping & interpolation

3.4 Signal analysis

4 Neurocognition

4.1 Music and language processing

4.2 Gestures and face expression

4.3 Other cognitive faculties

4.4 Motor function

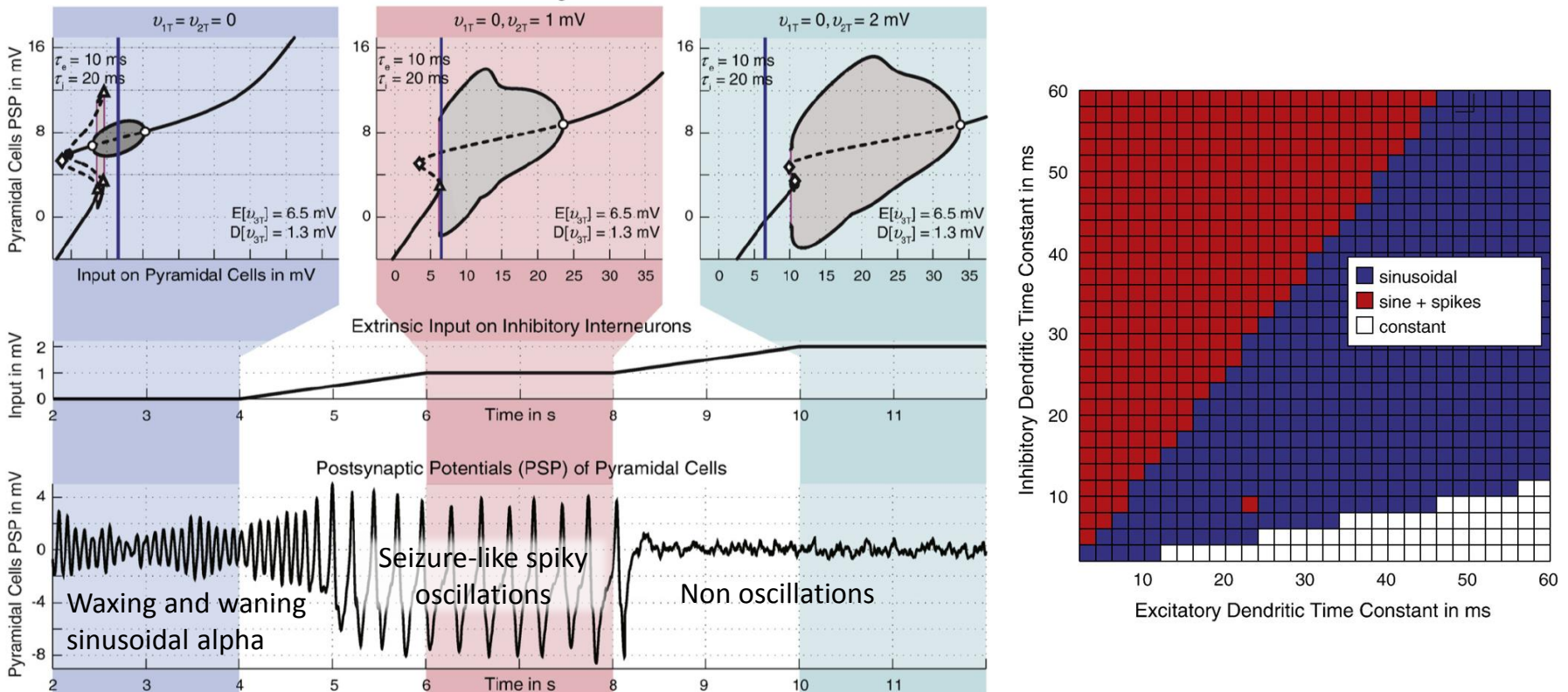
1 Computational Neuroscience

1.1 Neural mass modeling

Bifurcation analysis of neural mass models: Impact of extrinsic inputs and dendritic time constants

A. Spiegler, S.J. Kiebel, F.M. Atay, T.R. Knösche

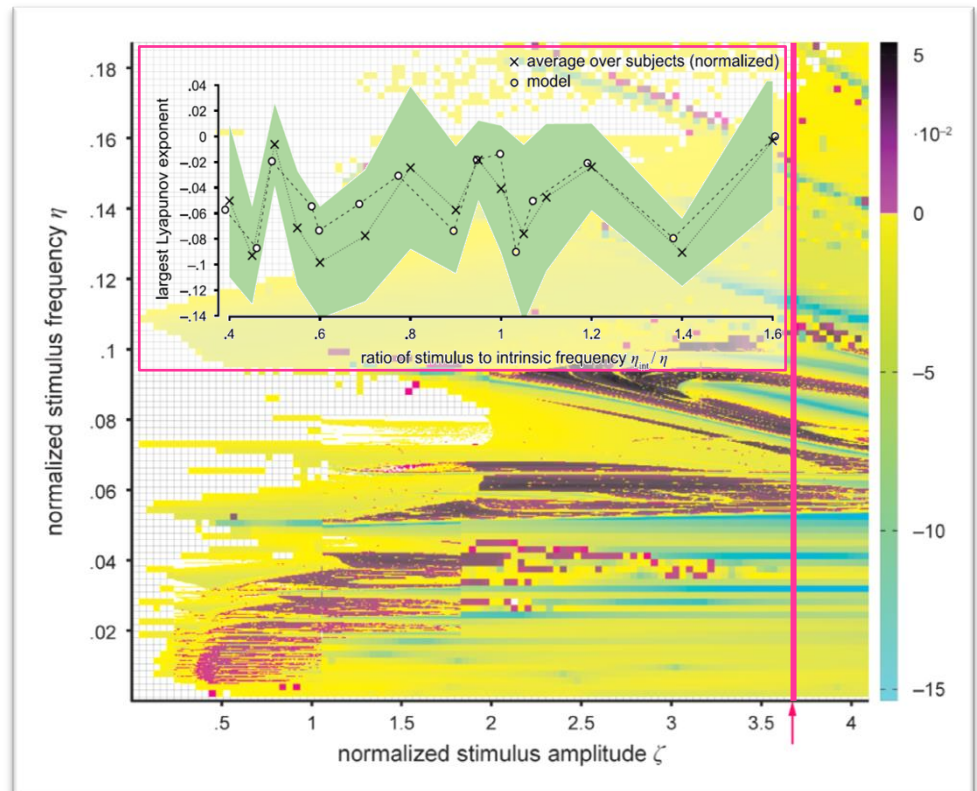
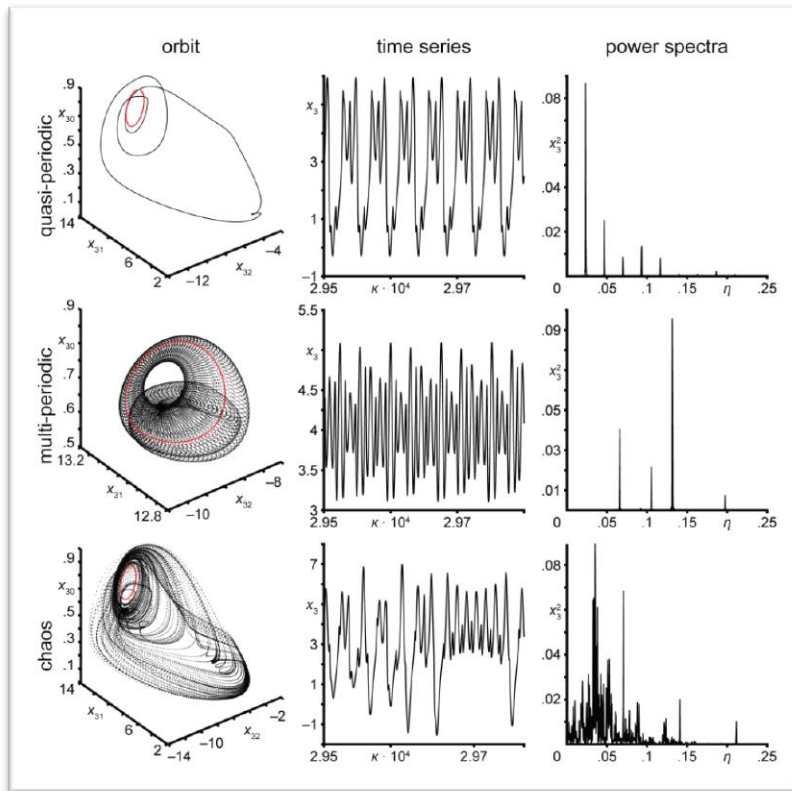
We use bifurcation analysis to systematically classify the oscillatory regimes of a NMM of a single cortical area. The resulting scheme is useful for applications where one needs to model an ordered sequence of qualitatively different oscillatory regimes, e.g., in pharmacological interventions, epilepsy, sleep, or context-induced state changes.



Modeling Brain Resonance Phenomena Using a Neural Mass Model

A. Spiegler, T.R. Knösche, K. Schwab, J. Haueisen, F.M. Atay

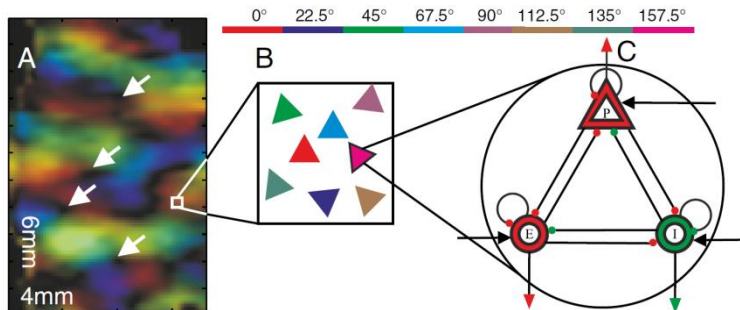
For an oscillatory driven Jansen & Rit circuit, we charted the entire stimulus parameter space (amplitude and frequency) by means of characteristic Lyapunov spectra and Kaplan-Yorke dimension, yielding a complex (fractal) pattern of rhythmic and chaotic states. This pattern of unpredictability matched well to EEG data from a photic driving experiment.



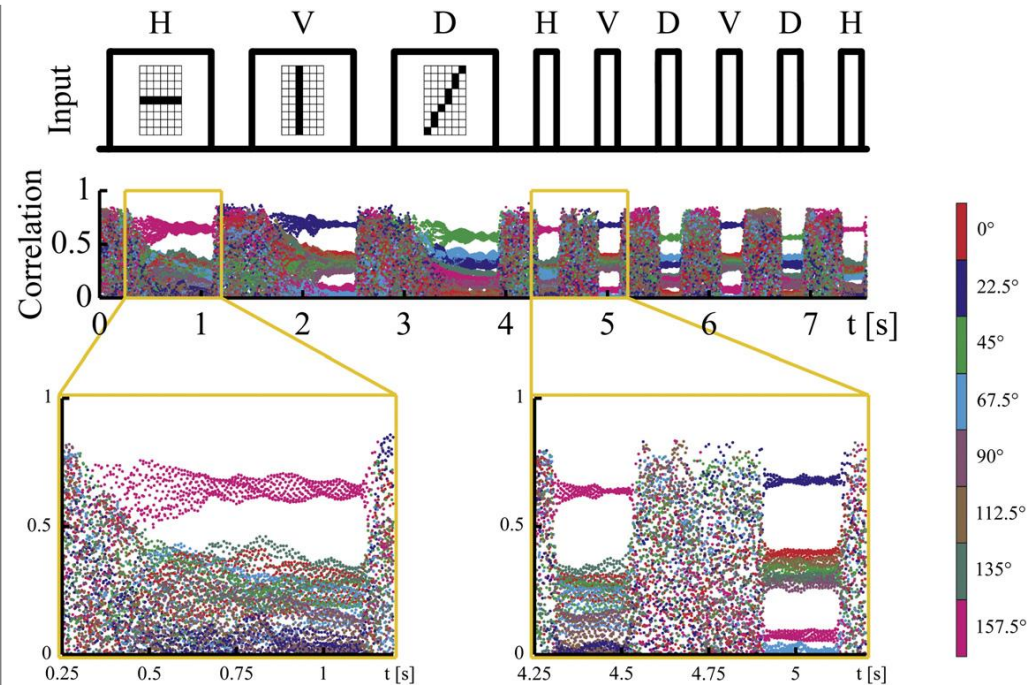
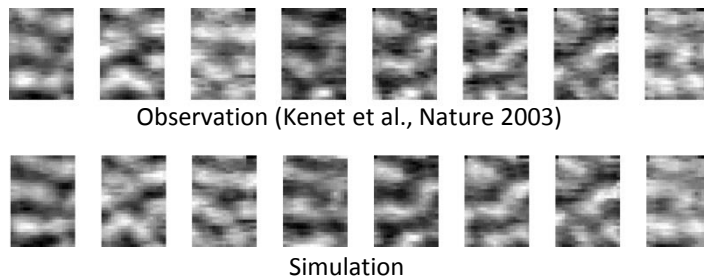
Associating spontaneous with evoked activity in a neural mass model of visual cortex

M. Nguyen Trong, I. Bojak, T.R. Knösche

We used a neural mass model to test if spontaneous brain activity provides a reservoir of cortical states, which are associated with stimuli through learning. Spontaneous transitions between orientation states established a stable heteroclinic channel. Unsupervised Hebbian learning associated visual inputs to particular states.



Orientation preference map (A), hypercolumn (B) and model of orientation preference column (C).

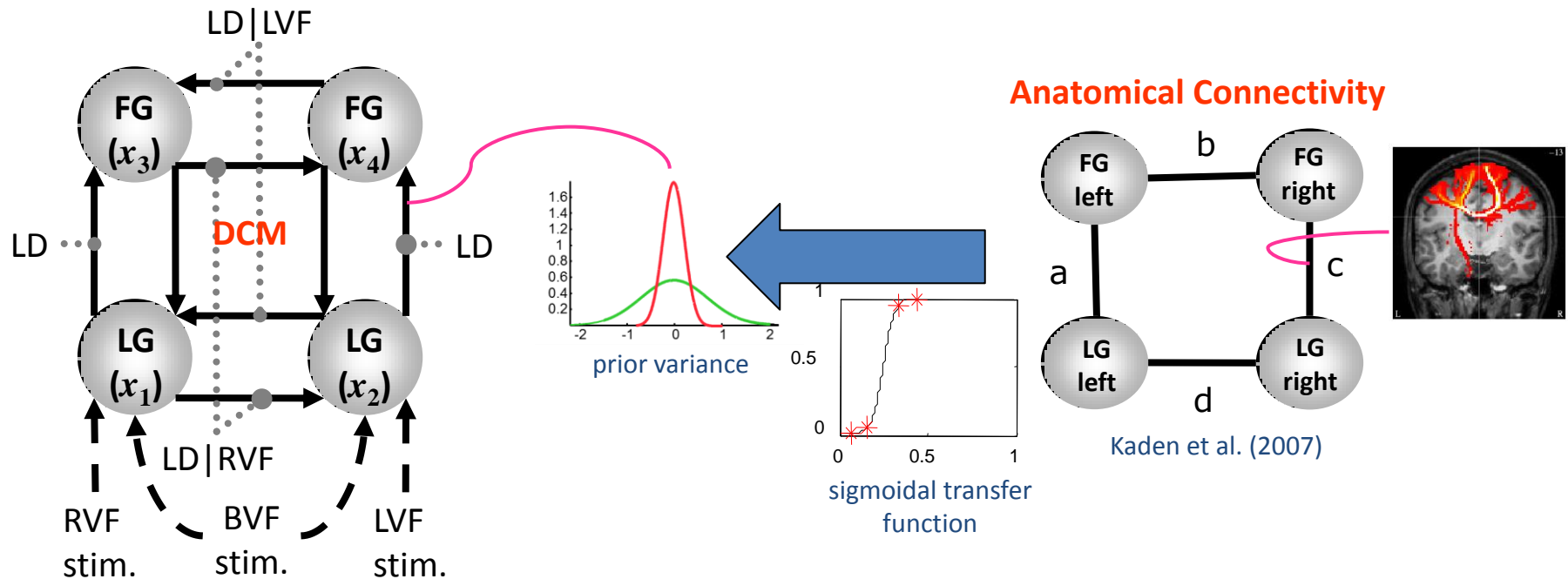


Association of internal states to stimuli through Hebbian learning.

Tractography-based priors for dynamic causal models

K.E. Stephan, M. Tittgemeyer, T.R. Knösche, R.J. Moran, K.J. Friston

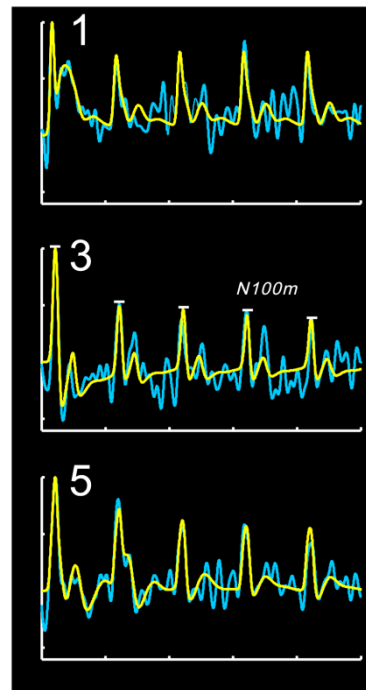
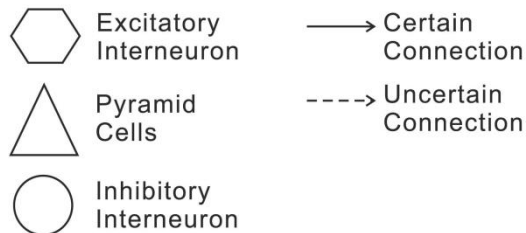
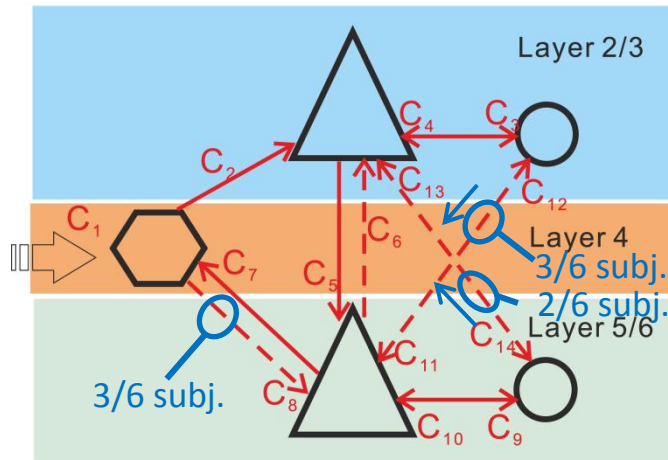
We use diffusion tractography to specify anatomically informed priors for DCM. We constructed 64 alternative DCMs, which embodied different mappings between anatomical connectivity and prior variance of effective connectivity, and fitted them to fMRI. Using Bayesian model selection, we show that the best model has a sigmoidal relationship.



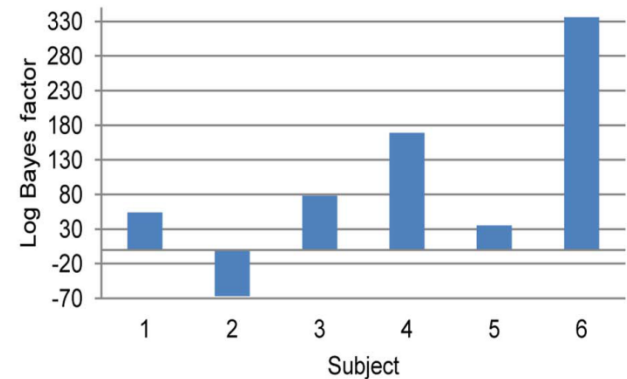
A Realistic Neural Mass Model of the Cortex with Laminar-Specific Connections and Synaptic Plasticity – Evaluation with Auditory Habituation

P. Wang, T.R. Knösche

Modeling auditory habituation with the proposed model, we found that: (1) besides the major excitatory pathway (L4→L2/3→L5/6), a “short-cut” (L4→L5/6) exists, (2) the signal flow PC→IIN is more intra-laminar, the signal flow IIN→PC is also inter-laminar, (3) forward connections (L4→L2/3) are more strongly habituated than backward ones (L5/6→L4).



— observed
— modeled



Bayes factor new LCCM vs. Jansen & Rit

2 Diffusion MRI & Tractography

2.1 Diffusion imaging & image processing

White matter integrity, fiber count, and other fallacies: The do's and don'ts of diffusion MRI

D.K. Jones, T.R. Knösche, R. Turner

In order to encourage the use of improved diffusion MRI methods, which have a better chance than DTI of characterizing the actual fiber structure, and to warn against the misuse and misinterpretation of DTI, we review the physics of diffusion MRI, indicate currently preferred methodology, and explain the limits of interpretation of its results.

The Do's

- Carefully consider the questions asked and where to invest precious acquisition time (small voxels, many directions, high diffusion weighting, high SNR).
- Carefully consider the impact of pre-processing steps on the quantitative metrics.
- Use the highest b-value, but ensure $SNR > 3$.
- Use many directions, but even more important is the use of small voxels.
- Use fiber crossing models for tractography.

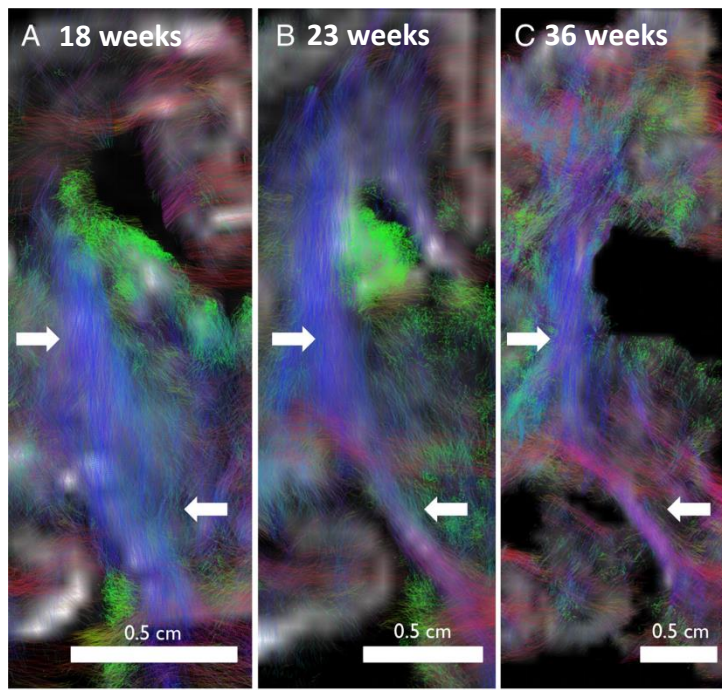
The Don'ts

- Don't assume that the principal tensor eigenvector is a good indication of the actual fiber orientations in all voxels.
- Except in the case of clinically-diagnosed conditions explicitly impacting on white matter don't use the term 'white matter integrity'. FA is not WM integrity!
- Don't use the phrase 'fiber count' for data derived from diffusion MRI.
- Don't use tractography to quantitatively estimate of 'connection strength'.

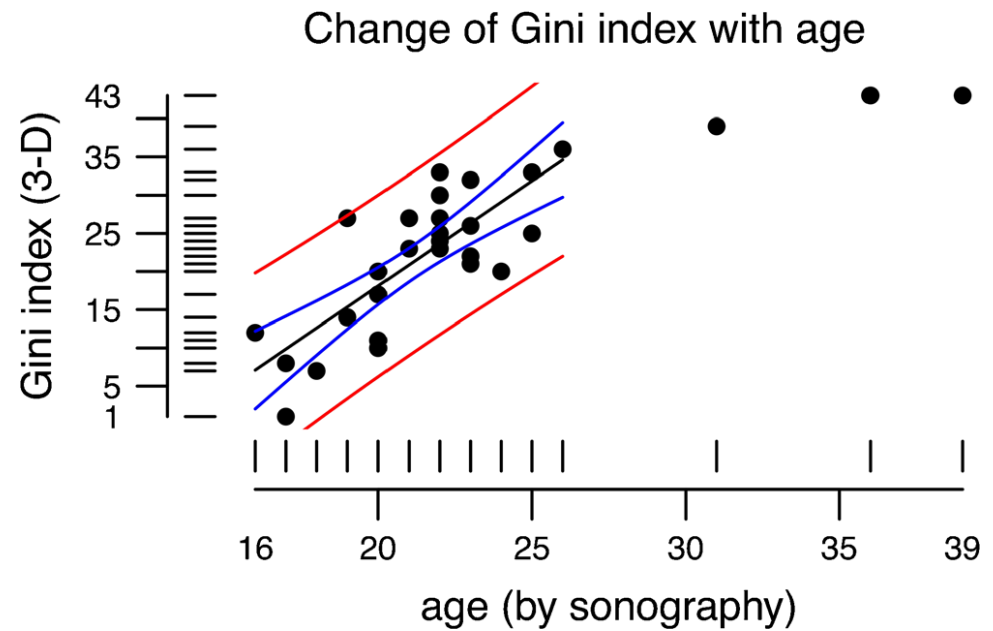
The Gini coefficient: a methodological pilot study to assess fetal brain development employing postmortem diffusion MRI

A. Viehweger, T. Riffert, B. Dhital, T.R. Knösche, A. Anwander, H. Stepan, I. Sorge, W. Hirsch

We demonstrate that the Gini coefficient can be a simple, intuitive parameter for modeling fetal brain development. Based on DWI constrained spherical deconvolution in postmortem fetal brains, FA, ADC and complexity (CX) maps were generated and used to compute the Gini coefficient. It correlated well with age between 17 and 26 gestational weeks.



Cortico-spinal tract (white arrows)

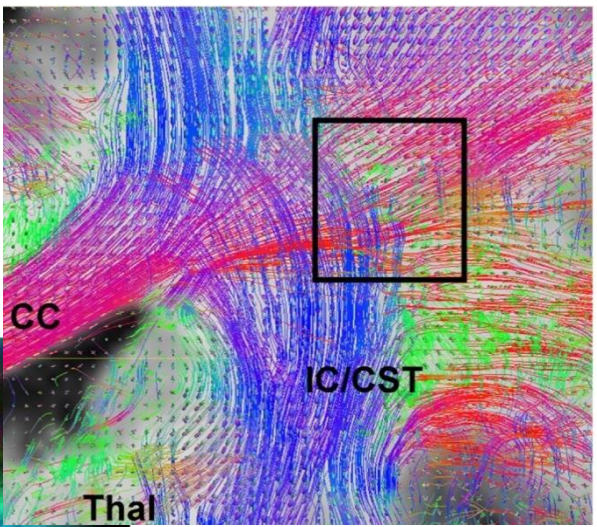
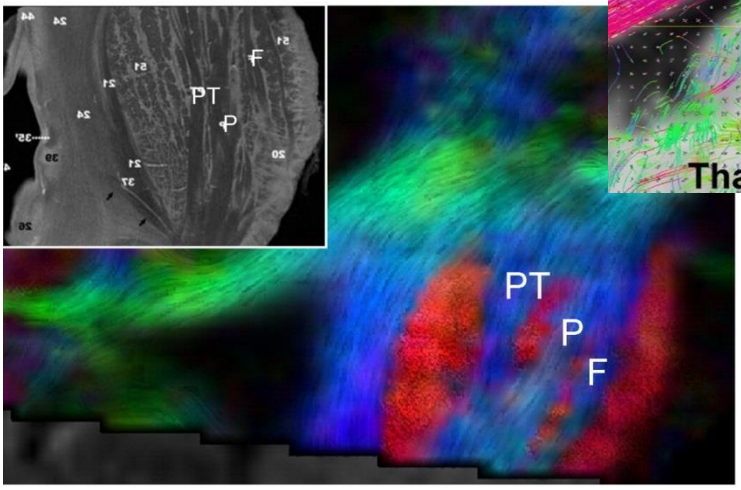


k-space and q-space: Combining ultra-high spatial and angular resolution in diffusion imaging using ZOOPPA at 7 T

R.M. Heidemann, A. Anwander, T. Feiweier, T.R. Knösche, R. Turner

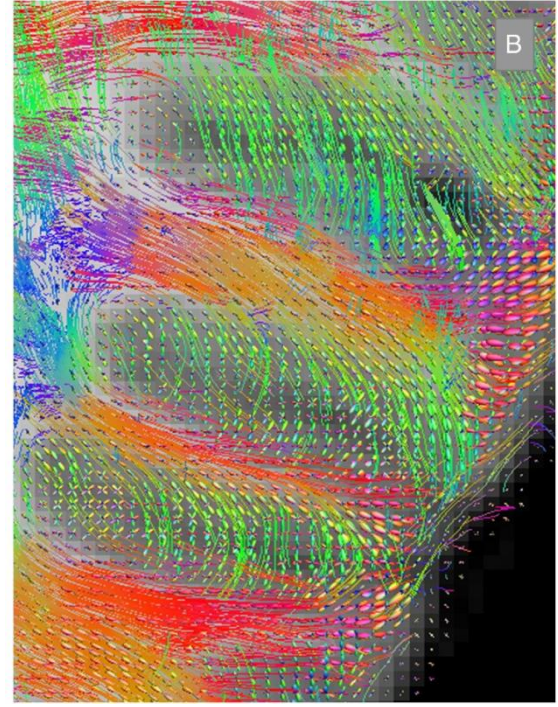
We introduce an adapted EPI sequence in conjunction with ZOOMed imaging and Partially Parallel Acquisition (ZOOPPA). The method can produce high quality diffusion-weighted images with high spatial (0.8 mm) and angular resolution at 7 T.

Interdigitated bundles in the pons, reconstructed at 1 mm.



Triple crossing in centrum semiovale at 0.8 mm.

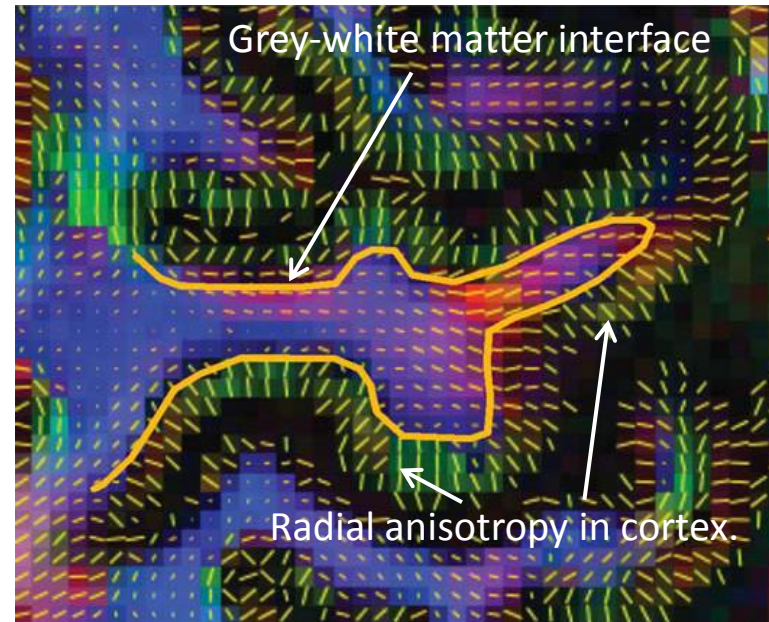
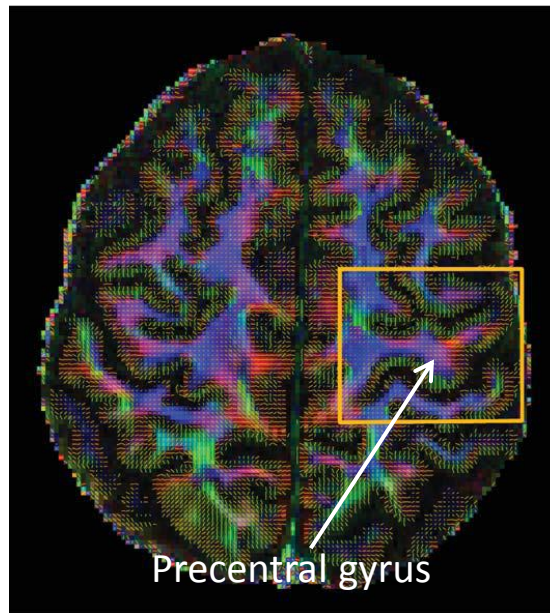
Fibers entering the cortex at 0.8 mm.



Diffusion Imaging in Humans at 7T Using Readout-Segmented EPI and GRAPPA

R.M. Heidemann, D.A. Porter, A. Anwander, T. Feiweier, K. Heberlein, T.R. Knösche, R. Turner

This study demonstrates that readout-segmented echo-planar imaging in conjunction with parallel imaging does provide a substantial improvement in image quality by reducing blurring and susceptibility-based distortions, as well as by allowing the acquisition of diffusion-weighted images with a high spatial resolution.

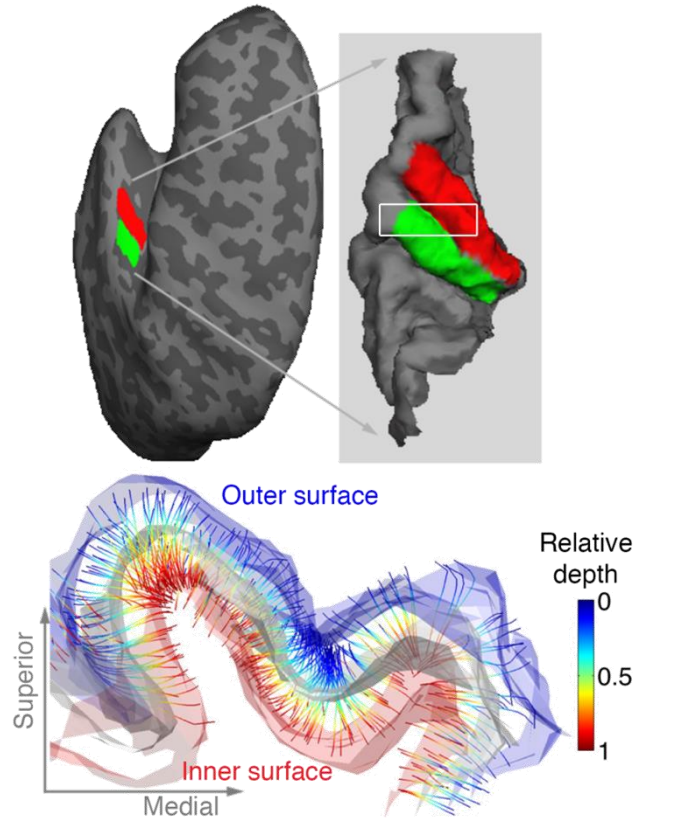


FA and principle eigenvectors, computed from 12 directions at $b=1000 \text{ s/mm}^2$.

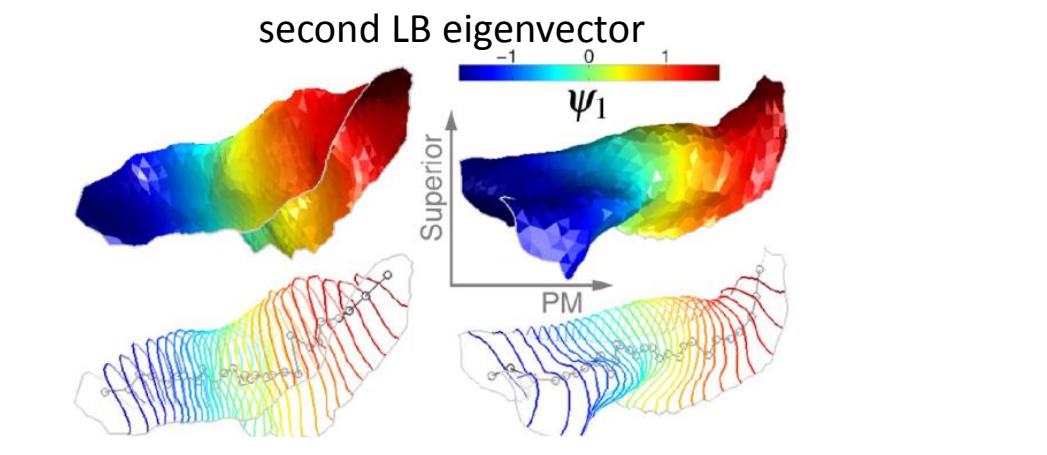
Group-wise analysis of myelination profiles of cerebral cortex using the second eigenvector of the Laplace-Beltrami operator

S.G. Kim, J. Stelzer, P.L. Bazin, A. Viehweger, T.R. Knösche

We present a novel framework to parameterize curved brain structures in order to construct correspondences across subjects without deforming individual geometry, using the second Laplace-Beltrami eigenfunction.

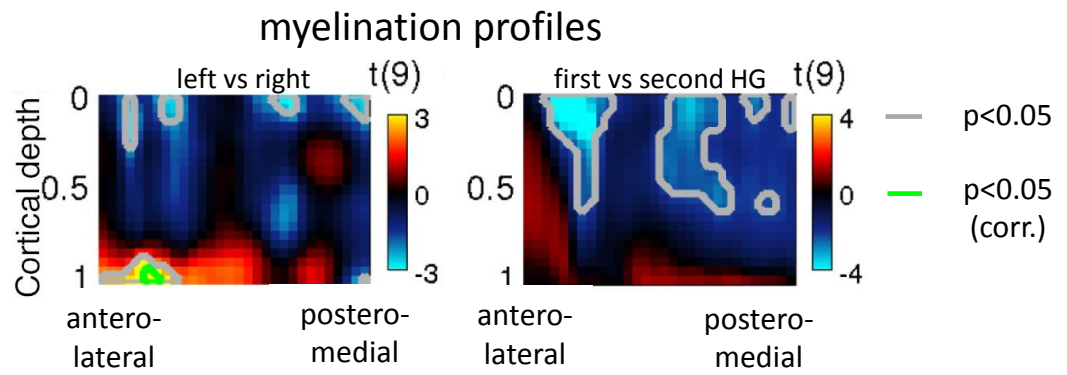


Cortical profiles of Heschl's gyrus.



second LB eigenvector

ψ_1



myelination profiles

left vs right

first vs second HG

Cortical depth

antero-lateral

postero-medial

antero-lateral

postero-medial

$p < 0.05$

$p < 0.05$ (corr.)

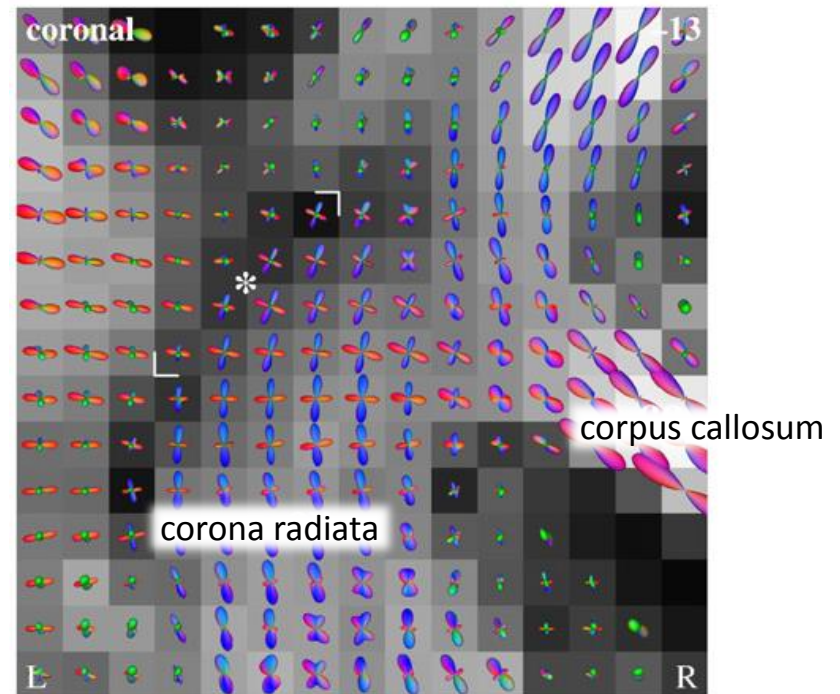
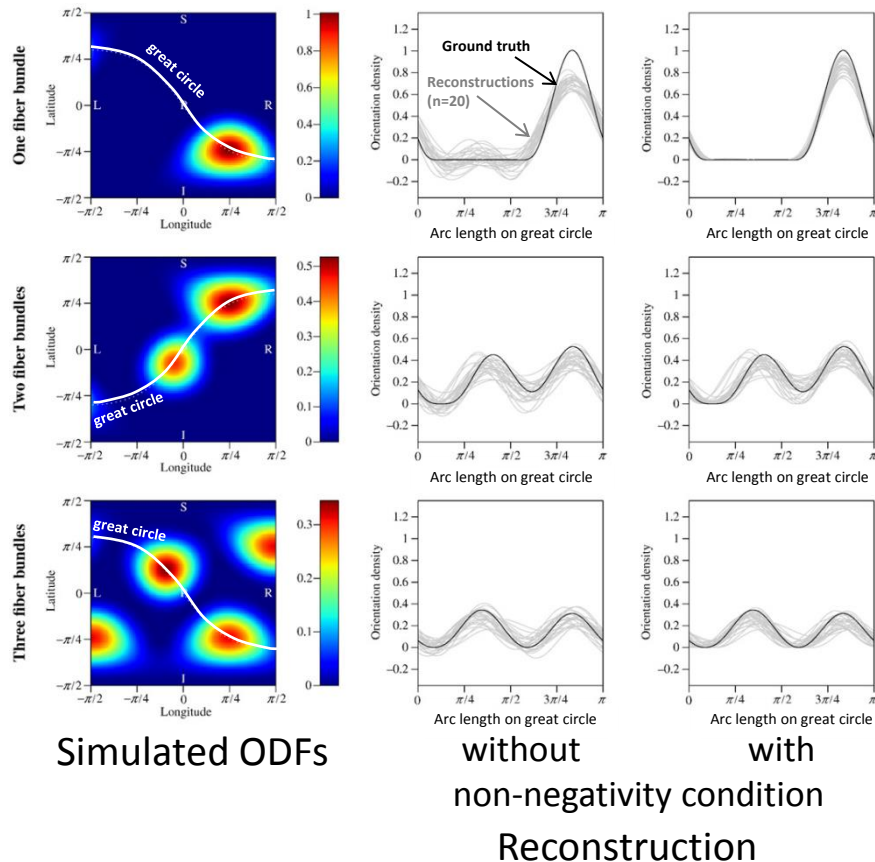
2 Diffusion MRI & Tractography

2.2 Local modeling & tracking

Variational inference of the fiber orientation density using diffusion MR imaging

E. Kaden, A. Anwander, T.R. Knösche

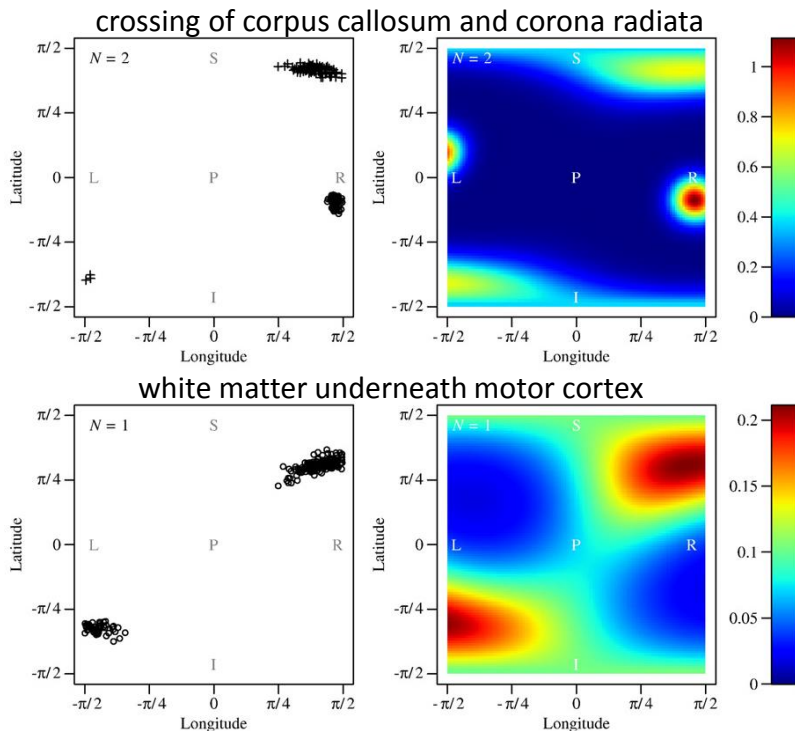
We propose the spherical deconvolution of the fiber orientation density in a reproducing kernel Hilbert space, thereby generalizing previous approaches. The novel approach is demonstrated with diffusion-weighted data of high angular resolution.



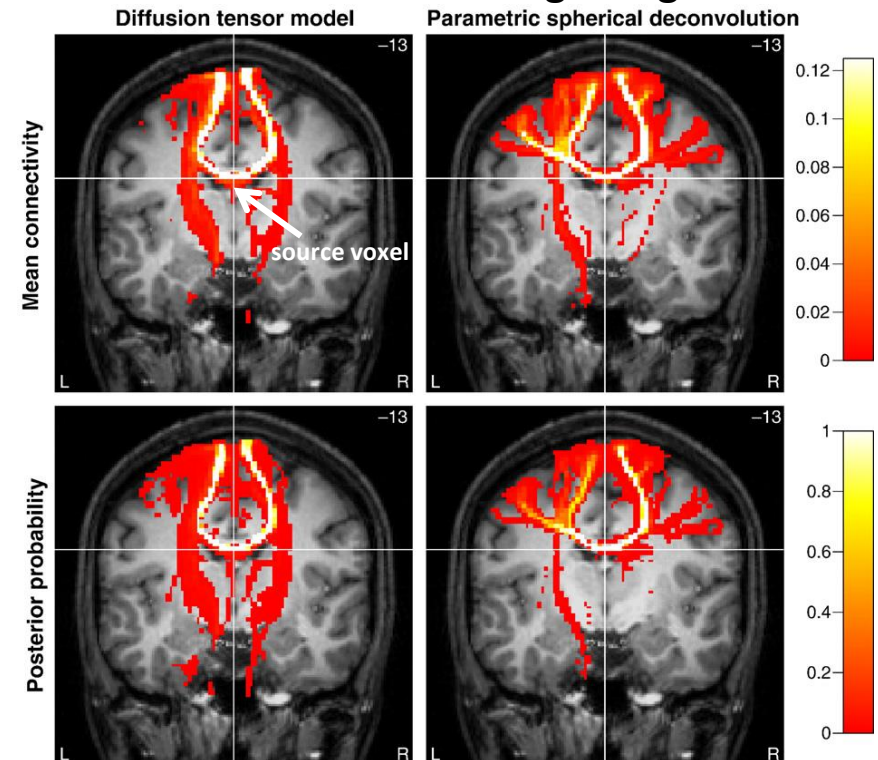
Parametric spherical deconvolution: Inferring anatomical connectivity using diffusion MR imaging

E. Kaden, T.R. Knösche, A. Anwander

We propose a spherical deconvolution approach describing the fiber orientation density by a mixture of Bingham distributions. We also define *anatomical connectivity* as the proportion of the fibers originating in a source area which intersect a target region.



Posterior distribution of the mean fiber orientation in voxels taken from the human brain.

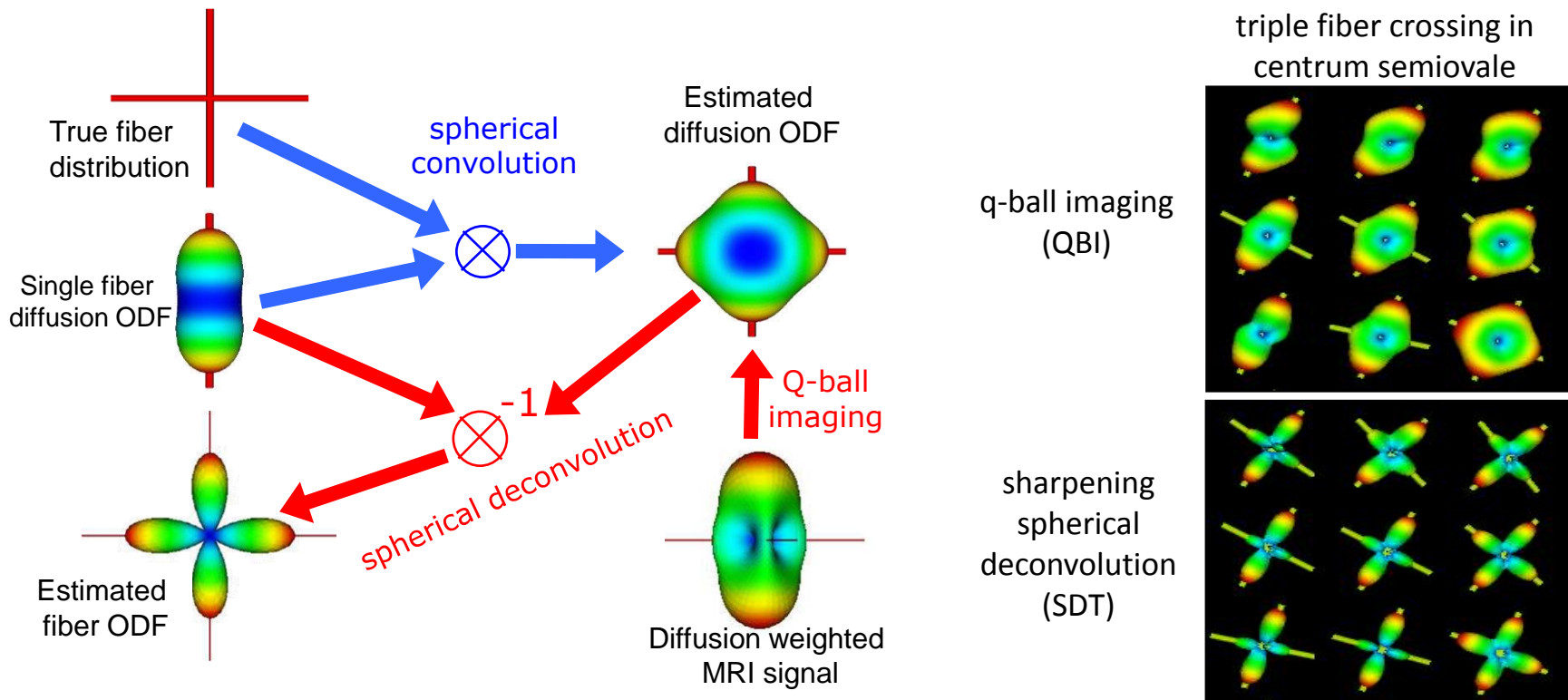


Posterior probability that the anatomical connectivity exceeds the threshold 0.1.

Deterministic and Probabilistic Tractography Based on Complex Fibre Orientation Distributions

M. Descoteaux, R. Deriche, T.R. Knösche, A. Anwander

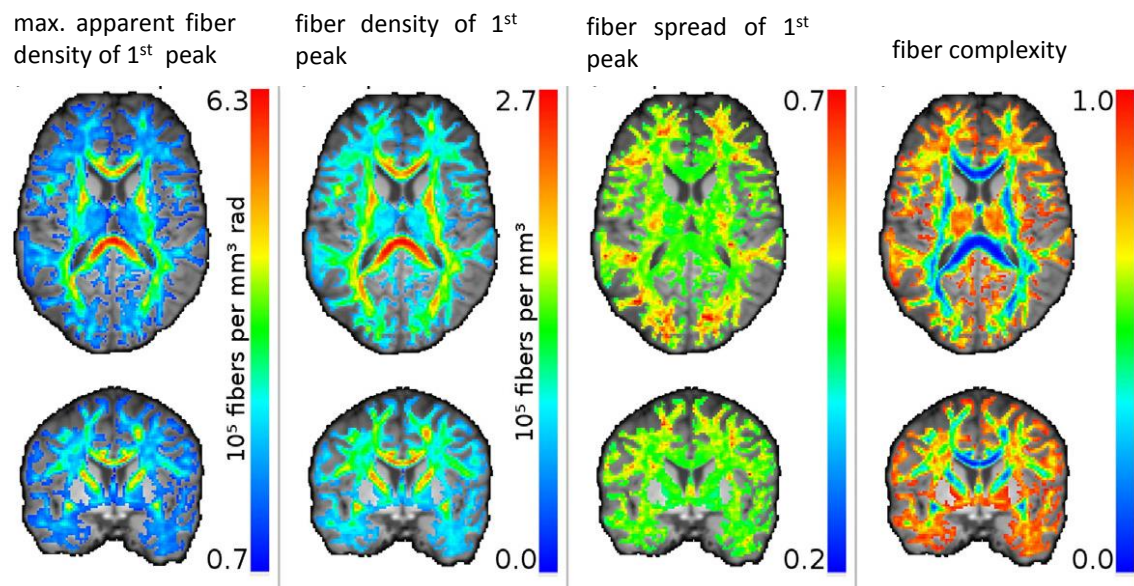
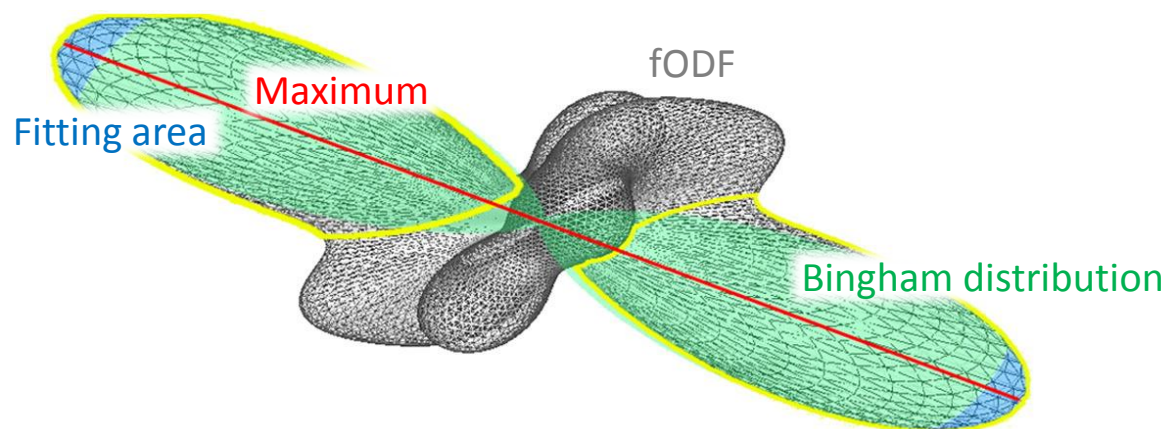
We propose an integral concept for tractography to describe crossing and splitting fiber bundles based on the sharpening deconvolution transform (SDT) of the diffusion ODF obtained from q-ball imaging. Moreover, we develop new deterministic probabilistic tractography algorithms using the full multidirectional information of the fibre ODF.



Beyond fractional anisotropy: Extraction of bundle-specific structural metrics from crossing fiber models

T.W. Riffert, J. Schreiber, A. Anwander, T.R. Knösche

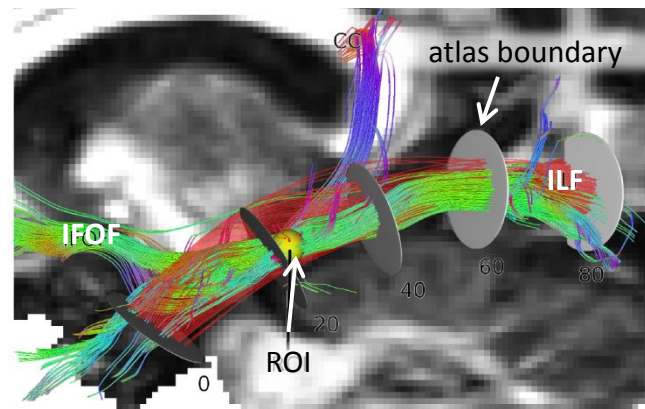
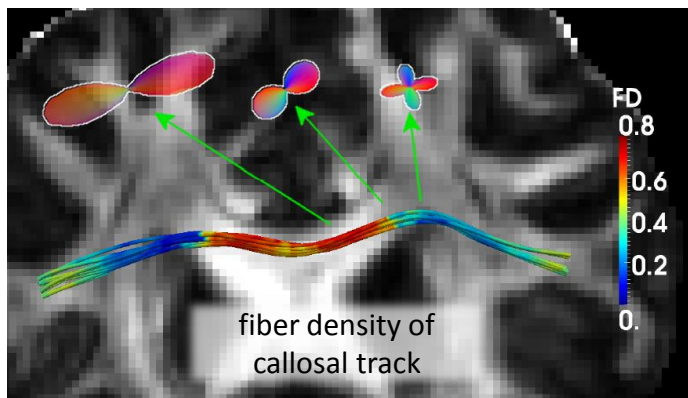
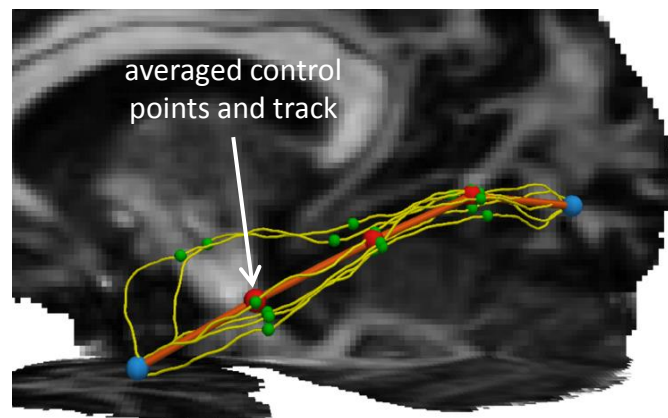
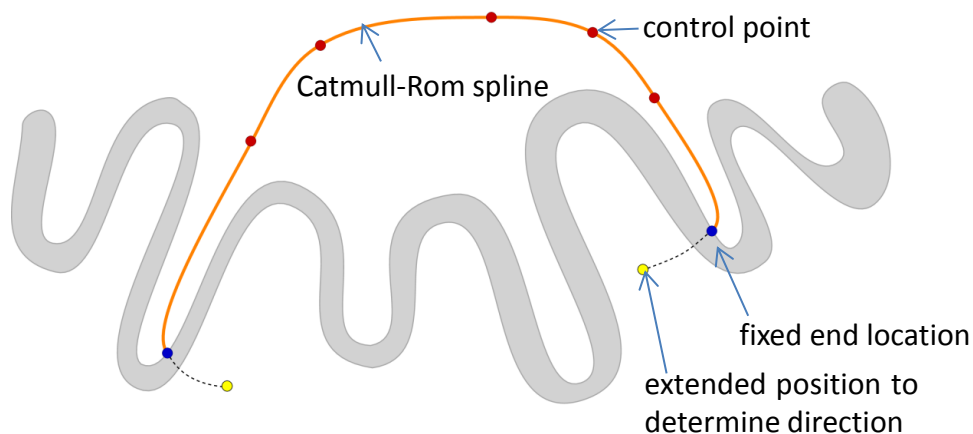
We offer a solution to combine the advantages of multi-compartment models and spherical deconvolution: first the fiber configuration is modeled as fODF and then its peaks are parameterized separately as Bingham distributions. We derive metrics for the characterization of fiber bundles and propose meaningful relationships to the underlying microstructure.



Plausibility Tracking: A method to evaluate anatomical connectivity and microstructural properties along fiber pathways

J. Schreiber, T. Riffert, A. Anwander, T. R. Knösche

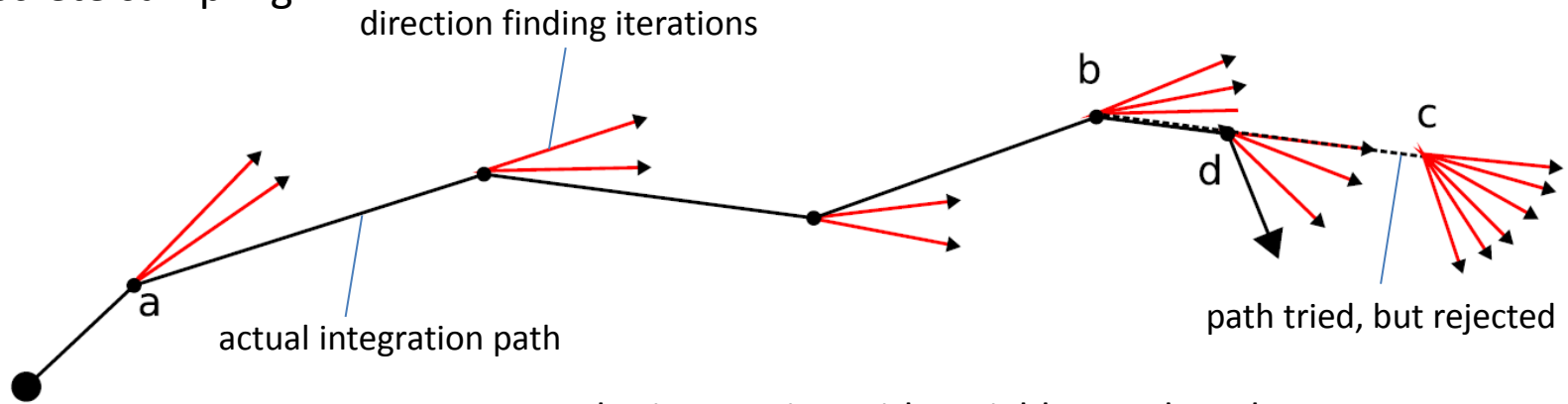
Plausibility Tracking combines the more complete connectivity pattern of probabilistic tractography with smooth tracks. It provides reliable local directions along fiber pathways, allowing for tract-based analysis of direction dependent indices of diffusion MRI.



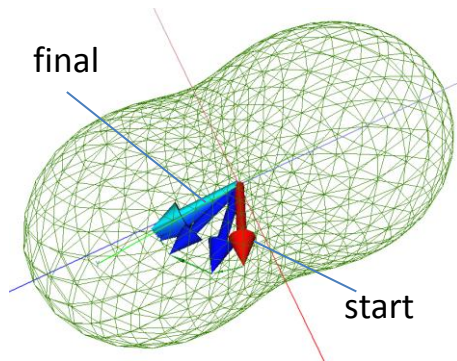
Tensor lines in tensor fields of arbitrary order

M. Hlawitschka, G. Scheuermann, A. Anwander, T.R. Knösche, M. Tittgemeyer, B. Hamann

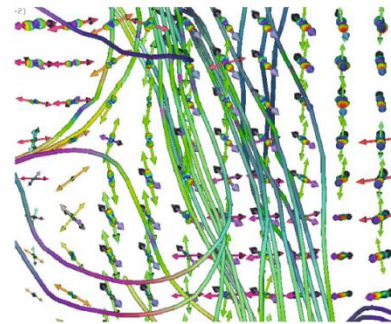
We present a method to reduce time complexity of the computation of higher-order tensor lines. It is based on a gradient descend technique and integrates well into fiber tracking algorithms. Furthermore, the method improves the angular resolution in contrast to discrete sampling.



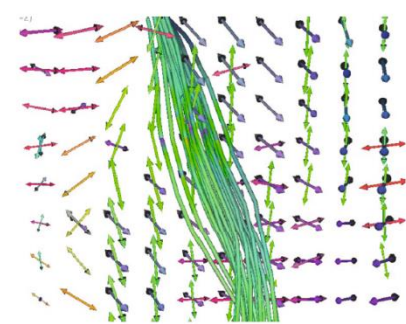
Euler integration with variable step length



Local direction finding



Second order tensor



Fourth order tensor

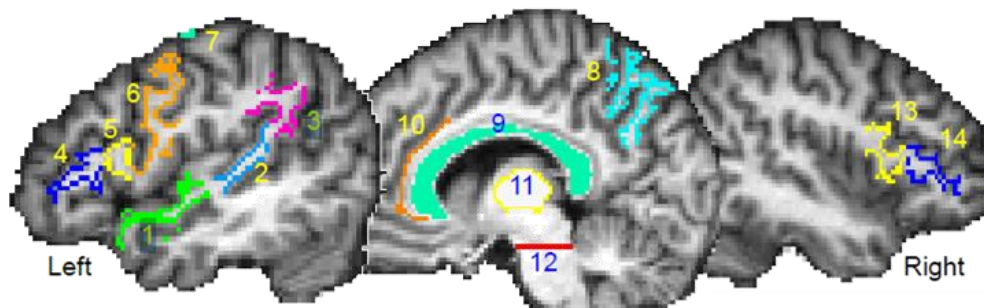
2 Diffusion MRI & Tractography

2.3 Validation of tractography

Quantifying Brain Connectivity: a Comparative Tractography Study

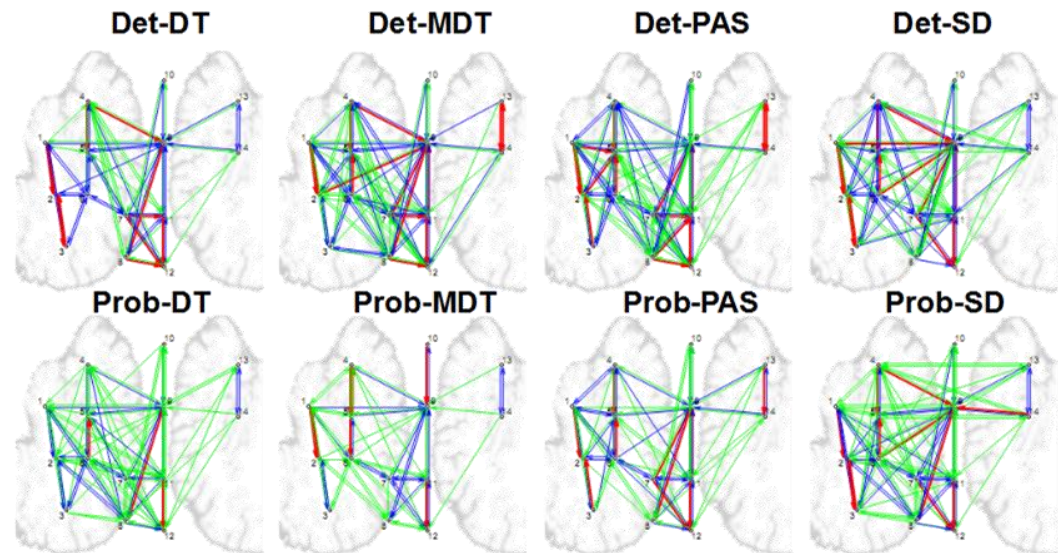
T.S. Yo, A. Anwander, M. Descoteaux, P. Fillard, C. Poupon, T.R. Knösche

We compare a representative selection of tractography algorithms and propose a novel way to quantify connectivity between brain regions. We find that fiber crossing models reveal more connections than the tensor model. Probabilistic approaches show more connected regions but lower connectivity values than deterministic ones.



Det – deterministic tracking
Prob – probabilistic tracking
DT – diffusion tensor
MDT – multiple diffusion tensors
PAS – persistent angular structure
SD – spherical deconvolution

1. anterior superior temporal gyrus (STG)
2. Posterior STG
3. angular gyrus
4. Brodmann area 45 (BA 45)
5. BA 44
6. precentral gyrus (PCG) ventral
7. PCG dorsol
8. precuneus
9. corpus callosum
10. anterior cingulate
11. Thalamus
12. cortical spinal tract
13. BA45, right hemisphere
14. BA44, right hemisphere

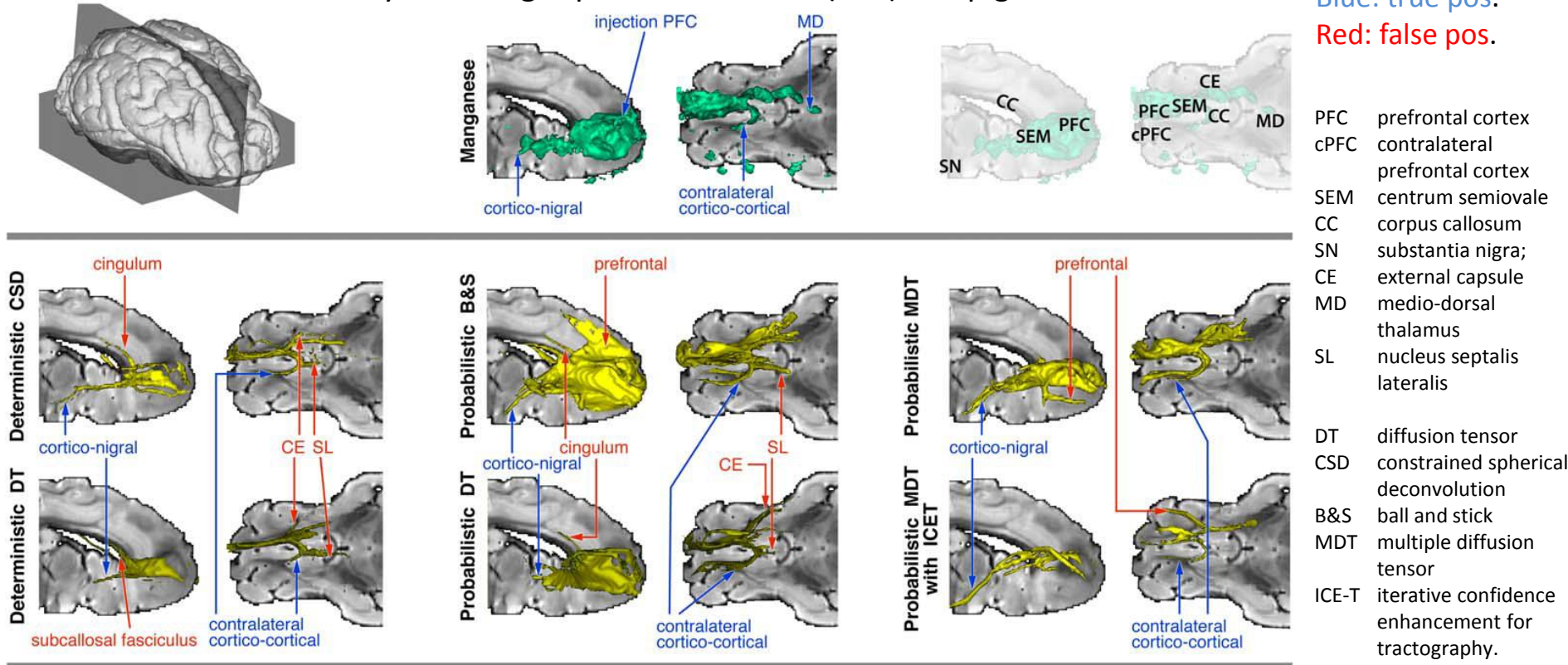


Validation of tractography – comparison with manganese tracing

T.R. Knösche, A. Anwander, M. Liptrot, T.B. Dyrby

We used invasive tracing to evaluate white matter tractography methods. High sensitivity and specificity could not be achieved at the same time, due to complex fiber arrangements in some areas. This is not easily resolved by more sophisticated local models alone, but requires better data, especially with higher spatial resolution.

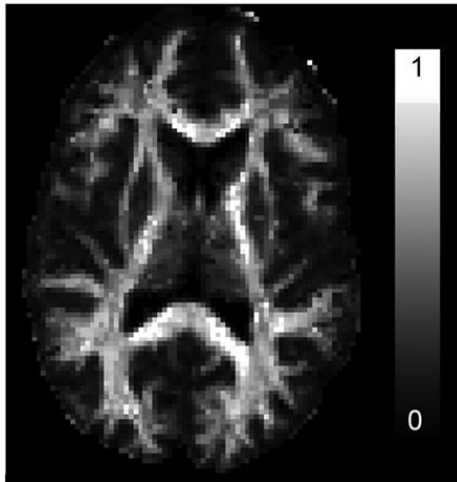
Connectivity of the right prefrontal cortex (PFC) in a pig brain



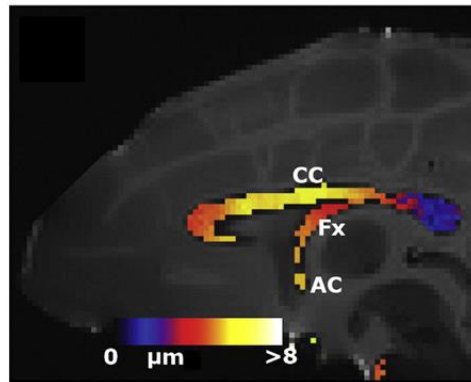
The CONNECT project: Combining macro- and microstructure

Y. Assaf , D.C. Alexander, D.K. Jones, A. Bizzi, T.E.J. Behrens, C.A. Clark, Y. Cohen, T.B. Dyrby, P.S. Huppi, T.R. Knösche, D. LeBihan, G.J.M. Parker, C. Poupon, CONNECT consortium

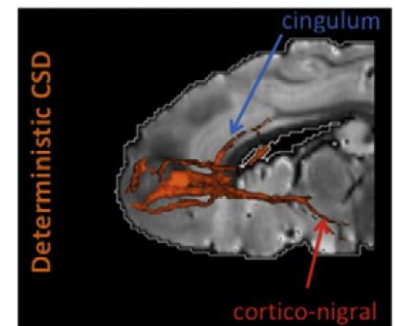
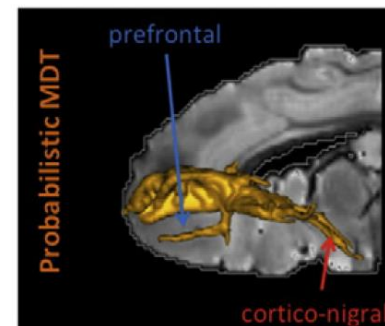
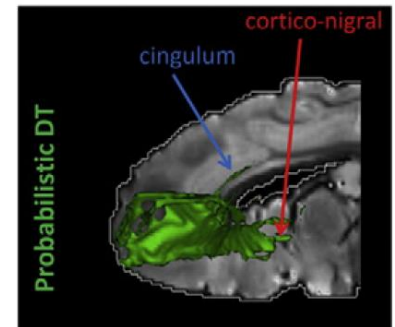
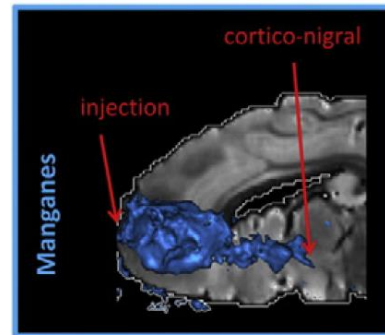
The CONNECT project aimed to combine tractography and micro-structural measures of the living human brain in order to obtain a better estimate of the connectome, while also striving to extend validation of these measurements.



Axonal density map computed from CHARMED for a healthy subject.



Axon diameter computed from ActiveAx from a fixed Vervet monkey brain.



Comparison between tractography and manganese tracing underscoring the false negative and false positive artifacts of tractography.

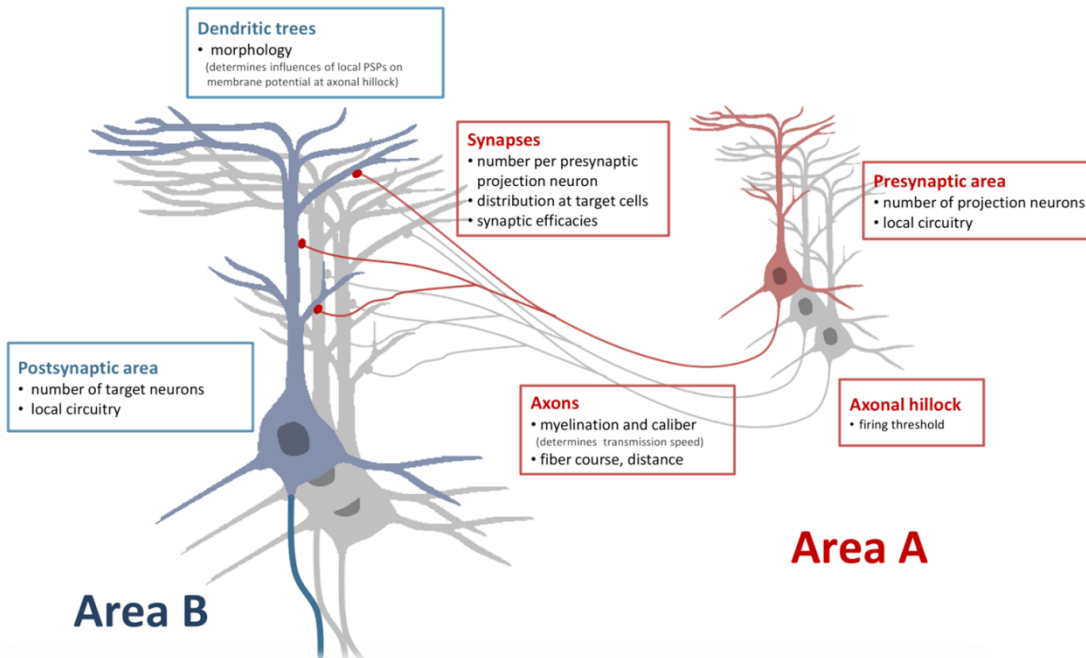
2 Diffusion MRI & Tractography

2.4 Connectivity based brain parcellation

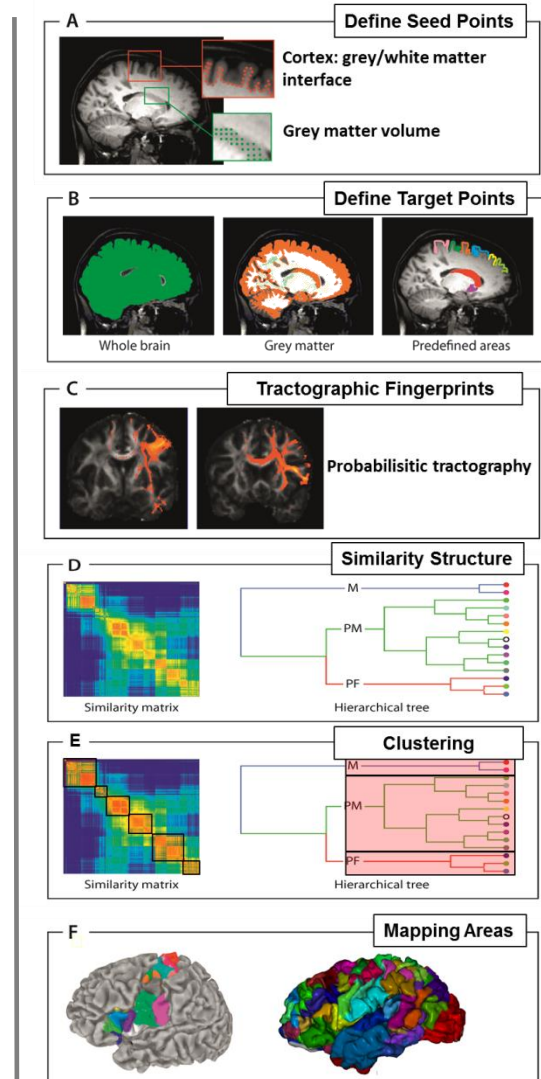
The role of long-range connectivity for the characterization of the functional–anatomical organization of the cortex

T.R. Knösche, M. Tittgemeyer

This review focuses on the role of long-range connectivity for the functional–anatomical organization of the cortex. We discuss connectivity-based parcellation and investigate techniques to estimate connectivity with emphasis to diffusion MRI and tractography.



Some factors contributing to anatomical connectivity.

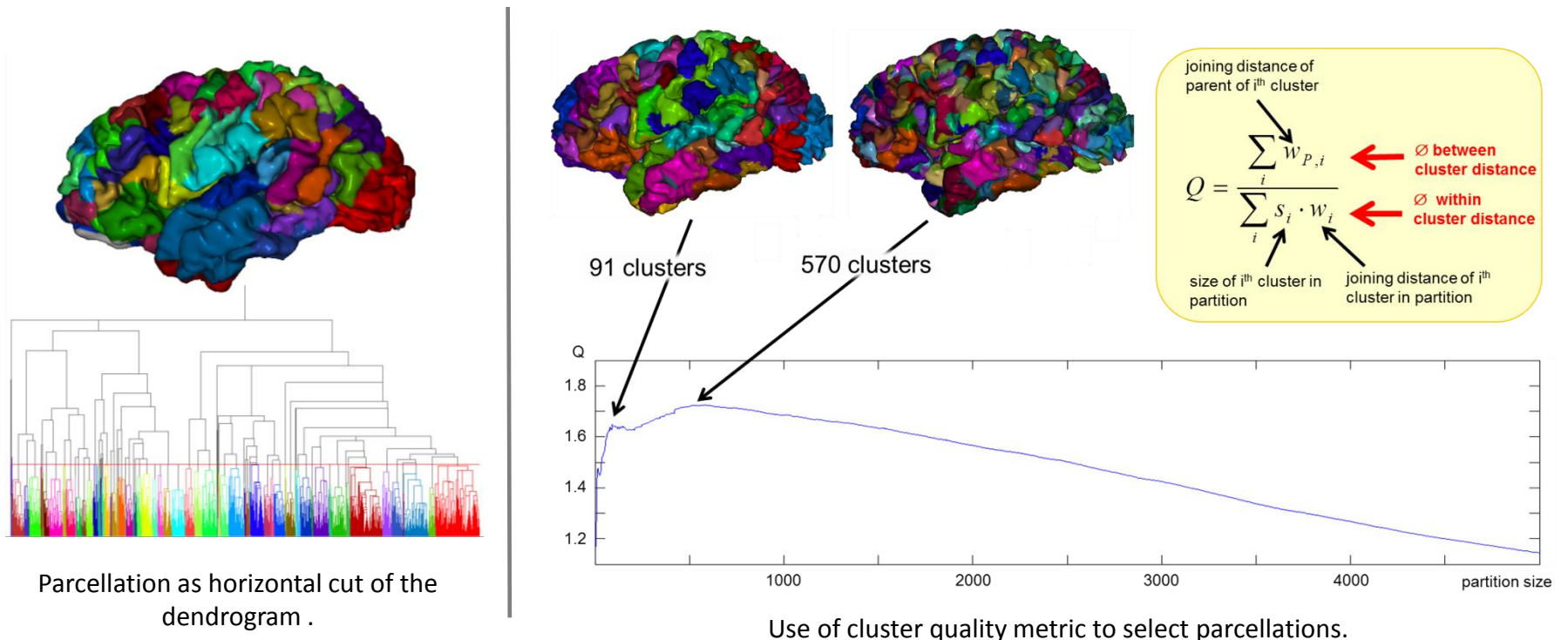


Stages of connectivity based parcellation.

A Hierarchical Method for Whole-Brain Connectivity-Based Parcellation

D. Moreno Dominguez, A. Anwander, T.R. Knösche

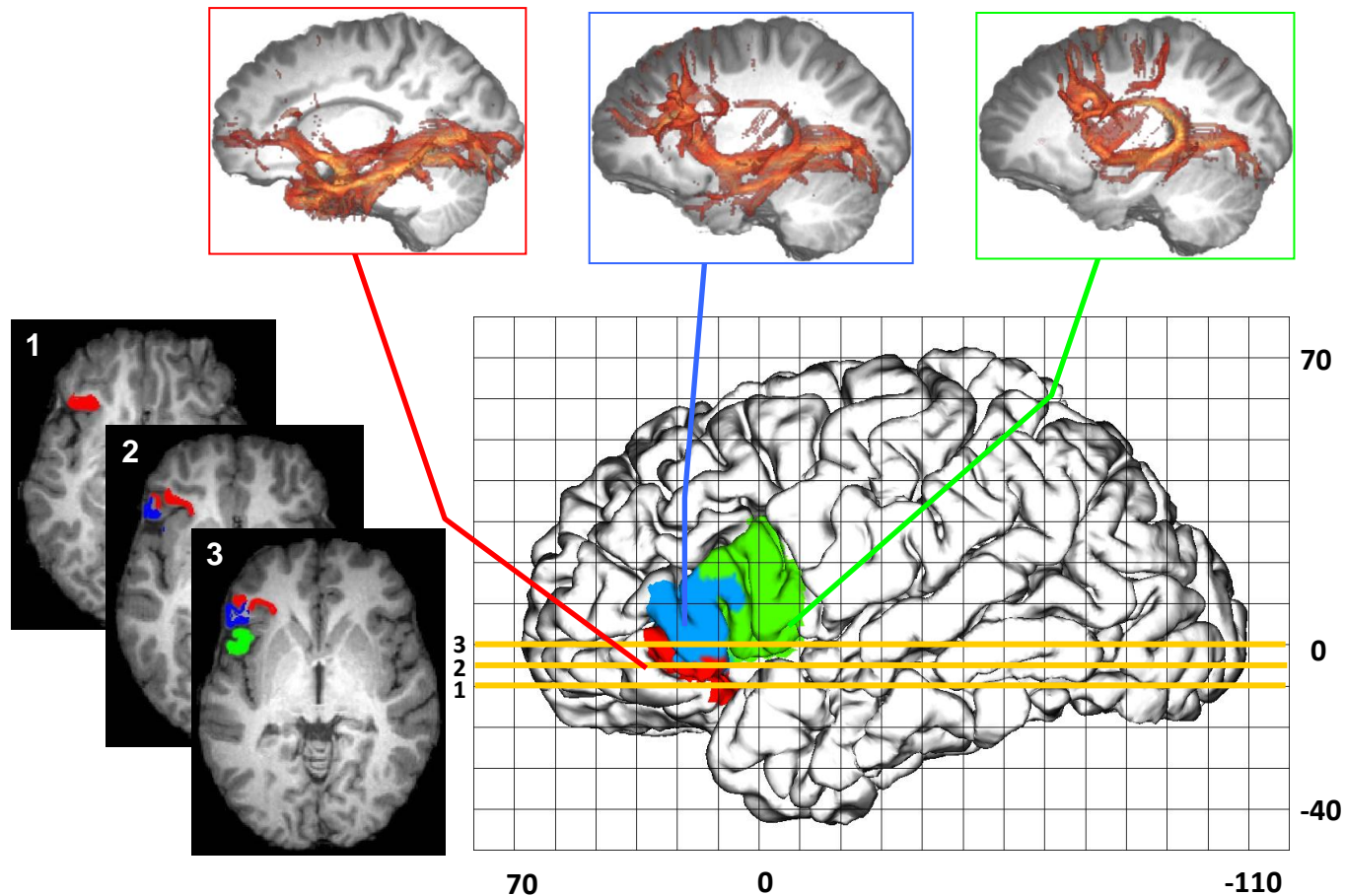
We propose hierarchical clustering to overcome the limitations of classical connectivity-based brain parcellation methods and achieve whole-cortex parcellation. We show how resulting dendrograms are used to compare the similarity structure of different subjects or recordings and how to extract parcellations from them.



Connectivity-Based Parcellation of Broca's Area

A. Anwander, M. Tittgemeyer, A.D. Friederici, D.Y. von Cramon, T.R. Knösche

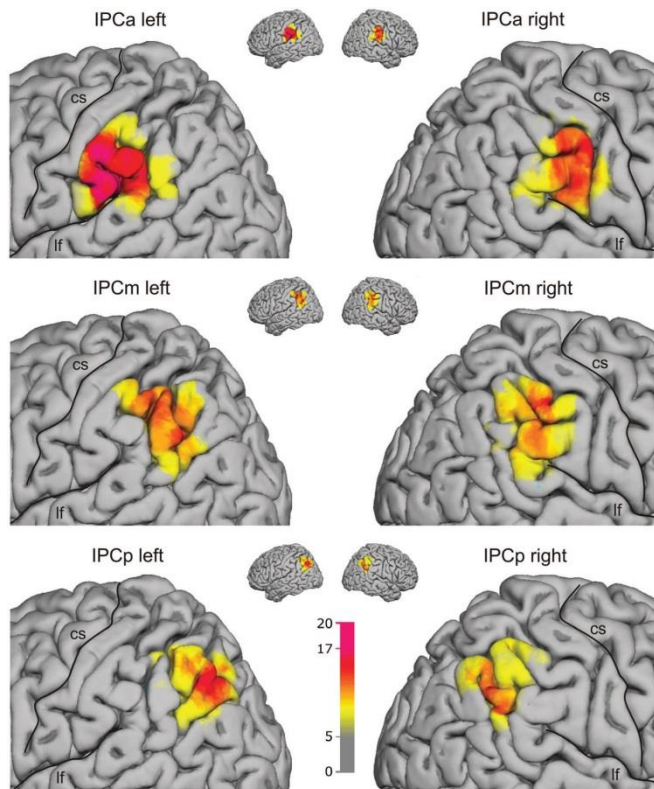
We used connectivity patterns based on diffusion tensor imaging to parcellate Broca's area. Three subregions are discernible that were identified as putative Brodmann areas 44 (green) and 45 (blue), as well as the deep frontal operculum (red).



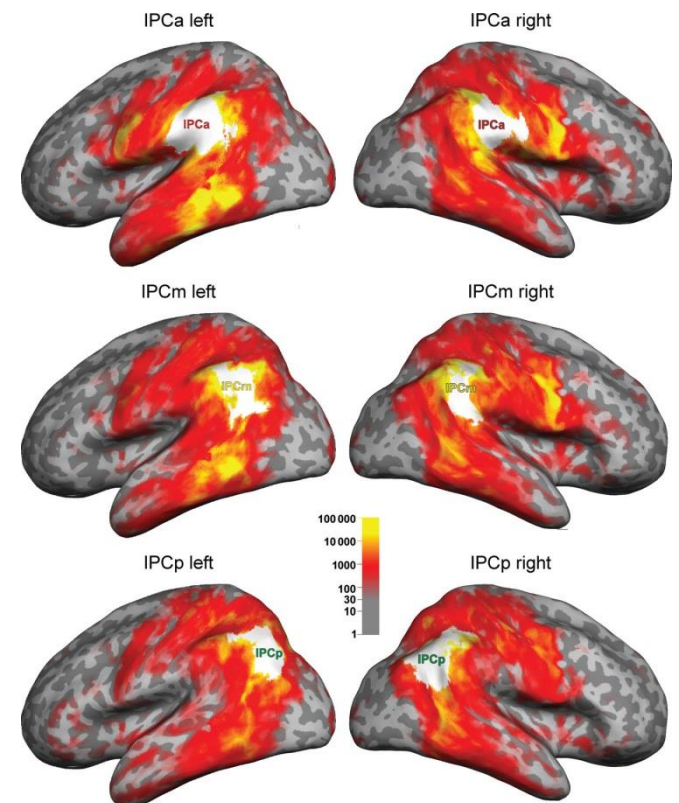
Connectivity architecture and subdivision of the human inferior parietal cortex revealed by diffusion MRI

M. Ruschel, T.R. Knösche, A.D. Friederici, R. Turner, S. Geyer, A. Anwender

We used diffusion-weighted MRI and probabilistic tractography to quantify the connectivity of the human IPCC and parcellate this cortex area. We found 3 subareas of comparable size in a rostro-caudal arrangement, which corroborates the subdivision reported for macaque IPCC. We also found additional features unique to human IPCC.



Population maps (left) and group averaged connectivity (right) of the three IPCC subareas for n=20.

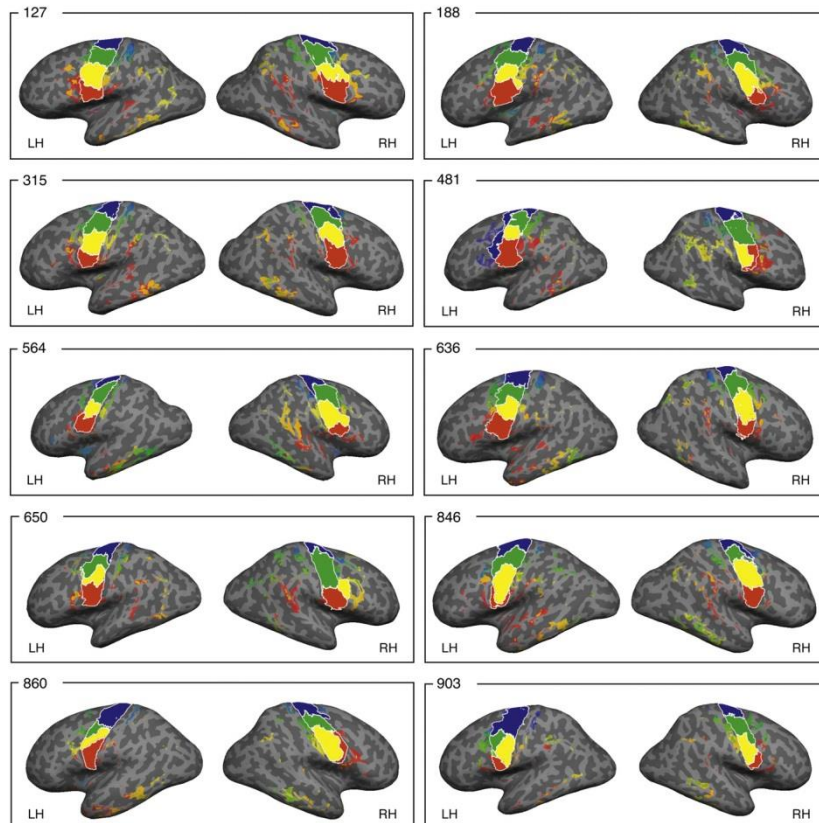


Anatomical and functional parcellation of the human lateral premotor cortex

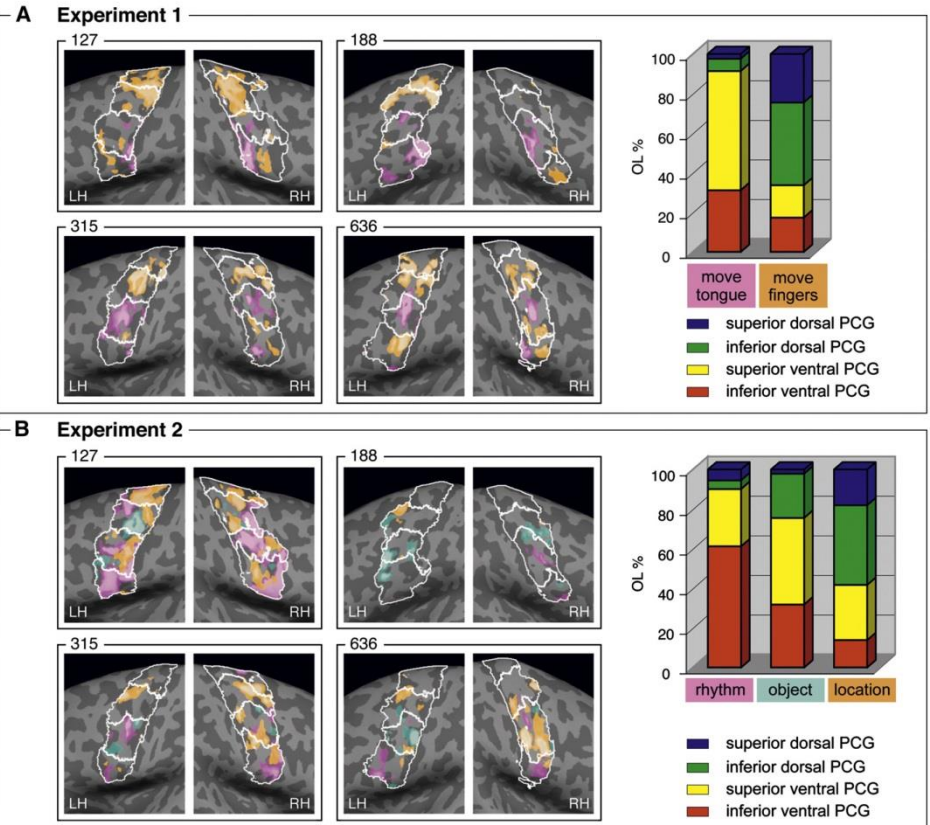
R.I. Schubotz, A. Anwander, T. R. Knösche, D.Y. von Cramon, M. Tittgemeyer

We used diffusion tractography and fMRI in cognitive and motor tasks to parcellate human precentral gyrus. The data suggest that anatomical parcellation predicts the distribution of functional activation and vice versa.

Anatomical parcellation and connectivity



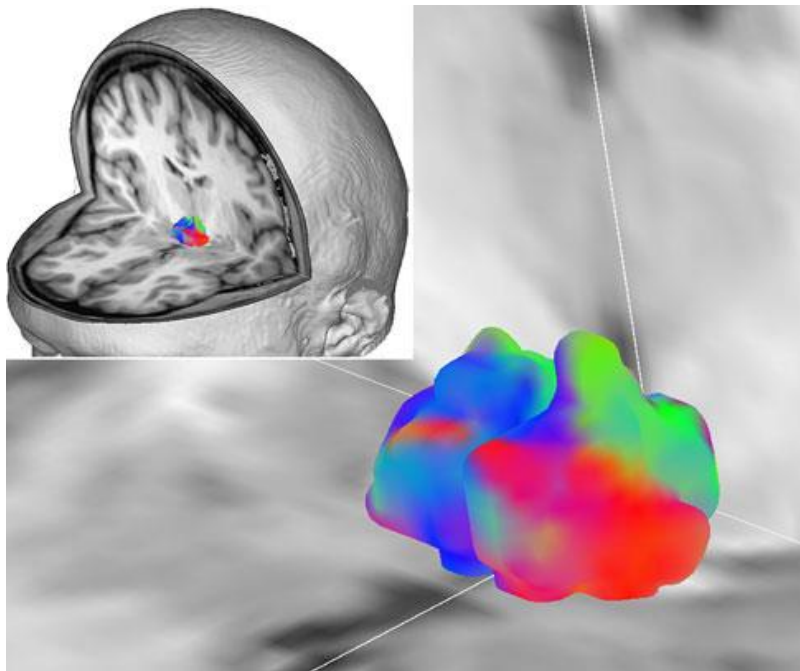
Functional localization



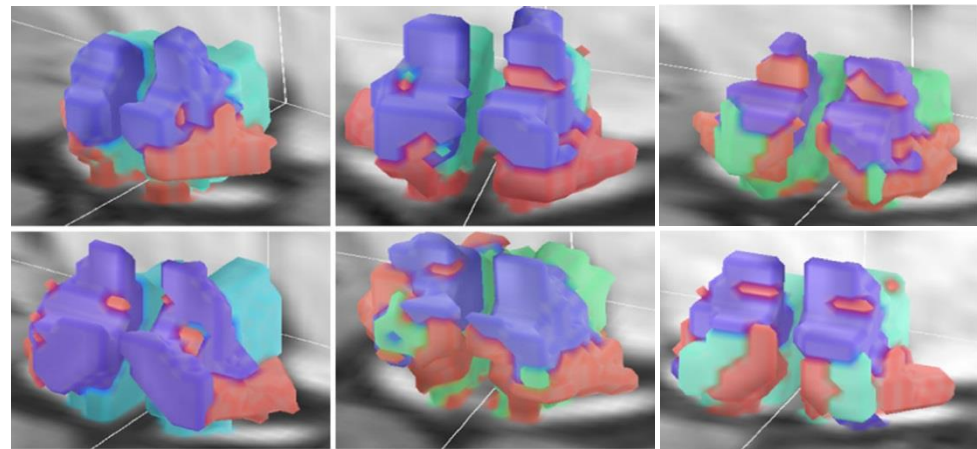
Diffusion imaging-based subdivision of the human hypothalamus: a magnetic resonance study with clinical implications

P. Schönknecht, A. Anwander, F. Petzold, S. Schindler,
T. R. Knösche, H.E. Möller, U. Hegerl, R. Turner, S. Geyer

We parcellated the hypothalamus by k-means clustering the main diffusion direction into three regions. We obtained anatomically coherent subdivisions across hemispheres and subjects: an anterior region with dorsoventral direction, a posteromedial region with rostro-caudal direction, and a lateral region with mediolateral direction.



Principal diffusion direction (red medial–lateral, green rostral–caudal, blue dorsal–ventral) in one subject.

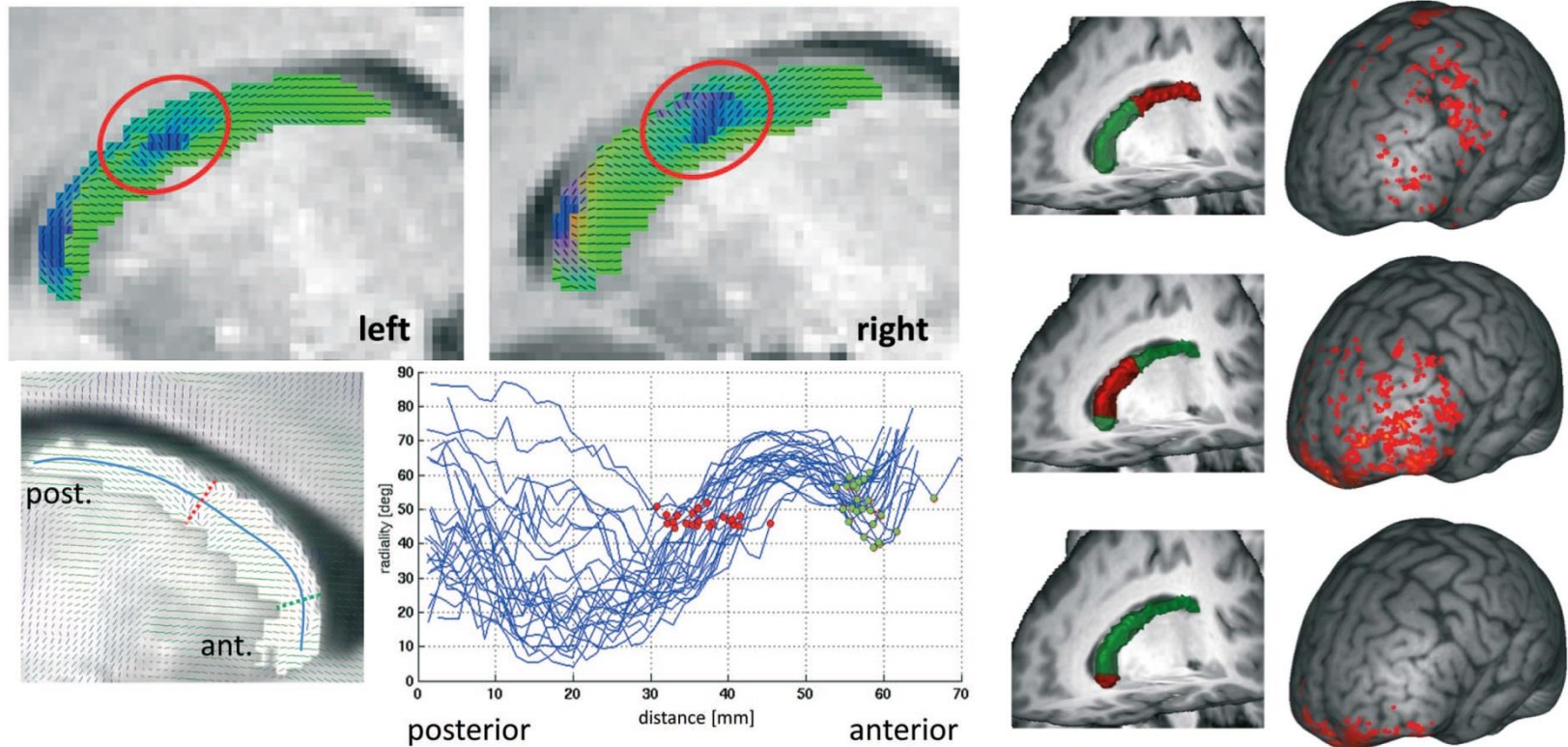


Hypothalamus parcellation into anterior (blue), posteromedial (green), and lateral (red) part for 6 subjects.

Beyond Cytoarchitectonics: The Internal and External Connectivity Structure of the Caudate Nucleus

S.A. Kotz, A. Anwander, H. Axer, T.R. Knösche

We applied diffusion MRI to characterize the local fiber structure of the CN and found a functionally meaningful structural tri-partition along the anterior-posterior axis of the CN. The connectivity of the subregions is in line with evidence from animal studies. Histological validation using polarized light imaging (PLI) confirms our results.



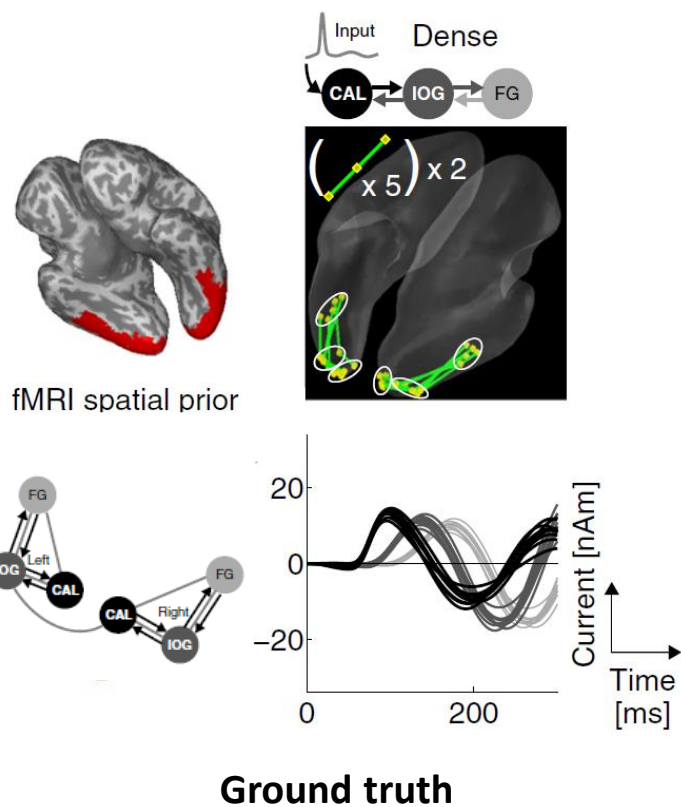
3 EEG/MEG Analysis & Source Modeling

3.1 Source reconstruction algorithms

MEG source reconstruction based on identification of directed source interactions on whole-brain anatomical networks

M. Fukushima, O. Yamashita, T.R. Knösche, M. Sato

We present a Bayesian framework for MEG source reconstruction that simultaneously reconstructs source amplitudes and source interactions across the whole brain, based on a full multivariate autoregressive (MAR) model. The MAR coefficients are constrained by diffusion tractography, while the source locations are constrained by fMRI.

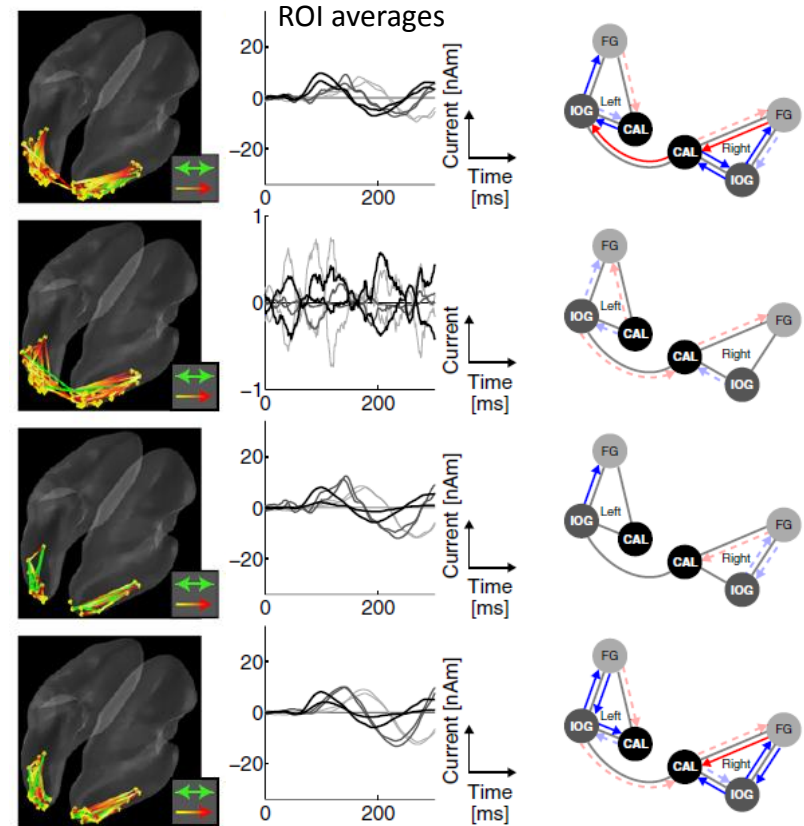


**weighted
minimum norm**

**LCMV
beamformer**

**hierarchical
var. Bayes (hVB)**

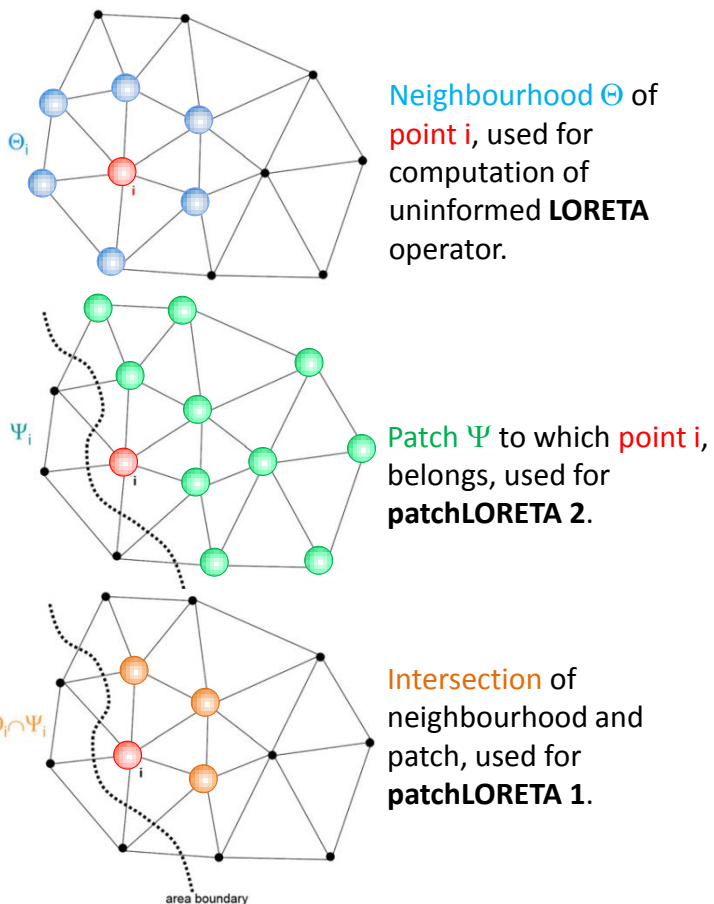
**dynamic hVB
(new method)**



Prior knowledge on cortex organization in the reconstruction of source current densities from EEG

T.R. Knösche, M. Gräser, A. Anwander

We propose two novel LORETA methods using parcellations as prior knowledge. The algorithms are evaluated using computer simulations and event-related potentials.

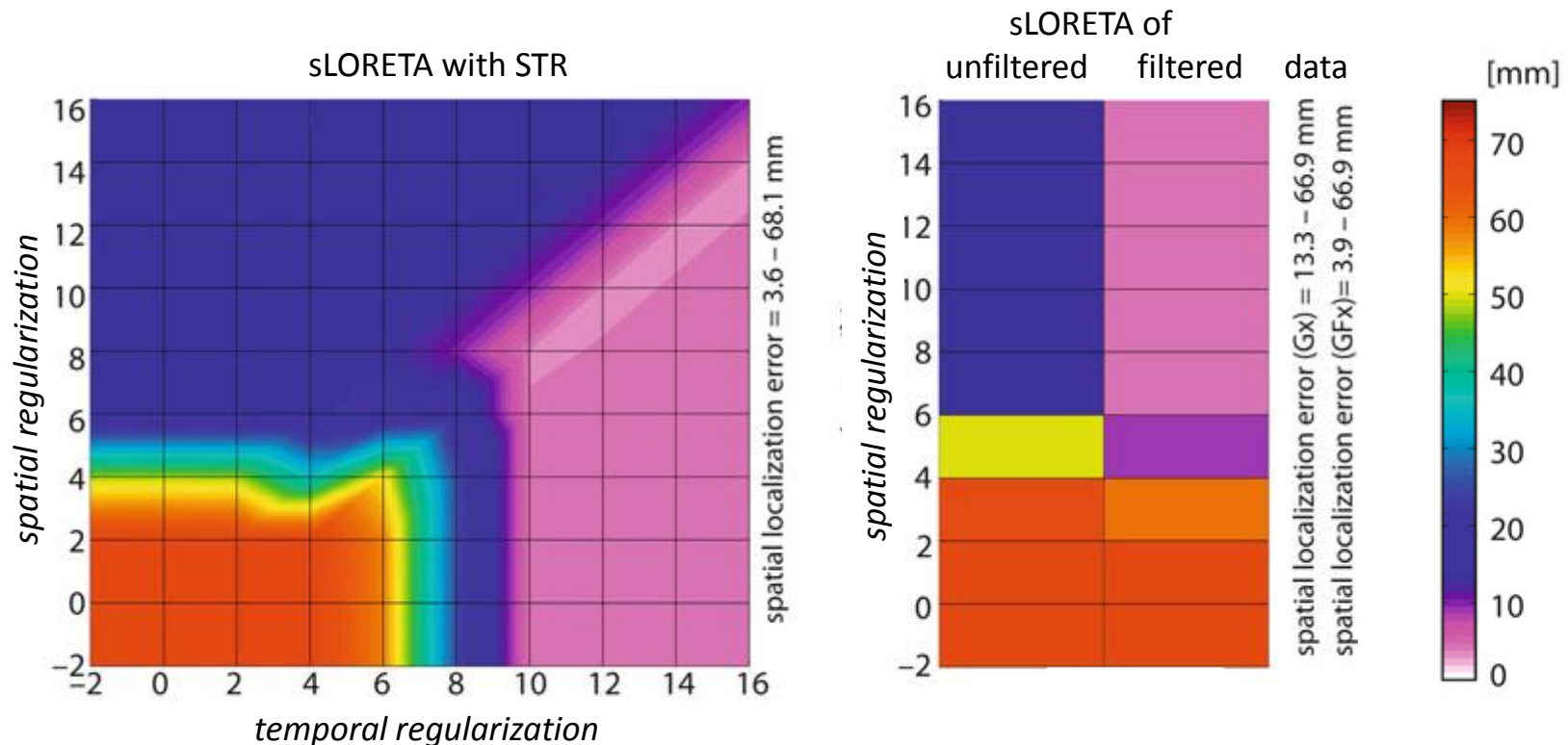


prior information	original	Minimum Norm	LORETA	patch LORETA 1	patch LORETA 2
		 0 13 local AUC = 0.976	 0 12 local AUC = 0.945	 0 13 local AUC = 0.996	 0 12 local AUC = 0.996
		 0 10 local AUC = 0.962	 0 10 local AUC = 0.926	 0 11 local AUC = 0.982	 0 12 local AUC = 0.959
		 0 13 local AUC = 0.985	 0 13 local AUC = 0.970	 0 14 local AUC = 0.974	 0 18 local AUC = 0.853
		 0 15 local AUC = 0.981	 0 16 local AUC = 0.980	 0 15 local AUC = 0.976	 0 16 local AUC = 0.777

Spatio-temporal Regularization in Linear Distributed Source Reconstruction from EEG/MEG: A Critical Evaluation

M. Dannhauer, E. Lämmel, C.H. Wolters, T.R. Knösche

We systematically compared the performance of spatio-temporal regularization (STR) in an sLORETA algorithm to simple *ad hoc* or *post hoc* filtering of the data or of the reconstructed current density, respectively. We did not find any evidence that STR-based methods outperform purely spatial algorithms combined with temporal filters.

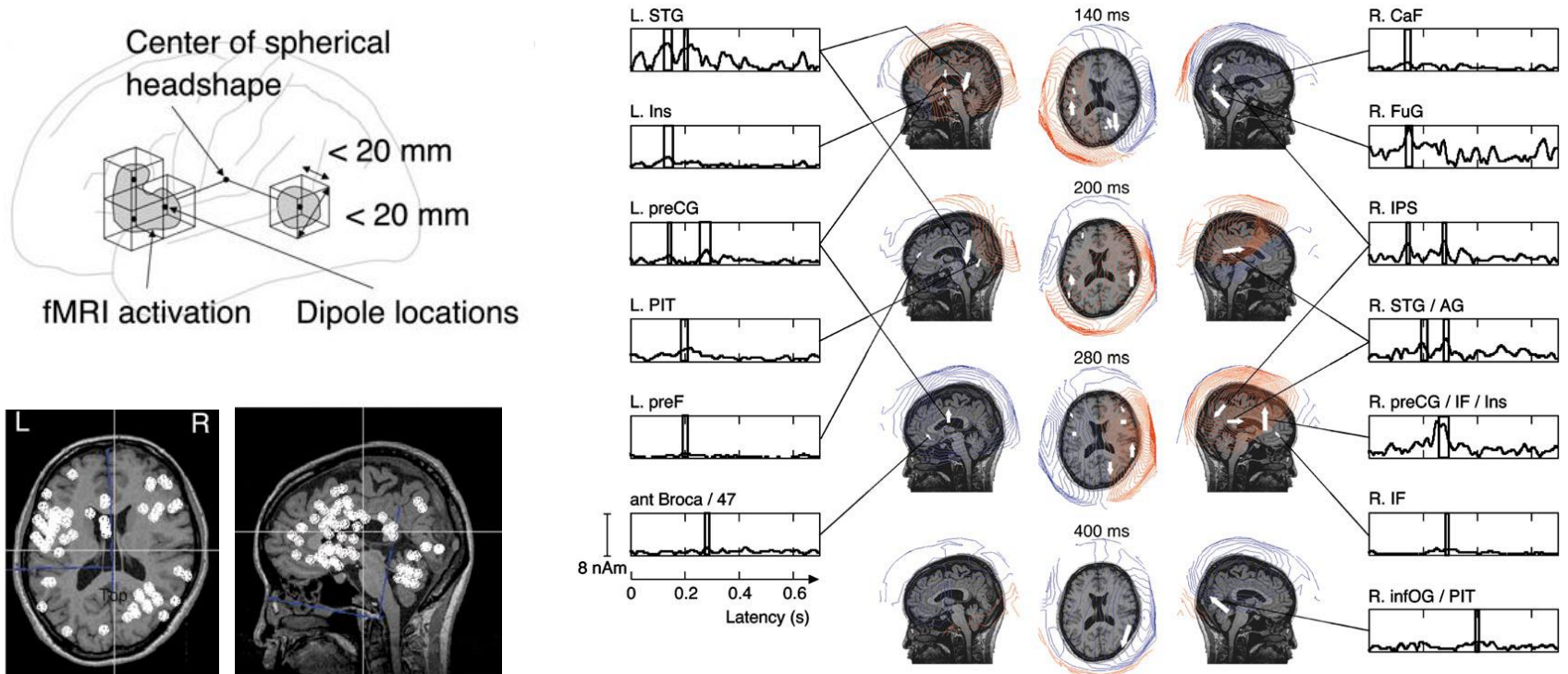


Localization errors for a single thalamic source pointing in dorsal direction.

An fMRI-Constrained MEG Source Analysis with Procedures for Dividing and Grouping Activation

N. Fujimaki, T. Hayakawa, M. Nielsen, T.R. Knösche, S. Miyauchi

We developed a method for combined source localization from MEG and fMRI. It involves dividing large fMRI activation volumes into subvolumes in each of which a dipole is placed, and grouping neighboring dipoles whose temporal changes are inseparable by MEG data. The method was explored using simulated and real data.



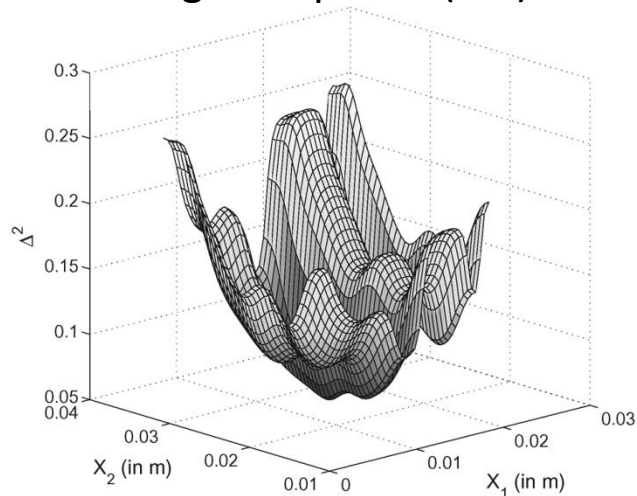
64 dipoles placed in fMRI blobs.

Results for language experiment: 13 group moments. Rectangles denote significance.

Reconstruction of Multiple Neuromagnetic Sources Using Augmented Evolution Strategies— A Comparative Study

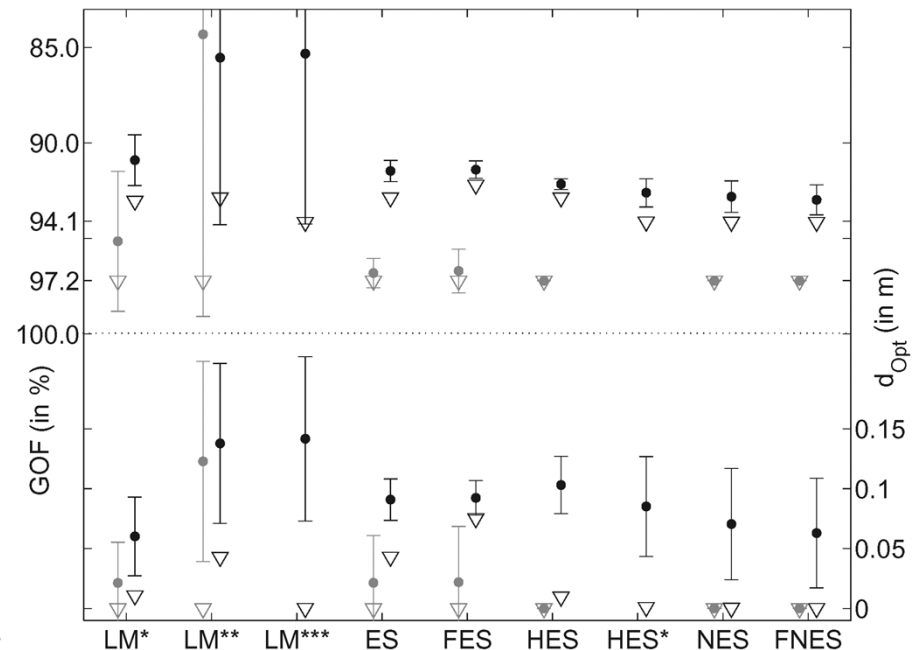
R. Eichardt, J. Haueisen, T.R. Knösche, E.G. Schukat-Talamazzini

Hybrid and nested evolution strategies (HES, NES), which both realize a combination of global and local search by means of multilevel optimizations, were newly designed and compared to established evolution strategies (ES), fast evolution strategies (FES), and the Levenberg-Marquardt (LM) method by conducting a two-dipole fit with MEG data.



Top: sample goal function projected into the plane of the two x positions of the dipoles.

Right: upper part (left axis): mean value (dot), standard deviation (bar), and best achieved value (triangle) for the GOF; lower part (right axis): distance to global optimum. Black and gray: two different data sets.



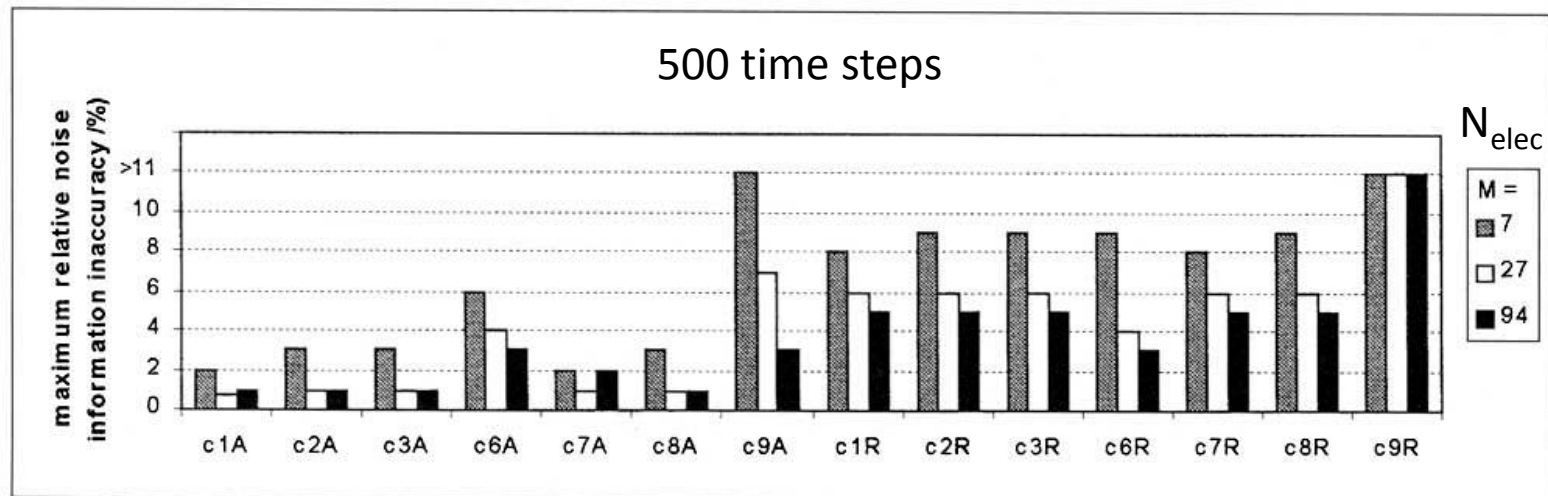
The asterisks (*) denote different parameterization choices.

Determining the Number of Independent Sources of the EEG: A Simulation Study on Information Criteria

T.R. Knösche , E.M. Behrens, H.R.A. Jagers, M.J. Peters

Information criteria (IC) to separate signal and noise subspaces in EEG/MEG were tested by simulations. We recommend two ICs best suited for **high noise and accurate covariances**, and for **low noise and less accurate covariances**, respectively.

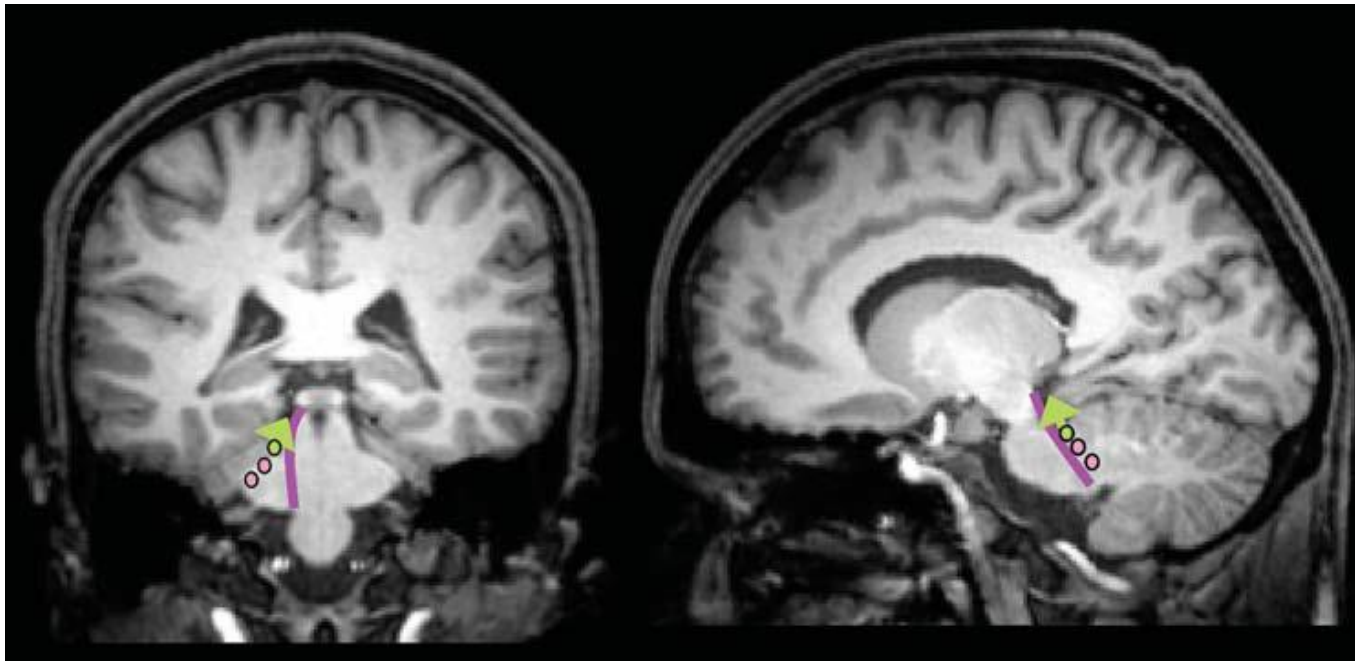
assumptions on noise	based on the distribution of ...					
	the measurements		all eigenvalues		the noise eigenvalues	
	Akaike	MDL	Akaike	MDL	Akaike	MDL
$\Sigma_N = \sigma^2 I$, σ unknown	C1A	C1R	C4A	C4R	C7A	C7R
$\Sigma_N = \sigma^2 I$, σ known	C2A	C2R	C5A	C5R	C8A	C8R
Σ_N arbitrary, sample known	C3A	C3R	C6A	C6R	C9A	C9R



Recent advances in modeling and analysis of bioelectric and biomagnetic sources

T.H. Sander, T.R. Knösche, A. Schlögl, F. Kohl, C.H. Wolters, J. Haueisen, L. Trahms

Current trends and results from major topics of electro- and magnetoencephalographic data analysis are presented. The following topics are discussed: source reconstruction using finite element modeling to locate deep sources; connectivity analysis; verification and validation of source reconstruction through animal and phantom measurements.



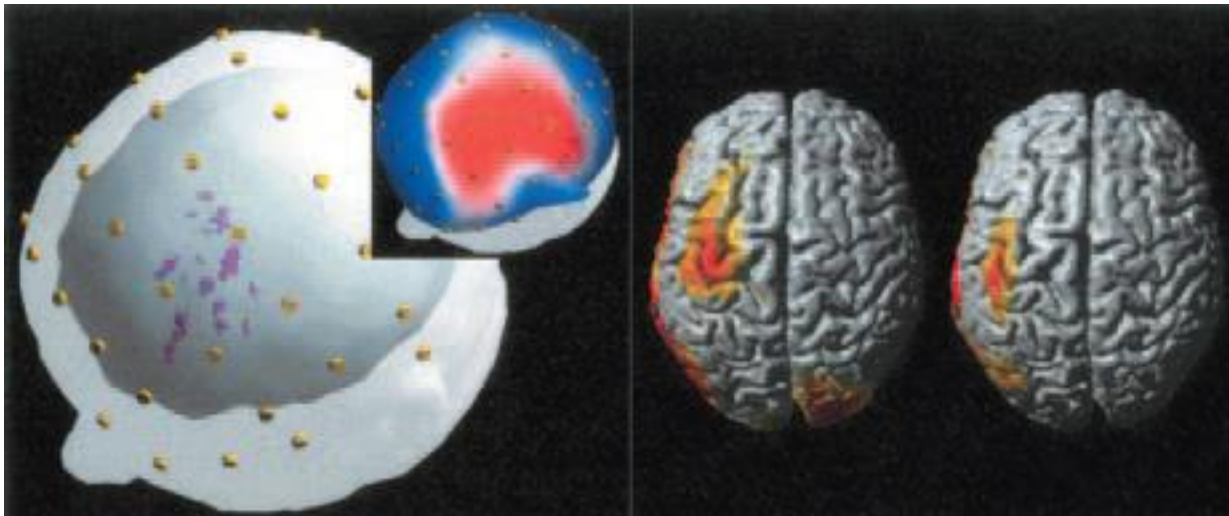
Localization of auditory brain stem potentials: localizations of wave V (7 ms after chirp offset) for different translation factors between diffusion anisotropy and conductivity anisotropy in the white matter (from low to high: 740, 1200, 1800); the green arrow indicates the dipole direction. The purple line denotes the course of the lateral lemniscus.

ASA - Advanced Source Analysis of Continuous and Event-Related EEG/MEG Signals

F. Zanow, T.R. Knösche

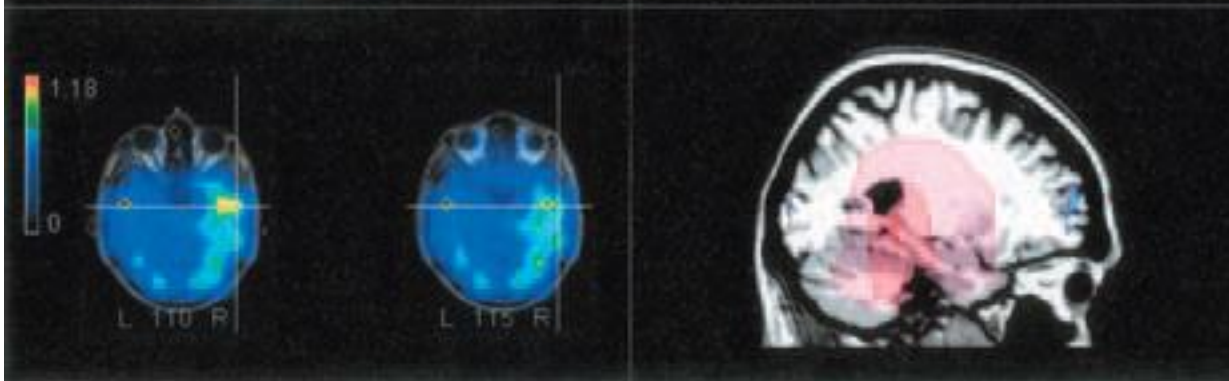
We present an overview on the currently available functionality of the ASA software (ANT Software BV, Enschede, Netherlands) and provide examples of its application.

Dipole locations
of epileptic
spike in EEG



Brain surface
current density
based on MEG in
musicians listening
to piano music

LORETA map
from EEG during
double cuing in
task switching



MUSIC map from
EEG during
perception of
musical phrase
boundaries.

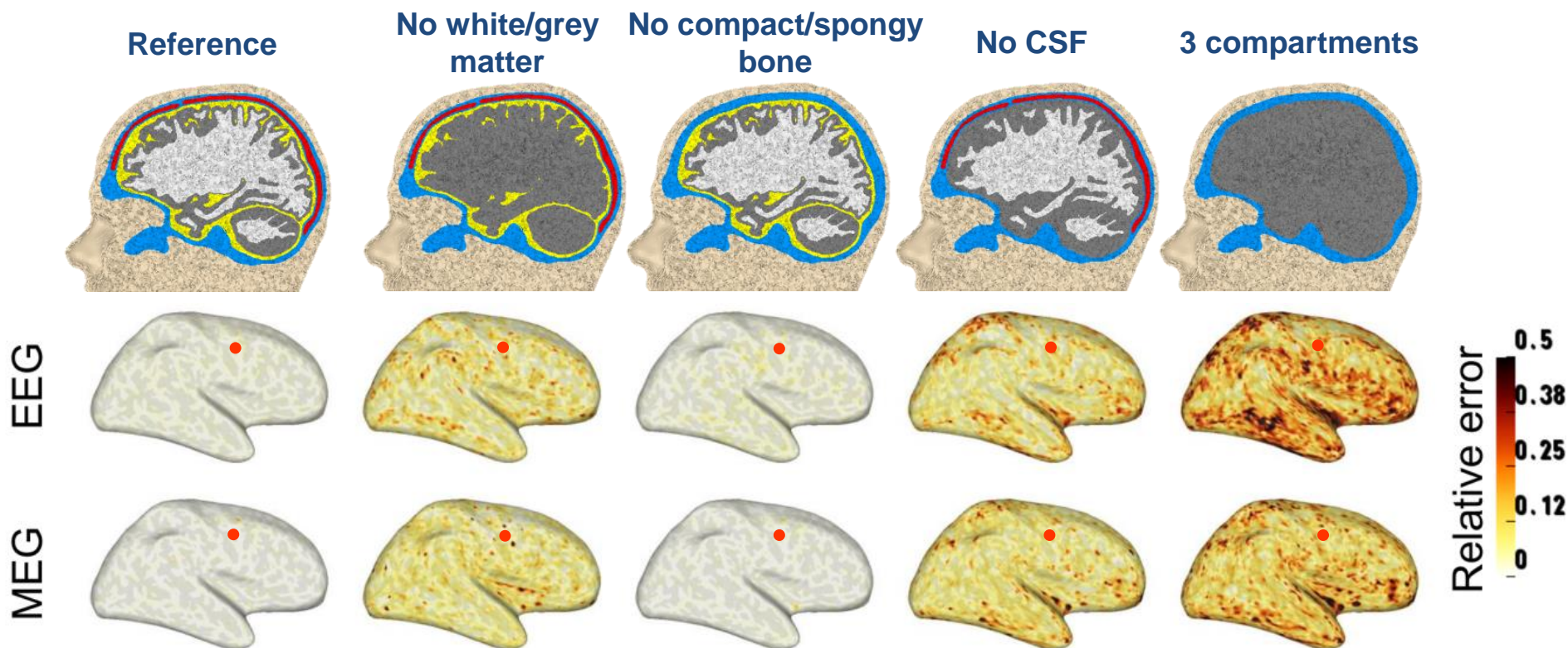
3 EEG/MEG Analysis & Source Modeling

3.2 Volume conductor modeling

Influence of the head model on EEG and MEG source connectivity analyses

J.H. Cho, J. Vorwerk, C.H. Wolters, T.R. Knösche

We studied the head model influence on EEG/MEG source connectivity analysis. Sources were reconstructed by beamforming, connectivity was estimated by imaginary coherence (ICoh) and generalized partial directed coherence (GPDC). Larger effects were found for white/gray matter and CSF, smaller ones for spongy/compact bone. ICoh is relatively safe from the crosstalk caused by imperfect head models, as opposed to the GPDC.

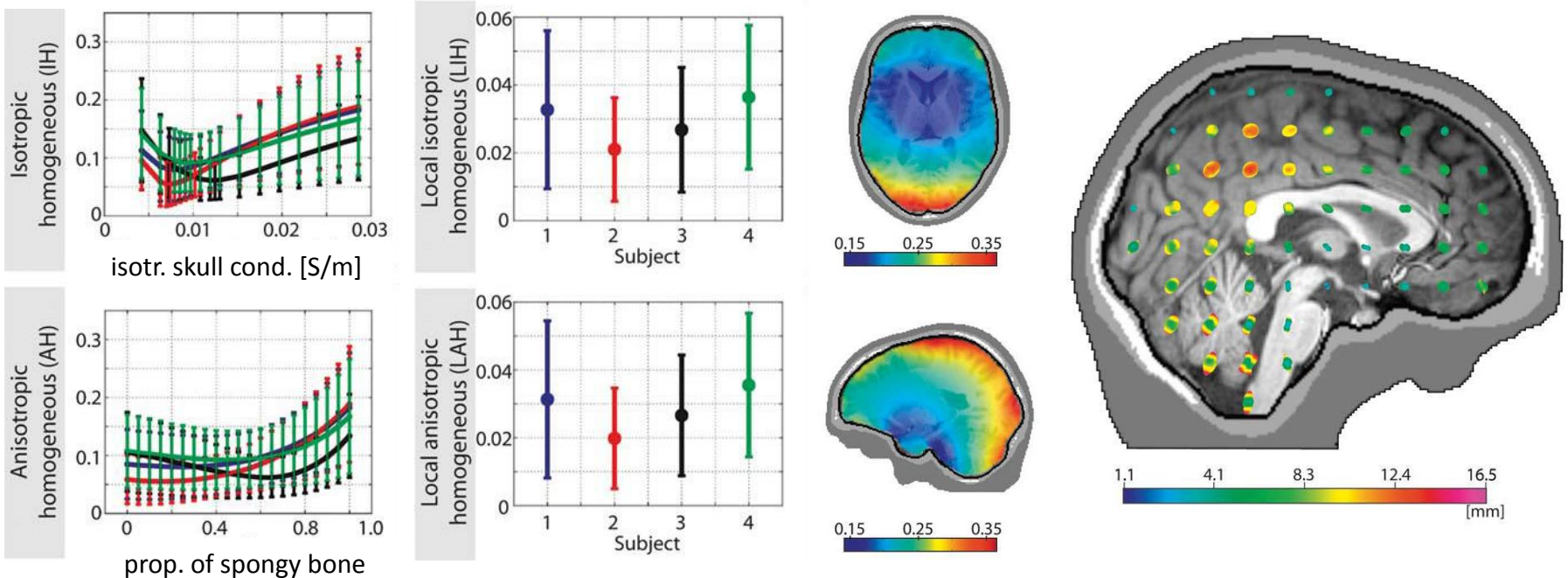


Reconstruction of connectivity, simulated by neural mass model (from red dot), with Imaginary Coherence.

Modeling of the Human Skull in EEG Source Analysis

M. Dannhauer, B. Lanfer, C.H. Wolters, T.R. Knösche

We used computer simulations to investigate finite element models of the layered structure of the human skull in EEG source analysis. We show that accounting for the local variations over the skull surface is important, whereas assuming isotropic or anisotropic skull conductivity has little influence. If using an isotropic and homogeneous skull model, the ratio between skin/brain and skull conductivities should be ca. 40:1.



Relative difference measure (RDM) in forward solution between full (tissues modeled separately) and simplified skull models.

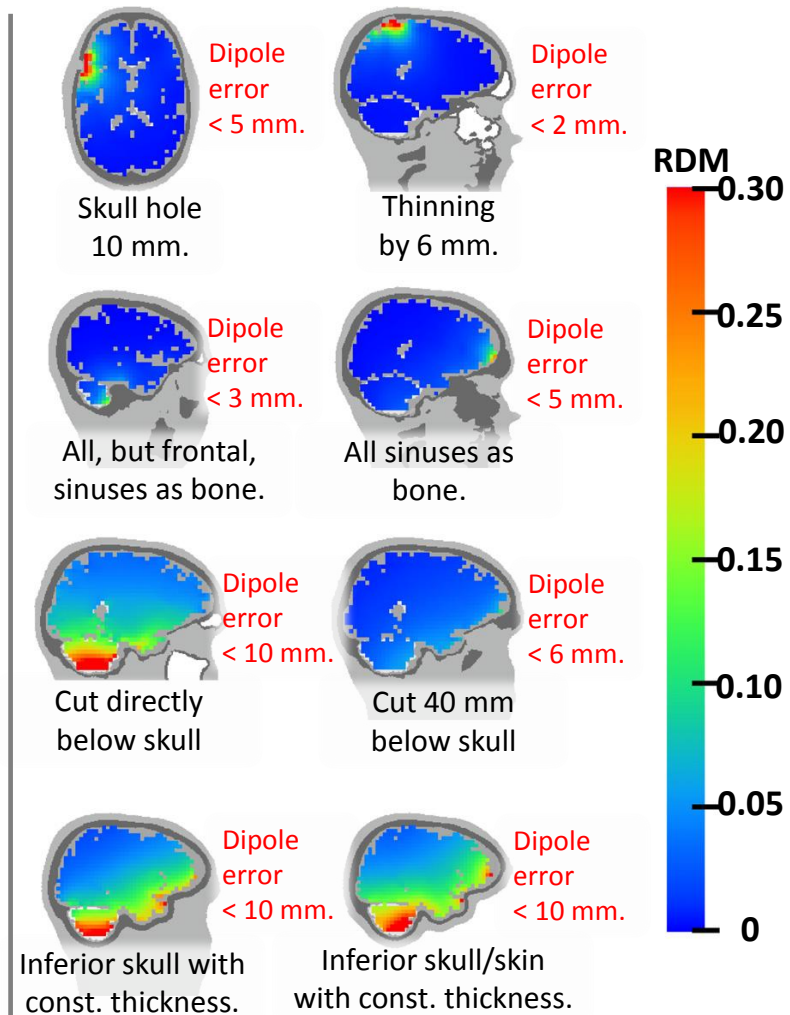
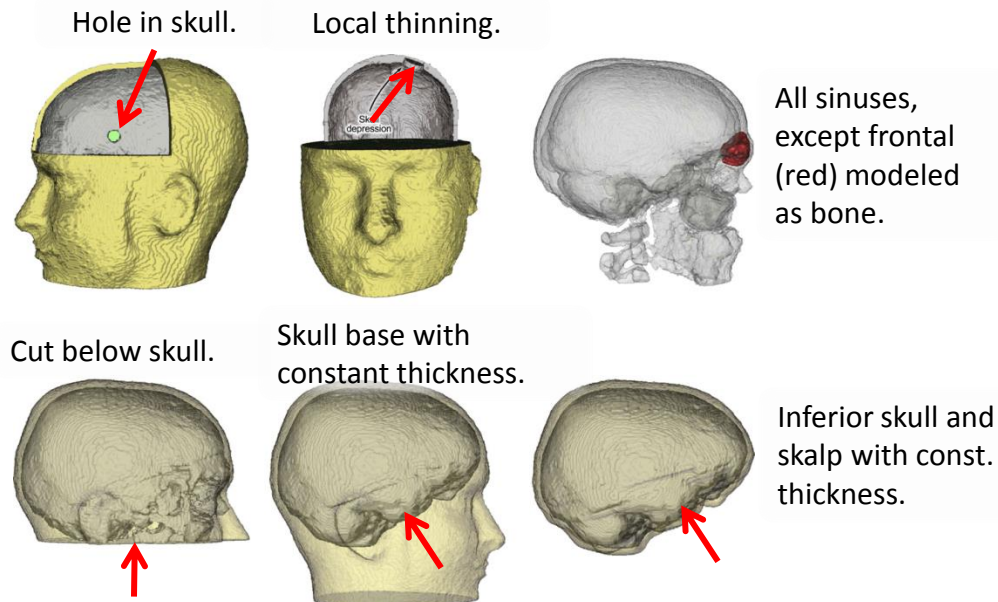
RDM for IH model with $\sigma_{\text{skull}}=4.2$ mS/m.

Dipole localization error for IH model with $\sigma_{\text{skull}}=4.2$ mS/m.

Influences of skull segmentation inaccuracies on EEG source analysis

B. Lanfer, M. Scherg, M. Dannhauer, T.R. Knösche, M. Burger, C.H. Wolters

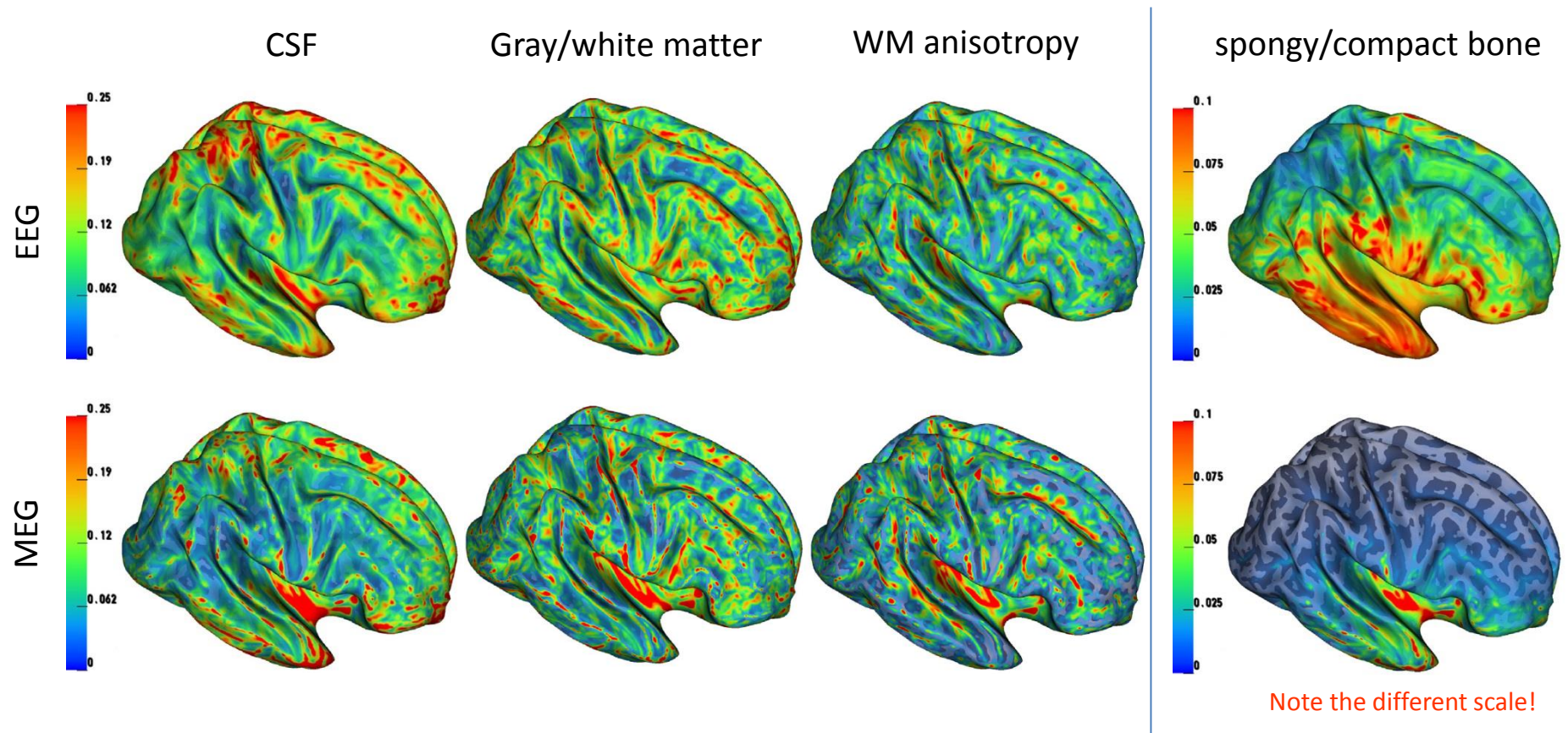
This computer simulation study investigated the influences of skull geometry deficiencies on EEG forward and inverse computations. These included erroneous skull holes, local errors in skull thickness, modeling cavities as bone, downward extension of the model and simplifying the inferior skull and scalp as layers of constant thickness.



A guideline for head volume conductor modeling in EEG and MEG

J. Vorwerk, J.H. Cho, S. Rampp, H. Hamer, T.R. Knösche, C.H. Wolters

We investigated the influence of (not) modeling skull spongiosa/compacta, CSF, gray/white matter, and white matter anisotropy on the EEG/MEG forward solution. CSF and gray/white matter distinction had strongest, WM anisotropy strong and skull spongiosa/compacta distinction weak effects (with optimized conductivity for the skull compartment).



Influence of Anisotropic Conductivity on EEG Source Reconstruction: Investigations in a Rabbit Model

D. Güllmar, J. Haueisen, M. Eiselt, F. Gießler, L. Flemming, A. Anwander, T.R. Knösche, C.H. Wolters, M. Dümpelmann, D.S. Tuch, J.R. Reichenbach

We quantify the influence of white matter anisotropy on EEG source reconstruction in a rabbit head using both simulations and source localization based on invasive measurements. In vivo anisotropic conductivity was obtained from DTI and included into a high-resolution finite-element model.

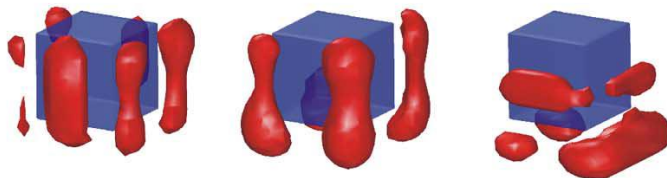
regions of strong influence of anisotropy



dipole orientation

ant.-post. left-right inf.-sup.

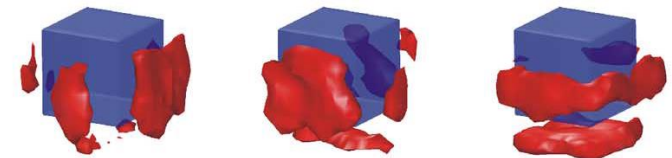
RDM*



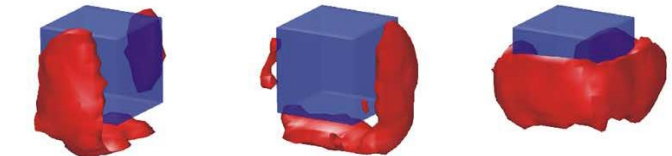
MAG



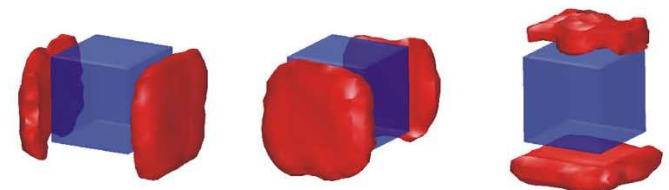
dipole shift



magnitude change



orientation change



ant.-post.

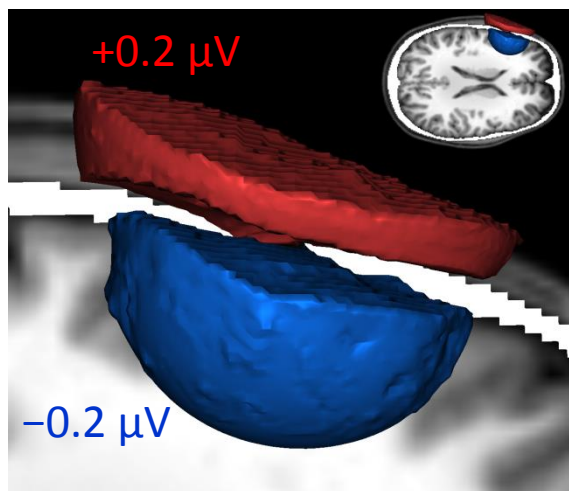
left-right

inf.-sup.

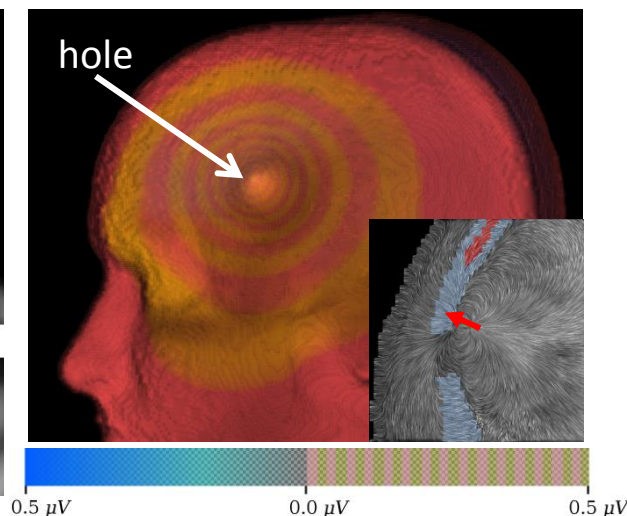
Visualizing Simulated Electrical Fields from Electroencephalography and Transcranial Electric Brain Stimulation: A Comparative Evaluation

S. Eichelbaum, M. Dannhauer, M. Hlawitschka, D. Brooks, T.R. Knösche, G. Scheuermann

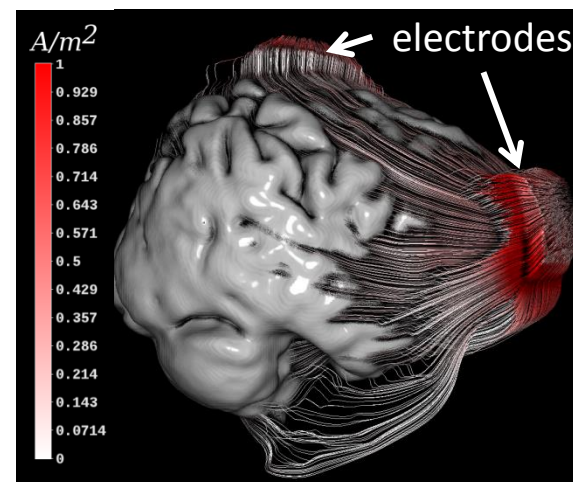
We evaluate widely used visualization techniques with respect to extractability of information, comparability, effective integration of anatomical context, and interactivity. We present illustrative examples and discuss pros and cons of the techniques.



Isosurfaces of potential differences between models with and without skull hole for a tangential dipole next to the hole.



Direct volume rendering of potential differences for a radial dipole next to the hole (see inset) using an alternating transfer function to highlight gradients.

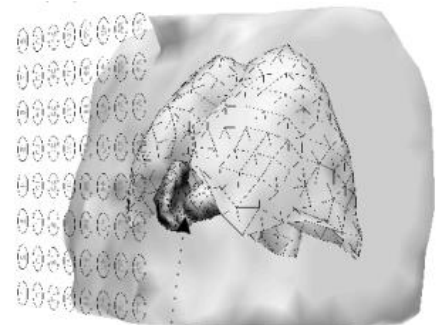


Streamlines of current flow during transcranial direct current stimulation (tDCS).

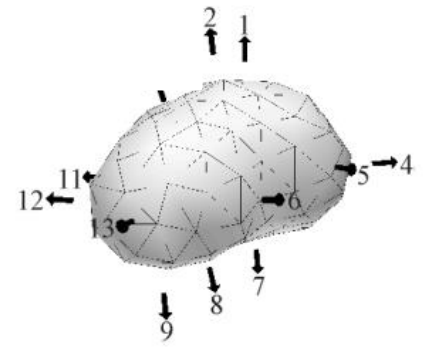
The Dependence of the Inverse Solution Accuracy in Magnetocardiography on the Boundary Element Discretization

J. Haueisen, J. Schreiber, H. Brauer, T.R. Knösche

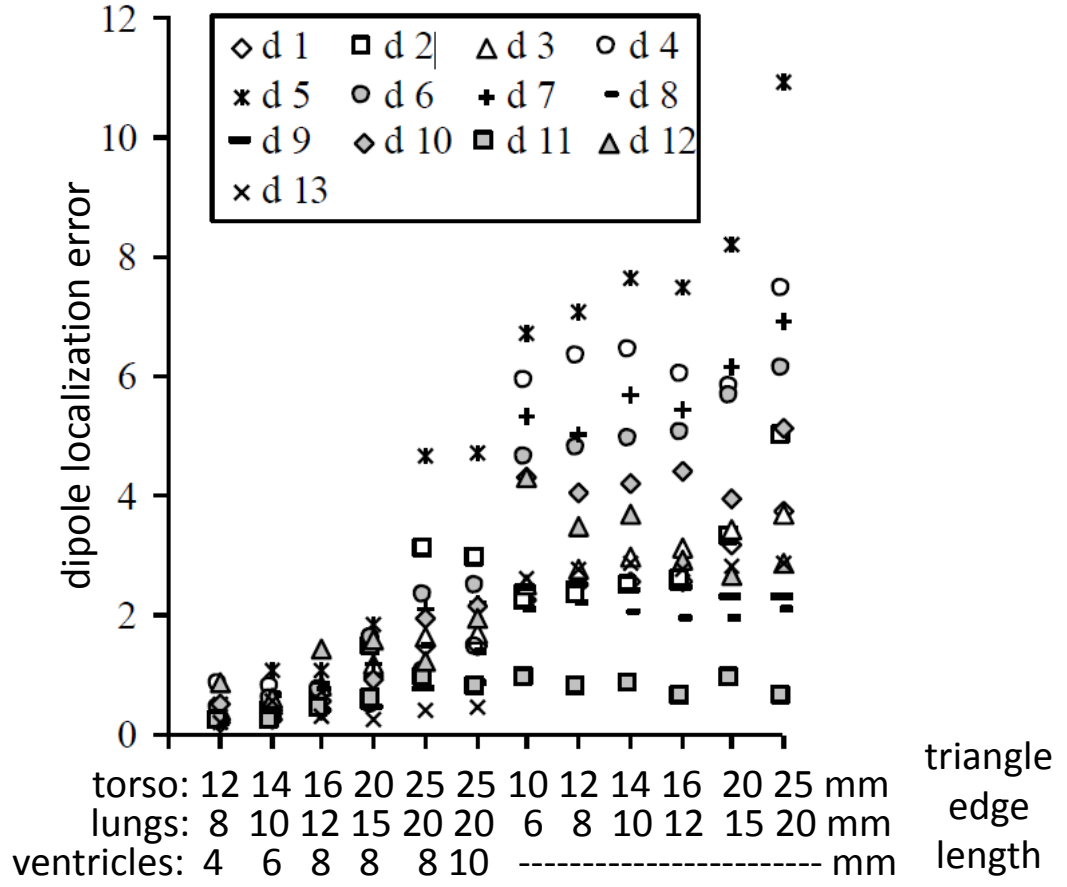
We quantify the influence of the boundary element discretization and model complexity (inclusion of blood masses) on the cardiomagnetic forward and inverse problem for different dipole depths and regions of the heart.



torso model with lungs, blood masses and sensor positions



left ventricle with dipoles



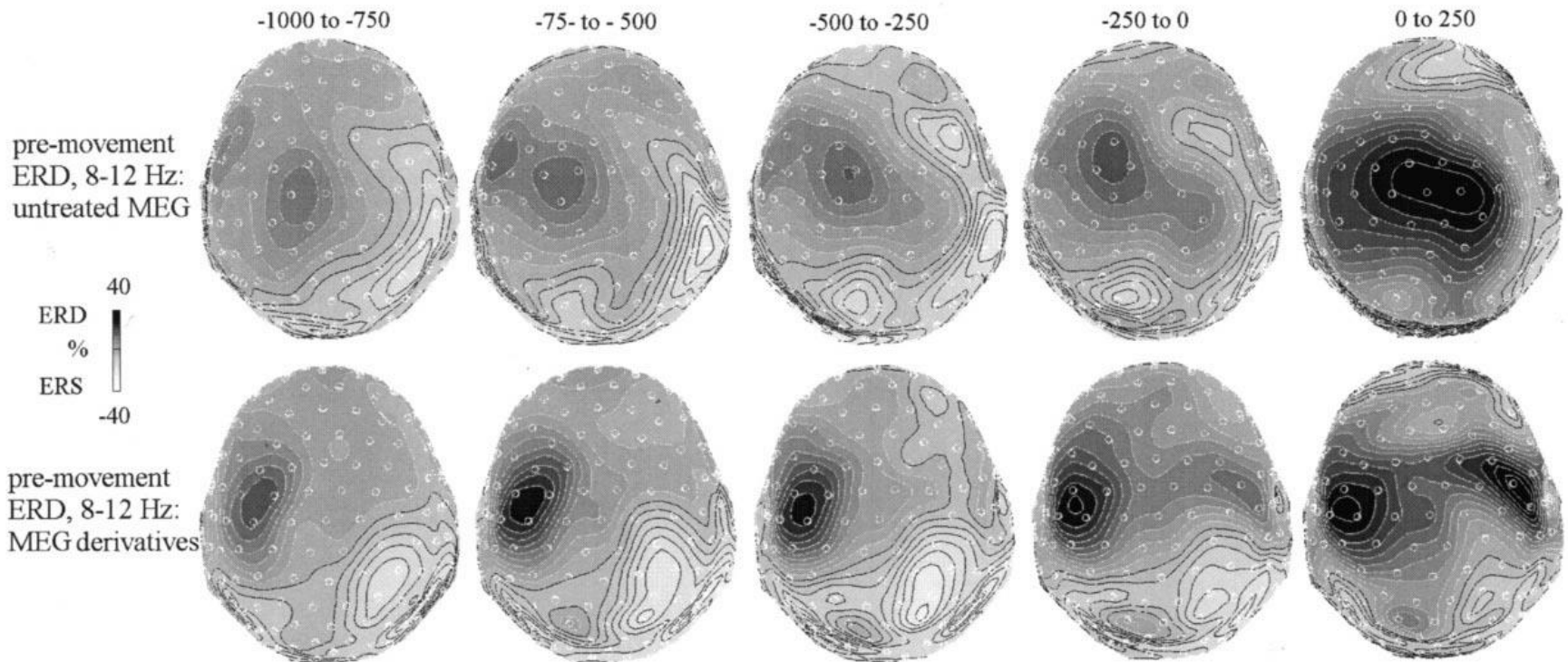
3 EEG/MEG Analysis & Source Modeling

3.3 Spatial mapping & interpolation

Tangential derivative mapping of axial MEG applied to event-related desynchronization research

M.C.M Bastiaansen, T.R. Knösche

We present a new method based on computing spatial derivatives of the MEG data. The limitations of this method were investigated by means of forward simulations, and the method was applied to a 150-channel MEG dataset.



Grand averages (N =6) of pre-movement ERD/ERS. Power decrease is depicted in dark gray with white contour lines, while power increase is depicted in light gray with black contour lines.

Transformation of Whole-Head MEG Recordings Between Different Sensor Positions

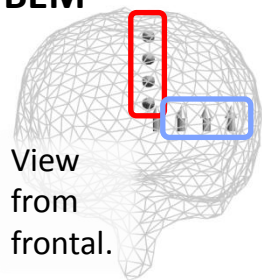
T.R. Knösche

A method is presented for the transformation of MEG recordings to a standard sensor position. It is based on the projection to a virtual source space. For an 148 channel magnetometer, the method was evaluated using simulations and phantom head recordings.

$$MEG_{new} = Leadfield_{new} \cdot Leadfield_{old}^{+} \cdot MEG_{old}$$

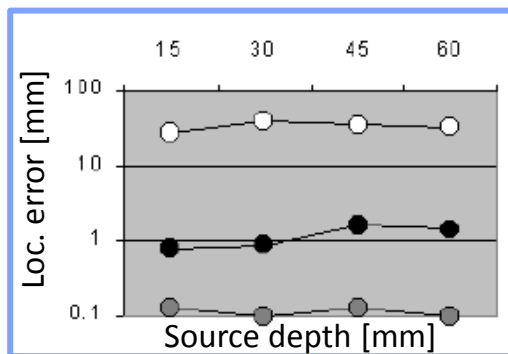
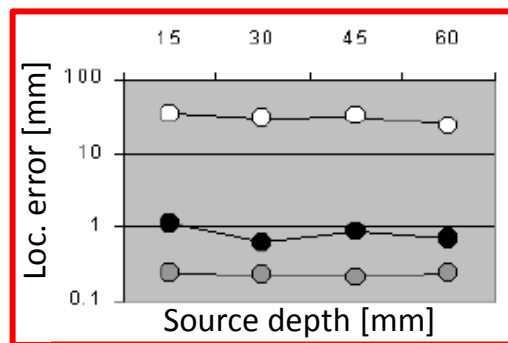
... with $(\cdot)^{+}$ being the truncated pseudoinverse.

Simulation with BEM

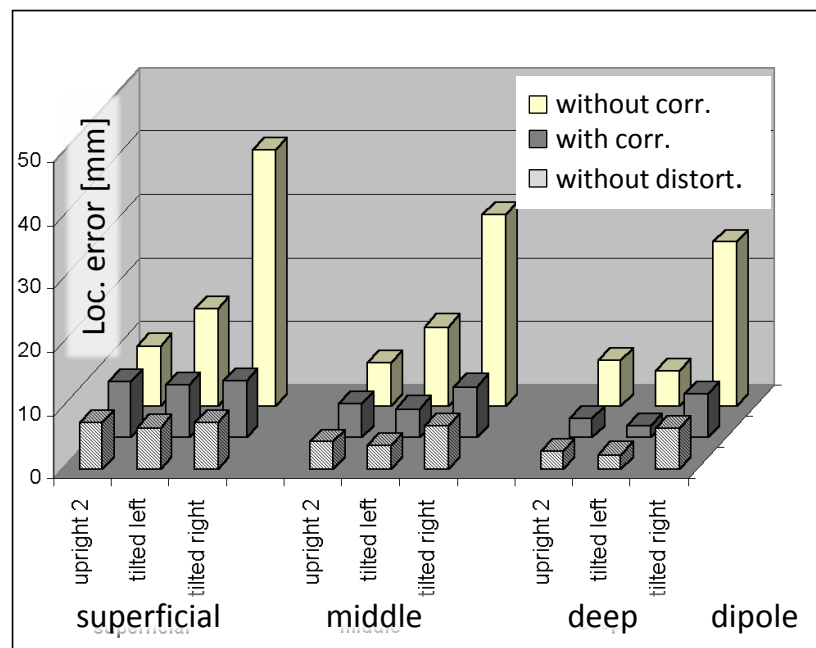


- Rotation of head by 10°.
- SNR=25

- without distortion
- with correction
- without correction



Phantom with sphere



3 EEG/MEG Analysis & Source Modeling

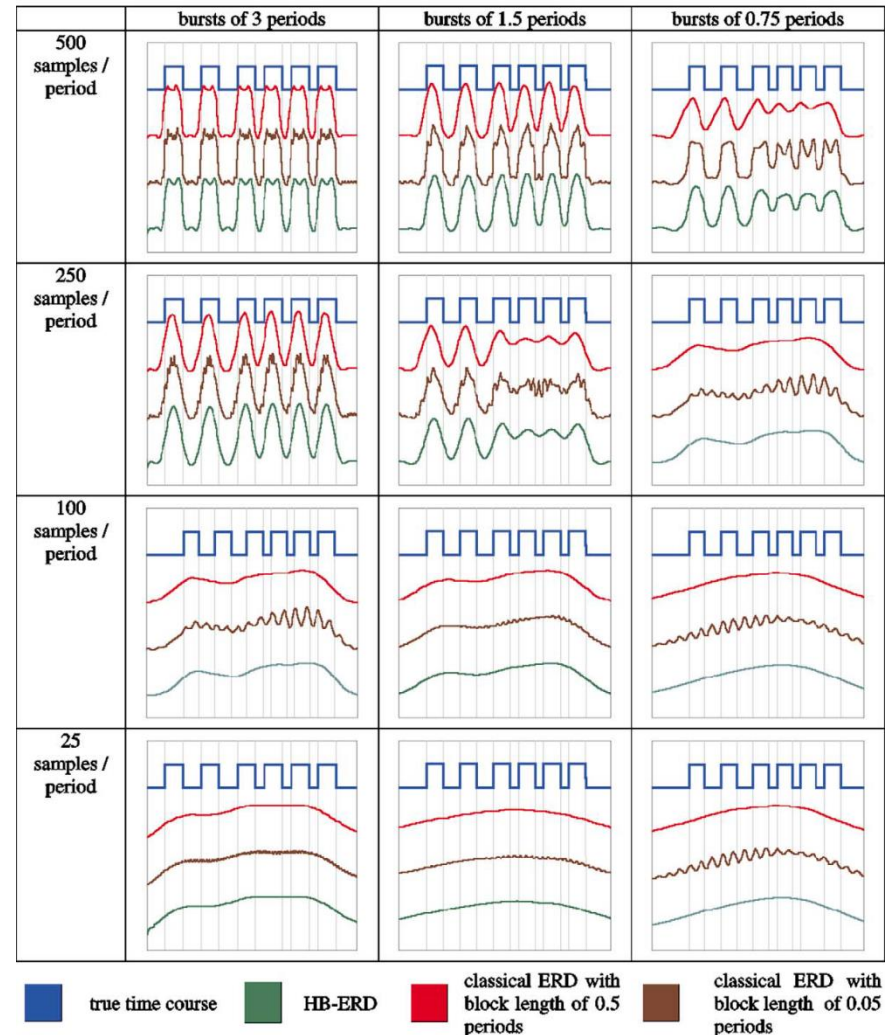
3.4 Signal analysis

On the time resolution of event-related desynchronization: a simulation study

T.R. Knösche, M.C.M. Bastiaansen

We investigated the time resolution of Hilbert transform and classical block integration methods for event-related desynchronization (ERD). We found:

- (1) block ERD is virtually identical to Hilbert-ERD, if the block length is half the period of the signal;
- (2) due to the slow impulse response, amplitude effects in ERD may in fact be caused by duration differences;
- (3) Hilbert-ERD still has important practical advantages, as no block length needs to be chosen.



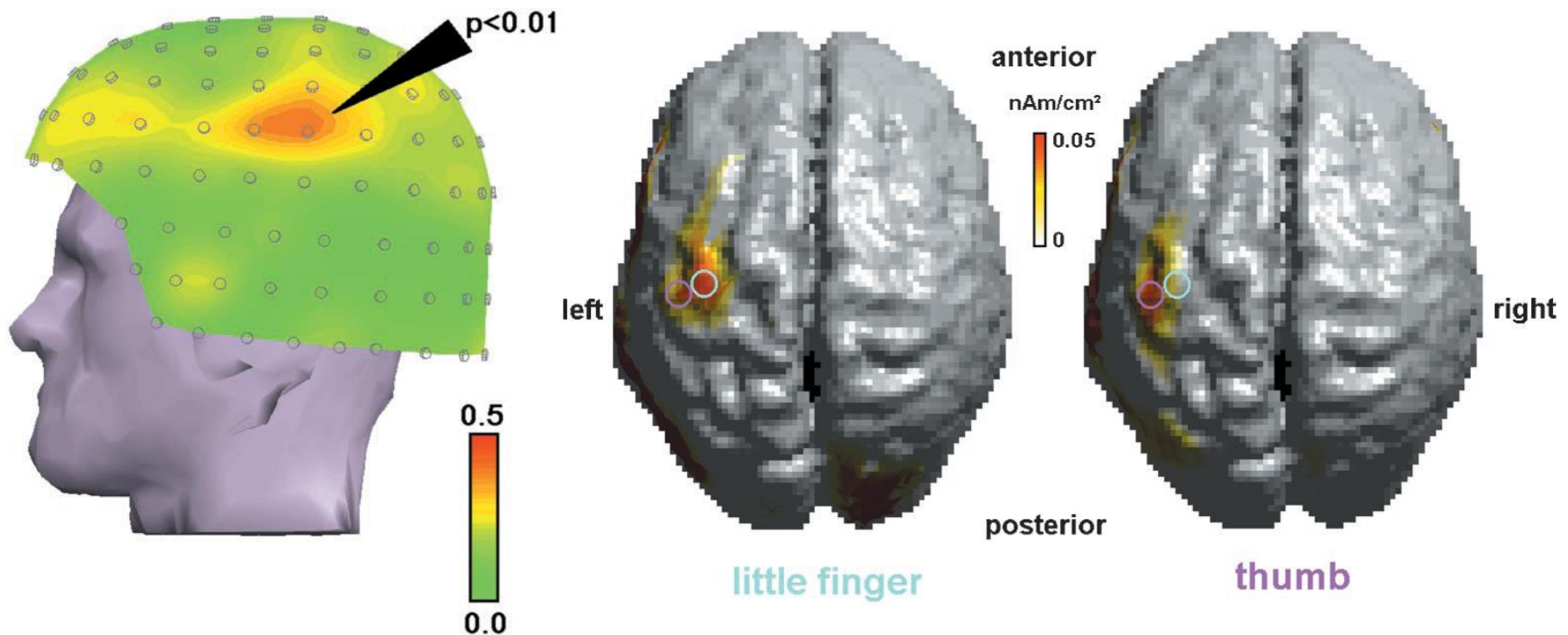
4 Neurocognition

4.1 Music and language processing

Involuntary Motor Activity in Pianists Evoked by Music Perception

J. Haueisen, T.R. Knösche

We used MEG to compare pianists and non-pianists while listening to piano pieces. Pianists have larger contralateral motor activity with spatial dissociation between notes preferably played by the thumb and the little finger. This shows that pianists, when listening to well-trained piano music, exhibit involuntary contralateral M1 activation.



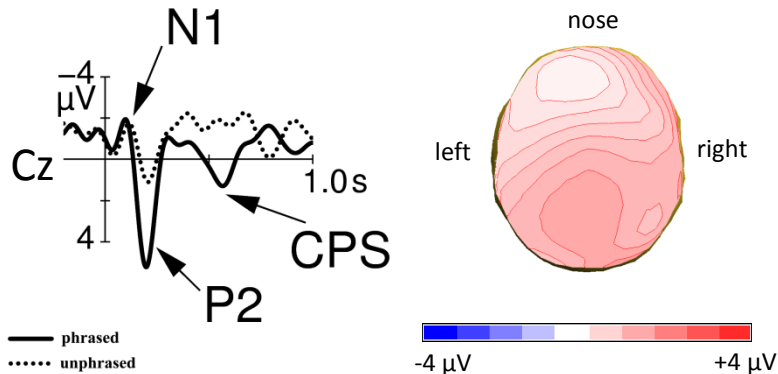
The perception of phrase structure in music

T.R. Knösche, C. Neuhaus, J. Haueisen, K. Alter, B. Maess, A.D. Friederici, O.W. Witte

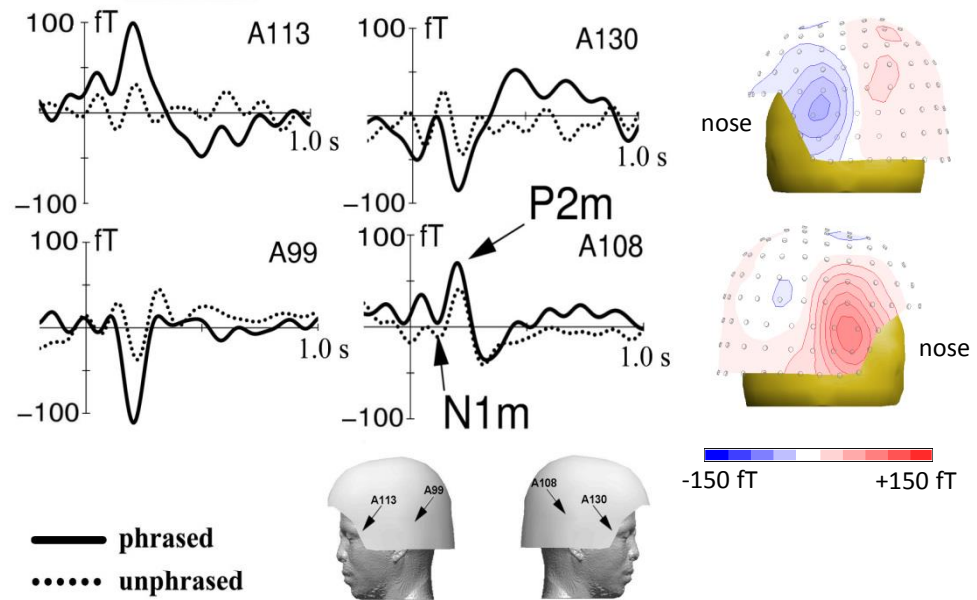
We discovered EEG/MEG correlates for musical phrase boundary perception. The EEG effect is similar to the closure positive shift (CPS) found for prosodic phrase boundaries in speech, suggesting that the underlying processes are related. Sources were found in the limbic system, suggesting they might reflect memory and attention processes.



Example piece with (top) and without (bottom) phrase boundary.



EEG response to musical phrase boundaries.

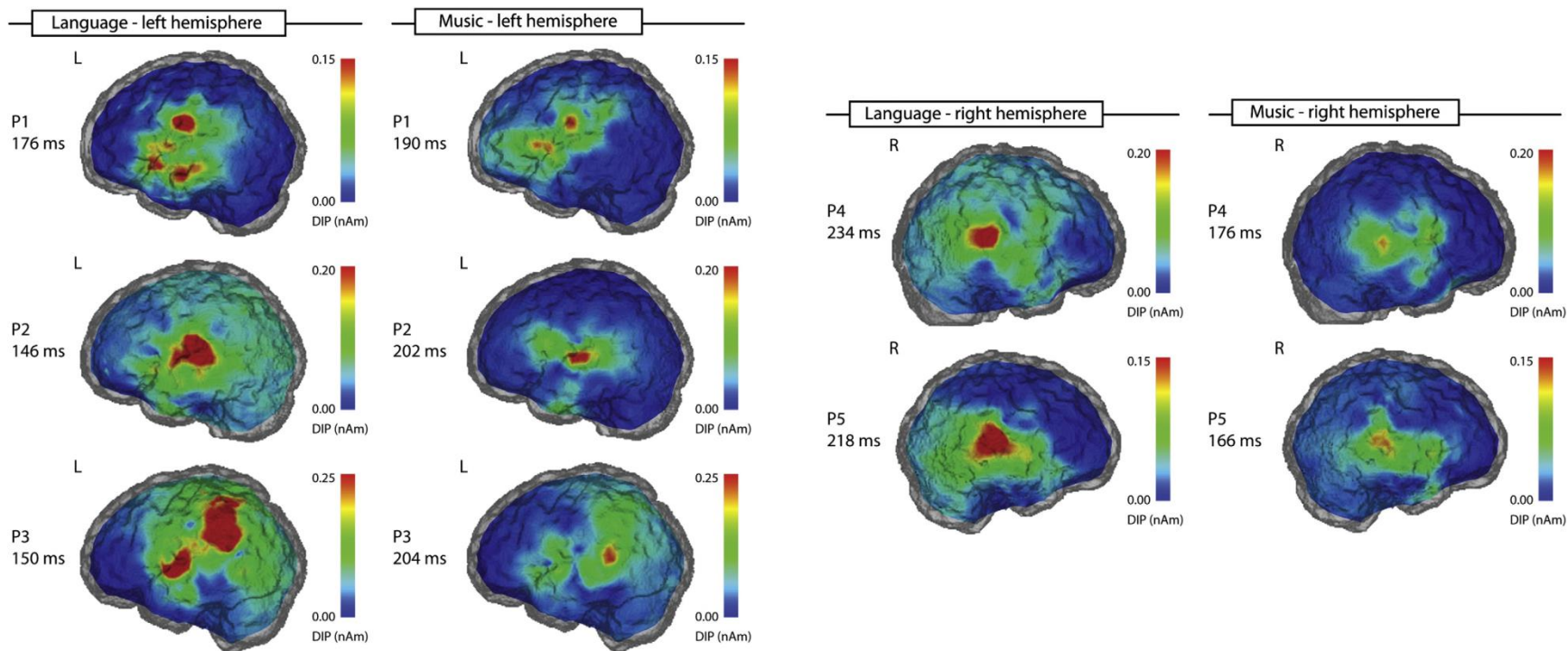


MEG response to musical phrase boundaries.

Co-localizing linguistic and musical syntax with intracranial EEG

D. Sammler, S. Koelsch, T. Ball, A. Brandt, M. Grigutsch, H.J. Huppertz, T.R. Knösche, J. Wellmer, G. Widman, C.E. Elger, A.D. Friederici, A. Schulze-Bonhage

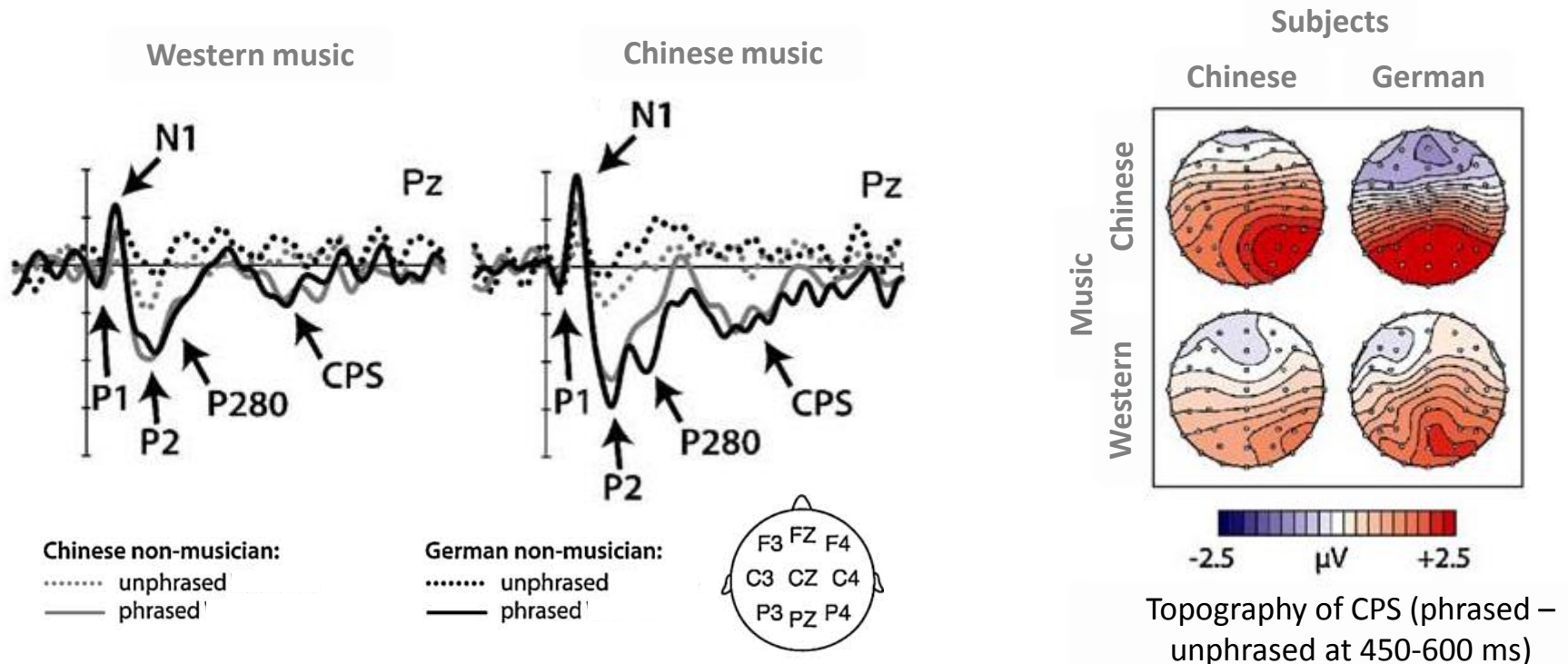
We use subdural EEG and minimum norm estimation to localize low-level syntax processes in music and language. In both domains we find a neural network with considerable overlap in the superior temporal lobe, supporting a co-localization of early musical and linguistic syntax processing in the temporal lobe.



Non-musicians' perception of phrase boundaries in music: A cross-cultural ERP study

Y. Nan, T.R. Knösche, A.D. Friederici

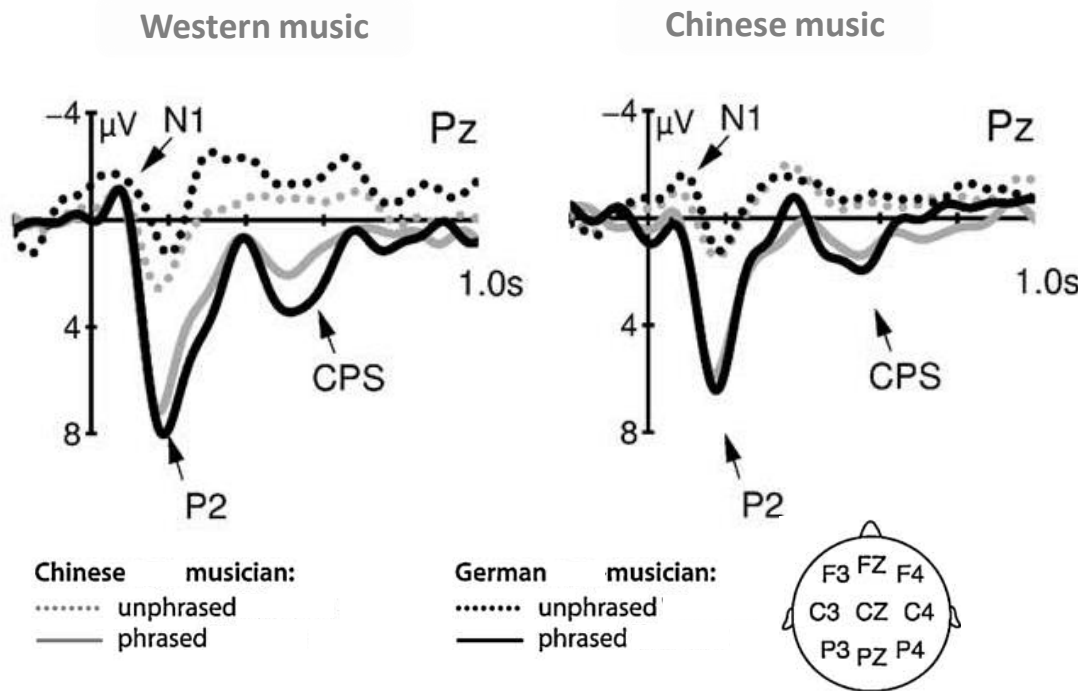
We studied neural responses to musical phrase boundaries in subjects without formal musical training, with emphasis on the relation between subjects' enculturation and cultural style of music. The results demonstrate the music CPS in non-musicians, suggesting that phrase boundary processing does not require formal musical training.



The perception of musical phrase structure: A cross-cultural ERP study

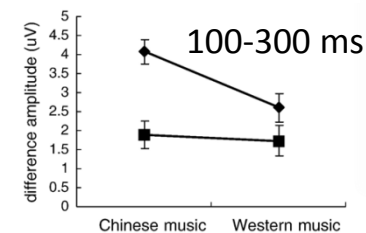
Y. Nan, T.R. Knösche, A.D. Friederici

The music CPS (450-600 ms) was found for Chinese and German musicians in response to phrase boundaries in classical Western and traditional Chinese music. At short latencies (100-450 ms) bottom-up (style properties of the music) and top-down (acculturation of the subjects) information interacted.

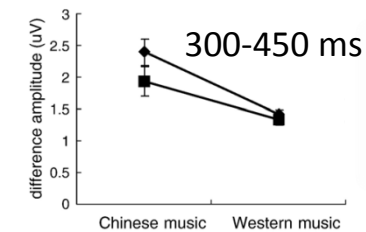


Chinese musician:
 unphrased
 — phrased

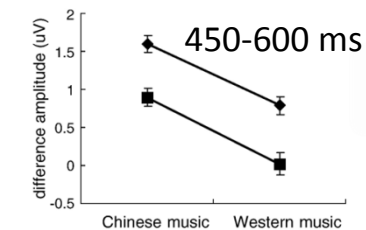
German musician:
 unphrased
 — phrased



Phrasing
 Phrasing × Style
 Phrasing × Group
 Phrasing × Style × Group



Phrasing
 Phrasing × Style
 Phrasing × Style × Group

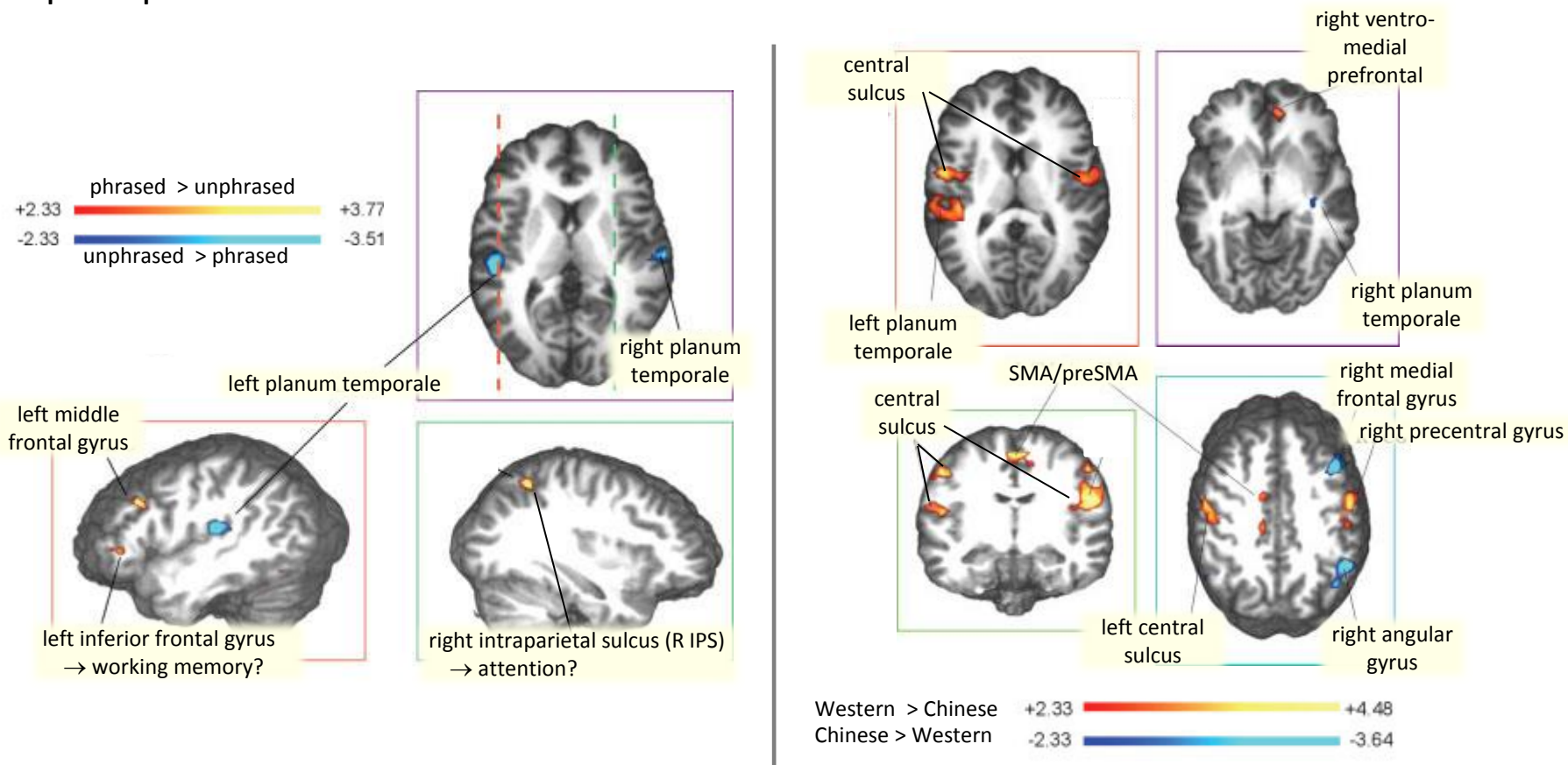


Phrasing
 Phrasing × Style

Cross-Cultural Music Phrase Processing: An fMRI Study

Y. Nan, T.R. Knösche, S. Zysset, A.D. Friederici

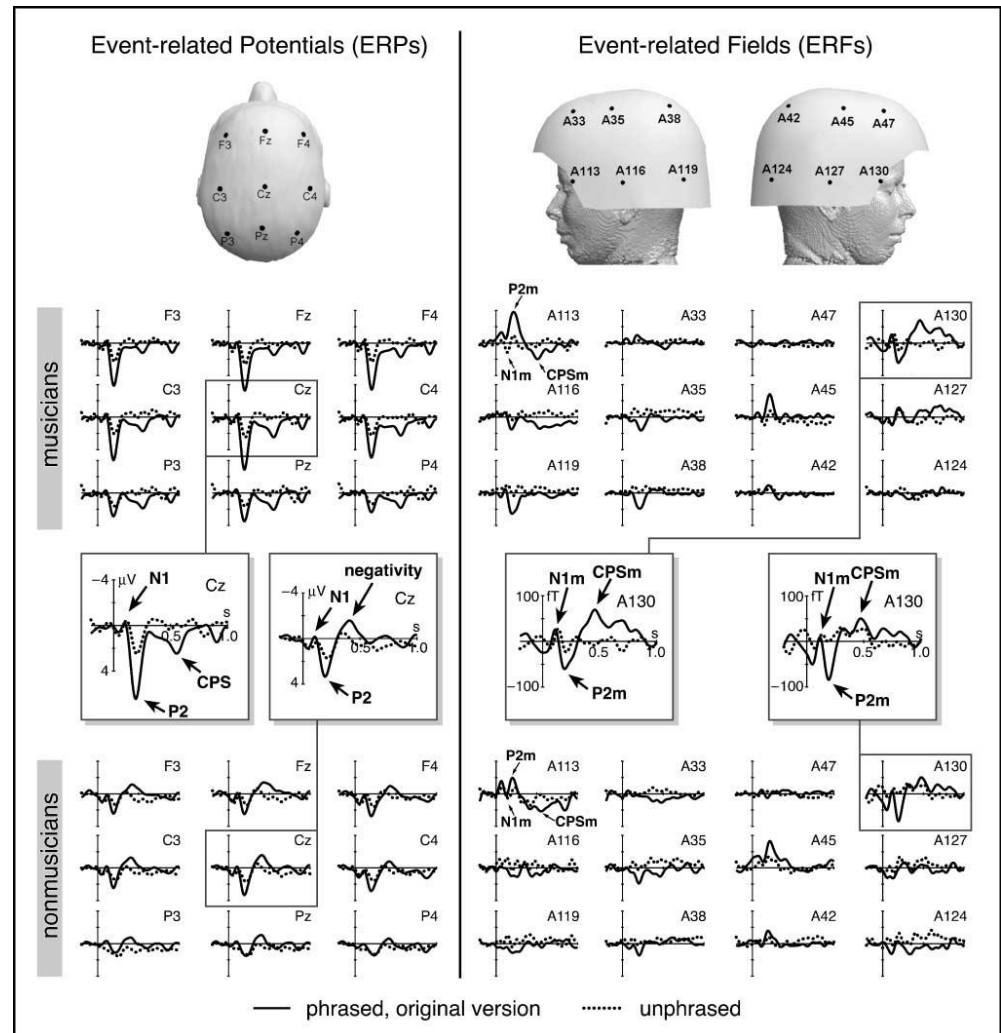
We used fMRI to investigate the neural basis of phrase boundary processing during the perception of music from native and nonnative cultures.



Effects of Musical Expertise and Boundary Markers on Phrase Perception in Music

C. Neuhaus, T.R. Knösche, A.D. Friederici

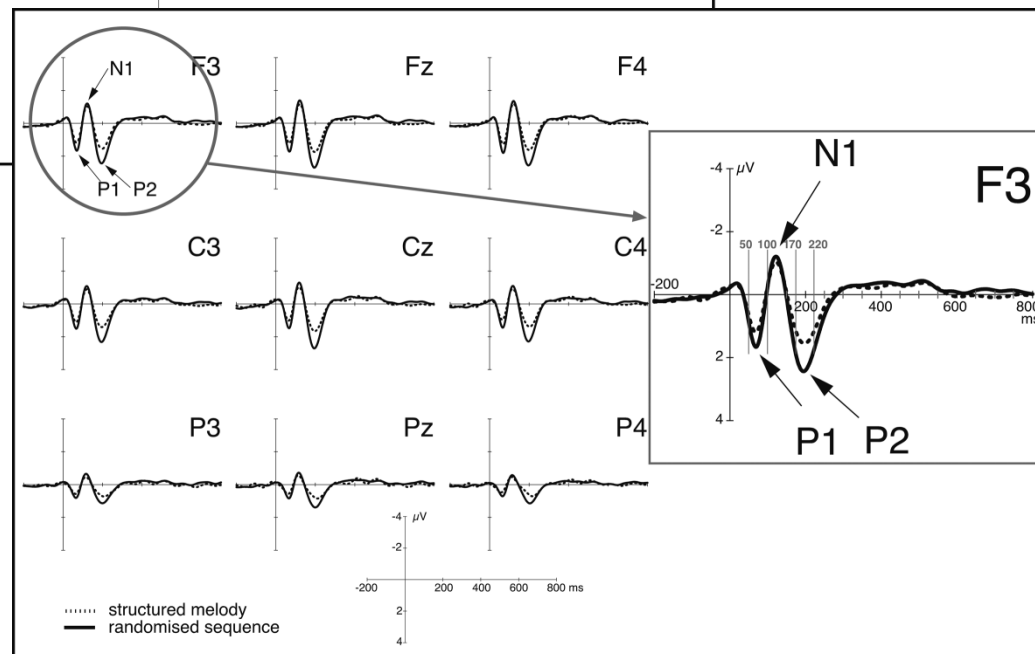
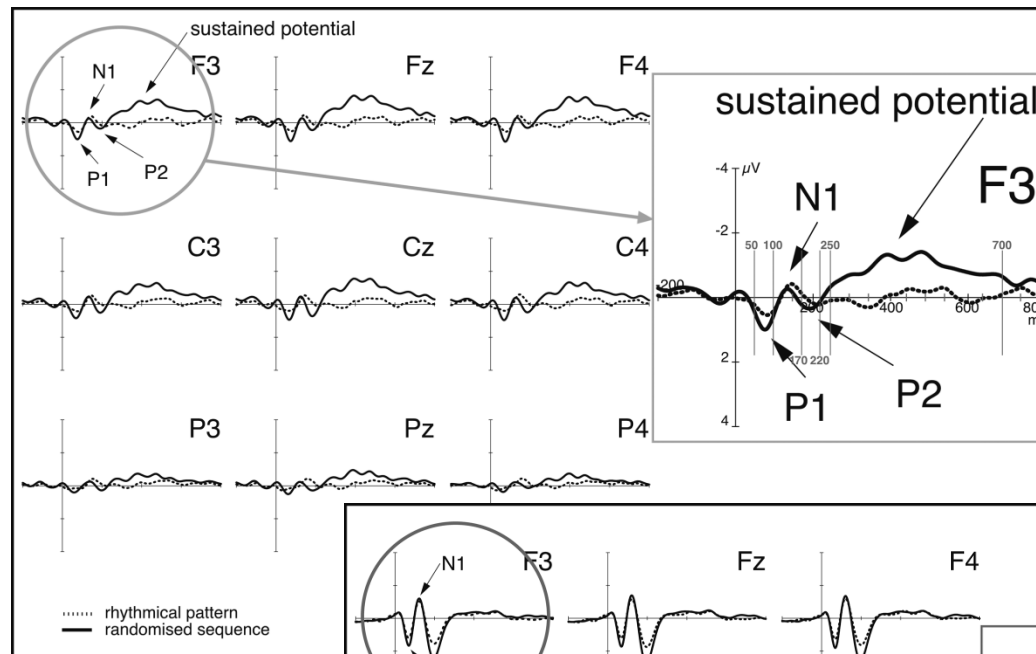
Musical phrase boundaries evoked CPS and CPSm in musicians, but an early negativity and a smaller CPSm in non-musicians, suggesting different perceptual strategies for both groups. Variations of acoustic cues revealed that the CPS is influenced by pause length, length of the tone preceding the pause, and harmonic function of this last tone. This is taken as evidence that the CPS mainly reflects higher cognitive processing of phrasing, rather than mere perception of pauses.



PROCESSING OF RHYTHMIC AND MELODIC GESTALTS— AN ERP STUDY

C. Neuhaus, T.R. Knösche

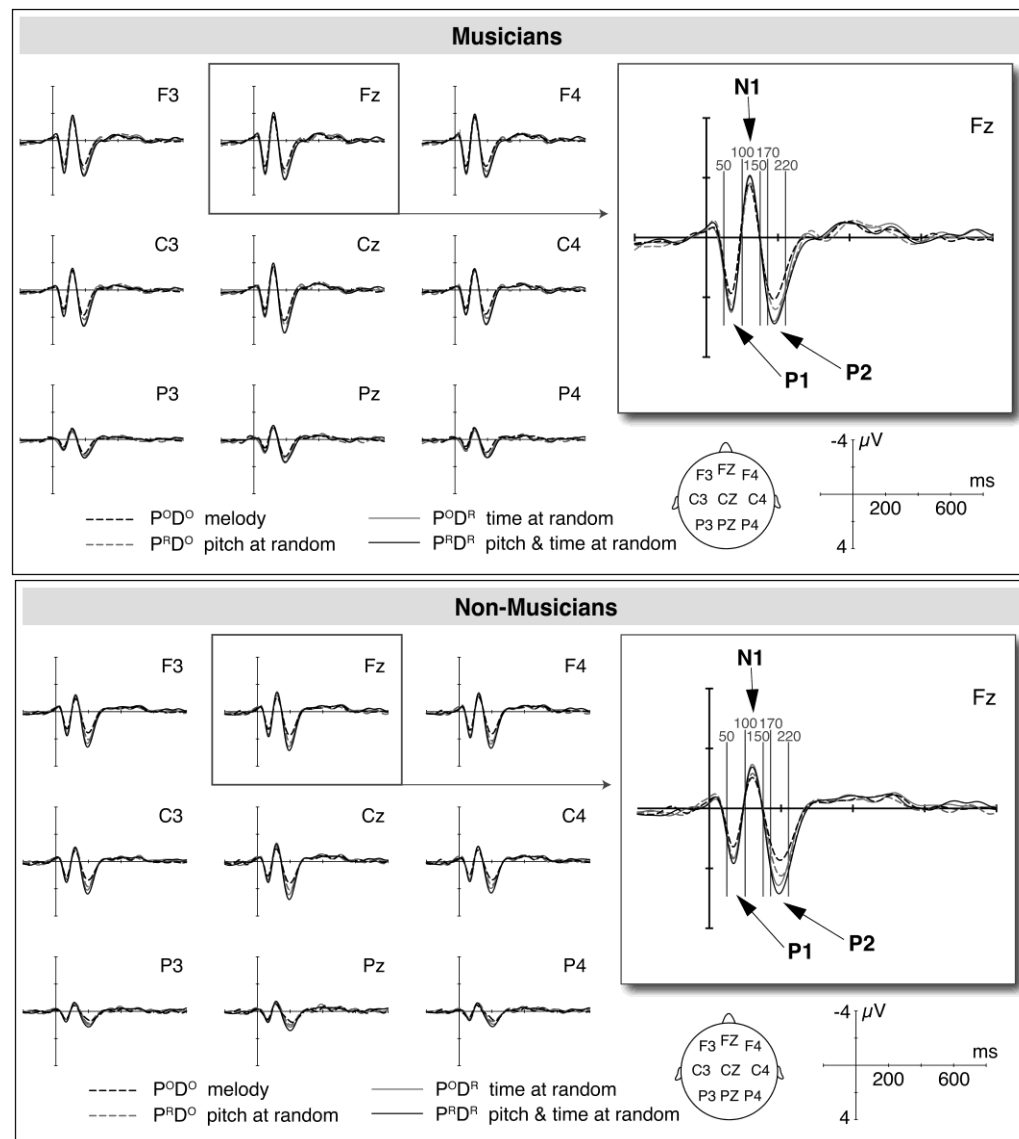
We used ERPs non-musicians to study the perception of auditory Gestalts in the rhythmic and melodic domains. We found differences in P1 and P2 amplitudes. Thus, already at the early stage of encoding, sequence processing might be top-down-driven.



Processing of pitch and time sequences in music

C. Neuhaus, T.R. Knösche

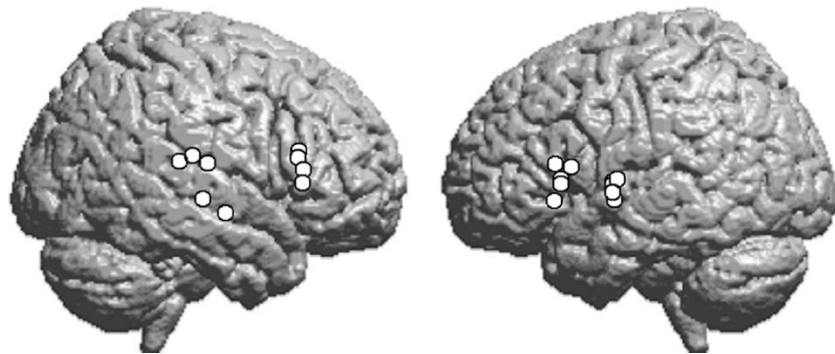
Either pitch and duration of tones, or both, were permuted randomly over a set of melodies. For musicians, strong interaction in the P1-N1-P2 complex corroborated the interdependence of pitch and time processing. Musicians also seem to rely on coherent time structure more than non-musicians and showed enlarged P1/P2 whenever tone duration, with or without preserved pitch, was random. Non-musicians tend to use ordered pitch relations for perceptual orientation, and main effects without interactions might indicate some kind of independent processing of both dimensions at some processing stages.



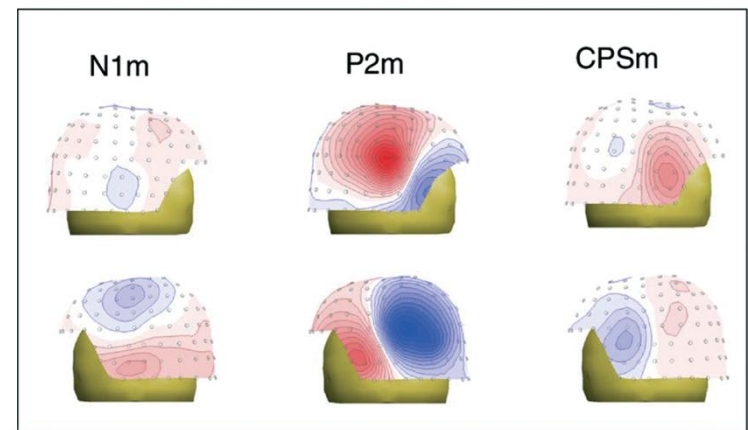
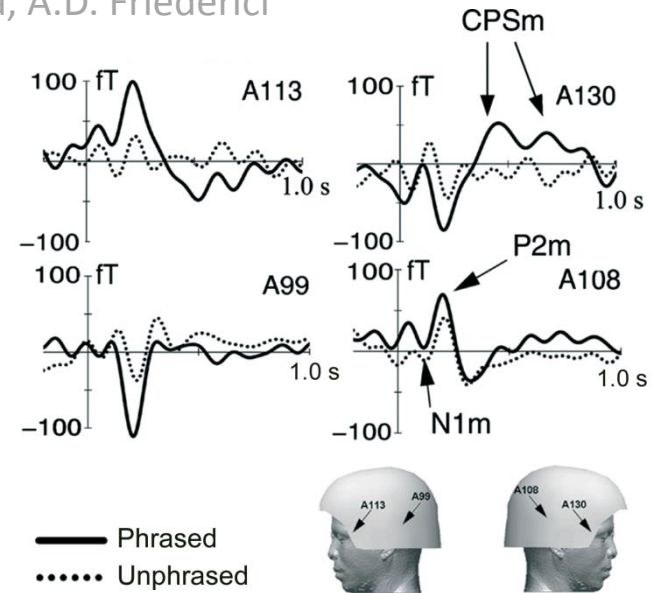
Human Communication Investigated with Magnetoencephalography: Speech, Music, and Gestures

T.R. Knösche, B. Maess, A. Nakamura, A.D. Friederici

We report a number of studies applying magnetoencephalography to elucidate the spatio-temporal organization of the processing of different levels of information during the perception of speech, music, and gestures.



Dipole locations reconstructed from MEG data recorded during early (100-200 ms after word onset) processing of syntactic word category violations.



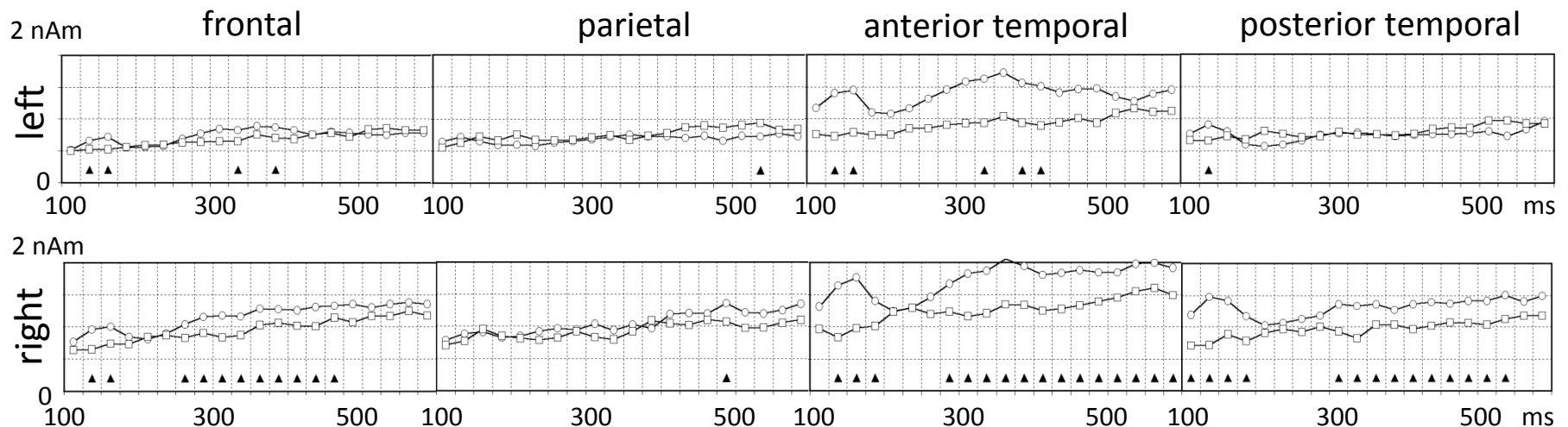
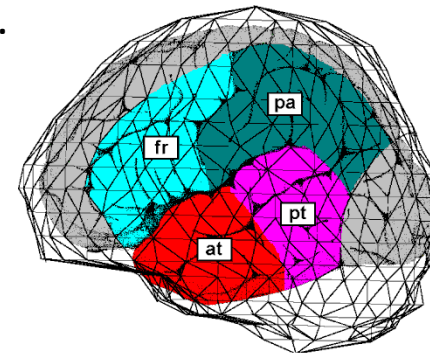
MEG response to musical phrase boundaries.

Processing of Syntactic Information Monitored by Brain Surface Current Density Mapping Based on MEG

T.R. Knösche, B. Maess, A.D. Friederici

Brain Surface Current Density mapping revealed differences between the brain responses to syntactically correct and incorrect sentences. For latencies >250 ms, differences are more prominent in the right hemisphere.

Correct: Die Kuh wurde im Stall gefüttert.
 Correct: Die Kuh wurde gefüttert.
 Incorrect: Die Kuh wurde im gefüttert.

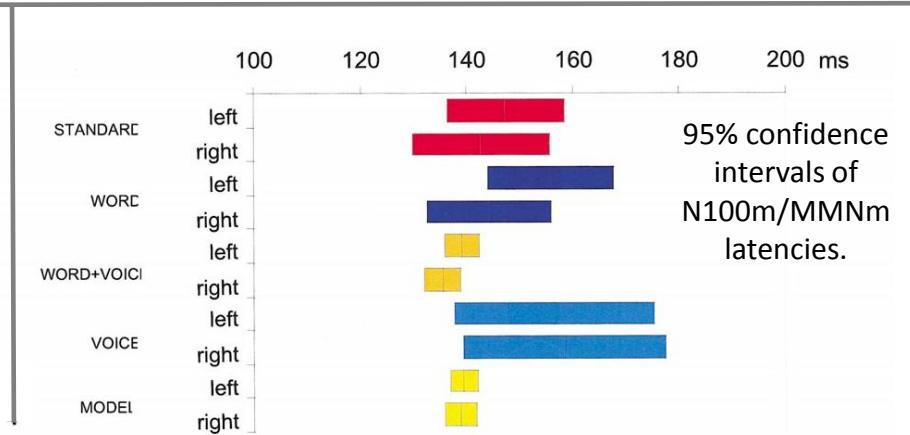
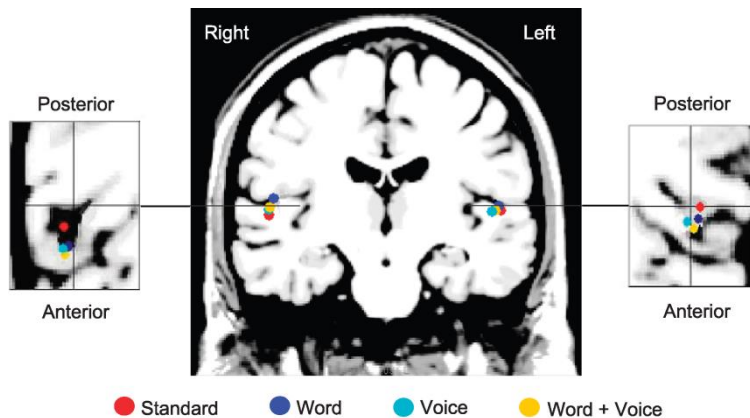
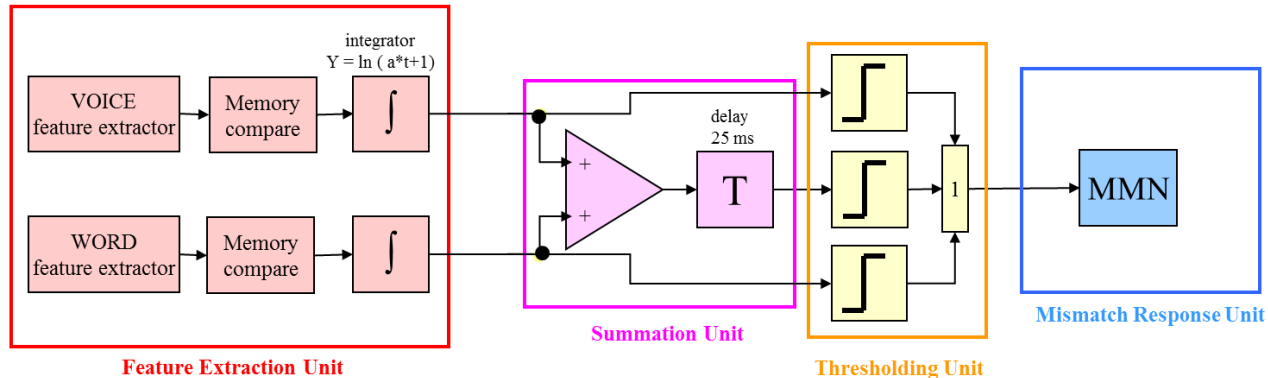


Circlets: incorrect; squares: correct; triangles: significant $p < 0.05$.

Early Parallel Processing of Auditory Word and Voice Information

T.R. Knösche, S. Lattner, B. Maess, M. Schauer, A.D. Friederici

We show that linguistic (phonetic) and extralinguistic (voice) information are processed in parallel at an early preattentive stage. We studied the conjunction of voice and word deviations in a mismatch negativity experiment using MEG and source reconstruction.



4 Neurocognition

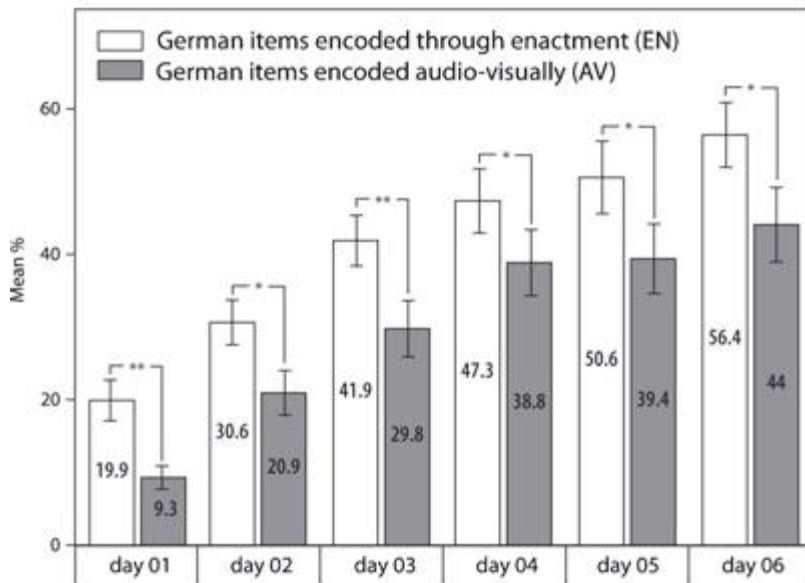
4.2 Gestures and face expression

Body in Mind: How Gestures Empower Foreign Language Learning

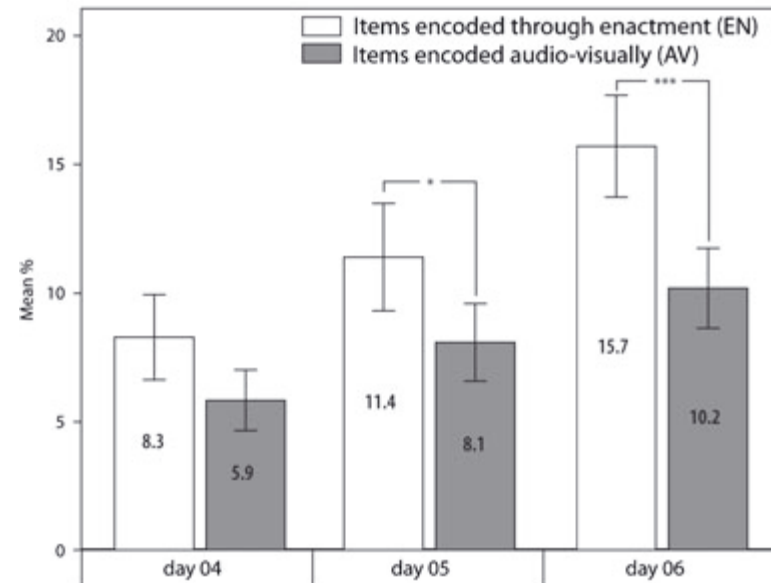
M. Macedonia, T.R. Knösche

We investigate the impact of enactment on abstract word learning and sentence production in a foreign language. We find that learners have better memory for words encoded with gestures, and use them more in sentences. The results are interpreted in terms of embodied cognition. Implications for teaching and learning are suggested.

Free recall of German words



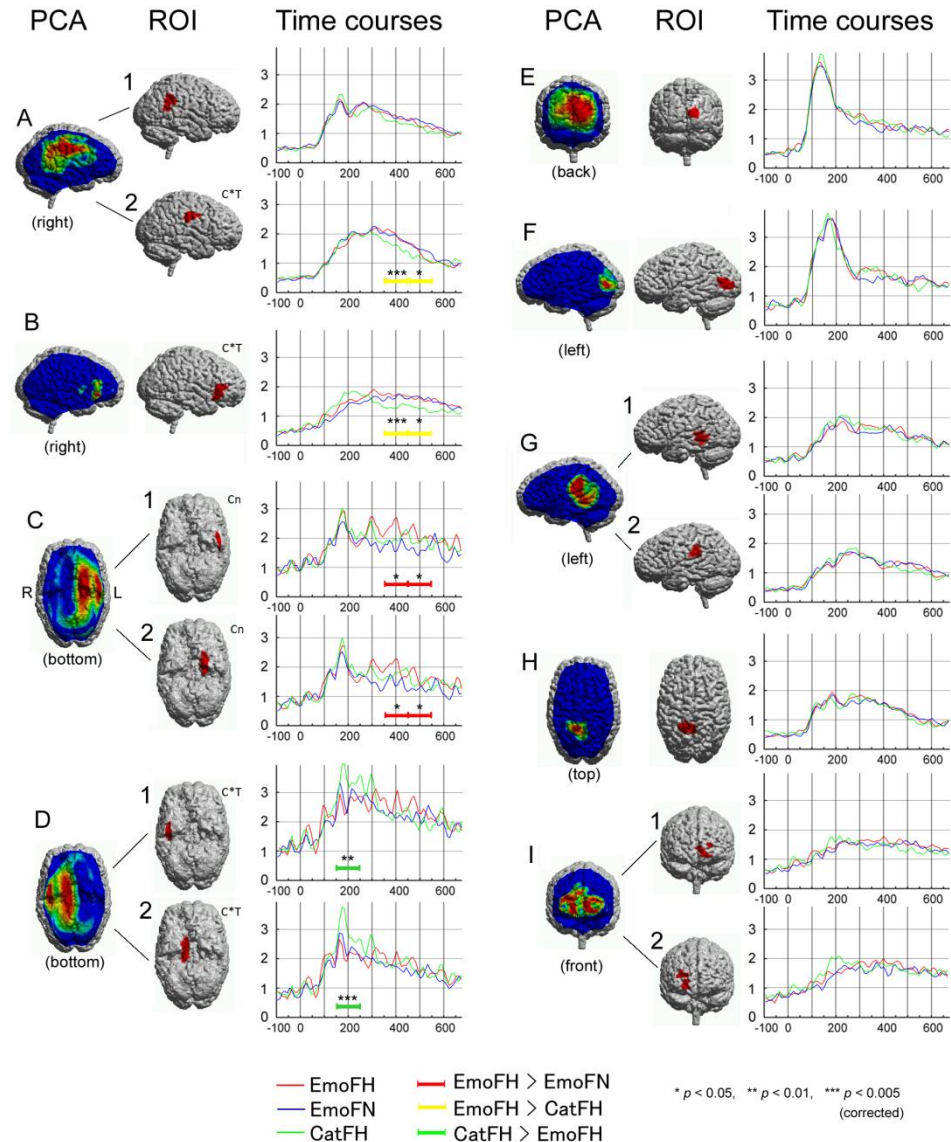
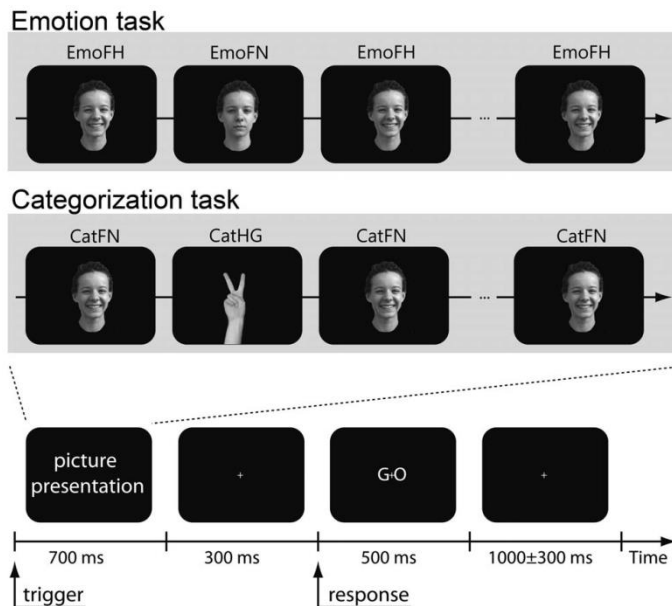
Sentence production in artificial language Vimmi.



Different Hemispheric Roles in Recognition of Happy Expressions

A. Nakamura, B. Maess, T.R. Knösche, A.D. Friederici

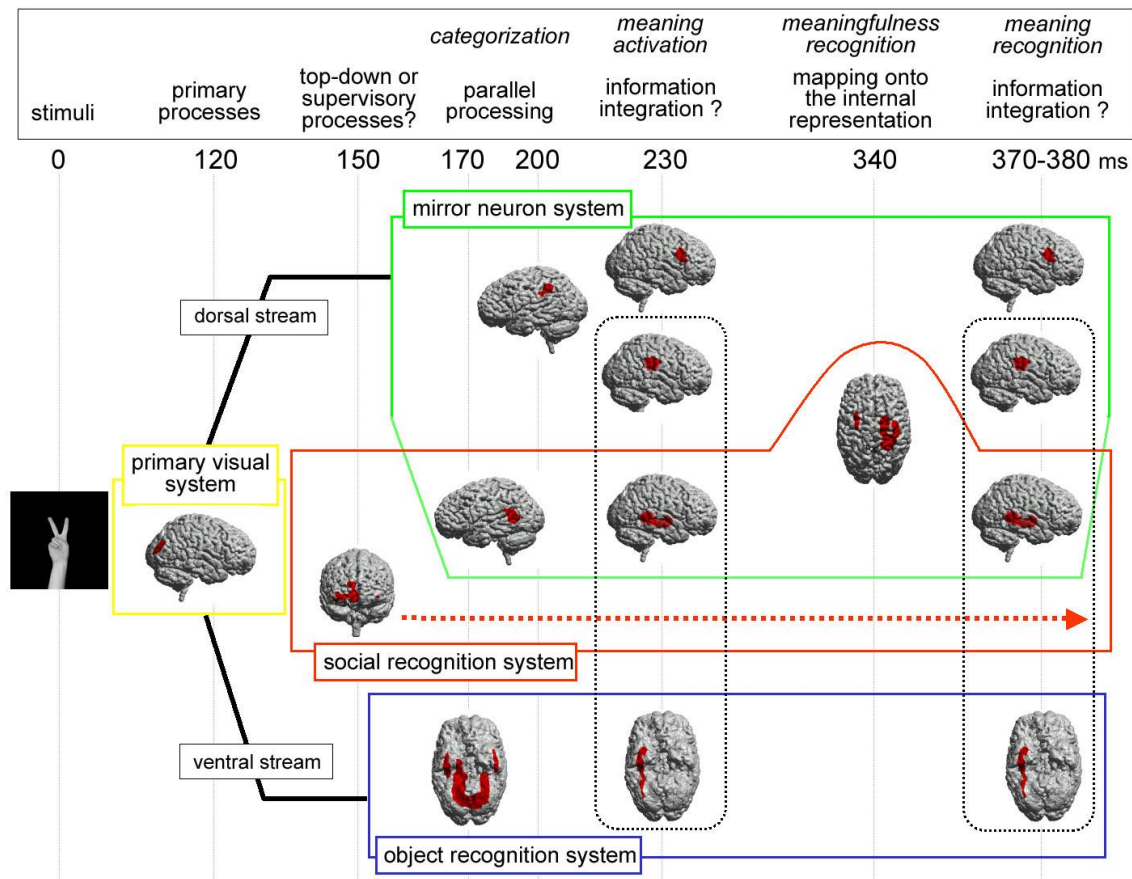
Using MEG, we analyzed the spatiotemporal structure of electrical brain activity during a categorization task (faces vs. hands) and an emotion discrimination task (happy vs. neutral faces). Brain regions that are specific for different aspects of processing emotional facial expressions showed interesting hemispheric dominance patterns.



Cooperation of different neuronal systems during hand sign recognition

A. Nakamura, B. Maess, T.R. Knösche, T.C. Gunter, P. Bach, A.D. Friederici

We use MEG to demonstrate that the primary visual, mirror neuron, social recognition and object recognition systems are involved in hand sign recognition.



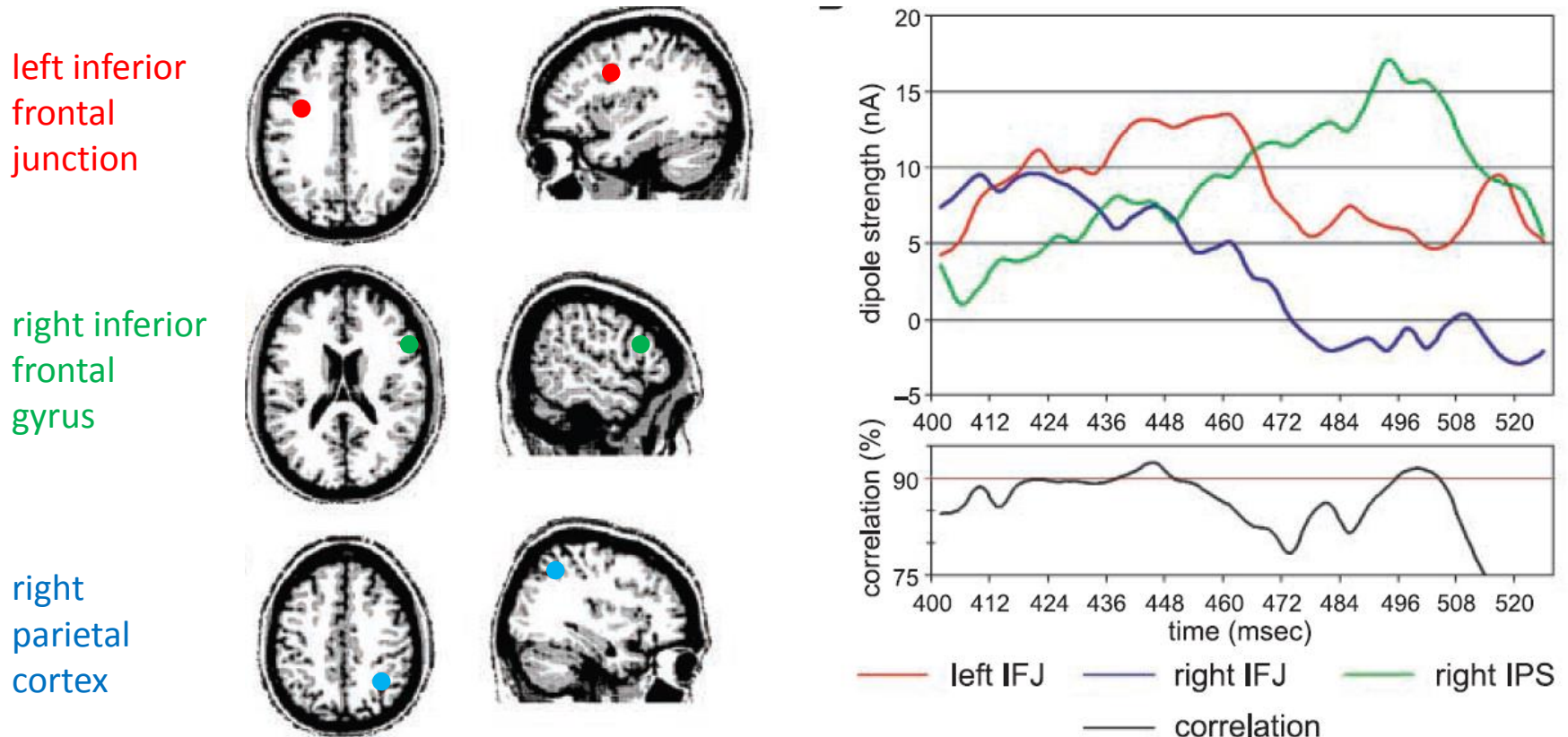
4 Neurocognition

4.3 Other cognitive faculties

Who Comes First? The Role of the Prefrontal and Parietal Cortex in Cognitive Control

M. Brass, M. Ullsperger, T.R. Knösche, D.Y. von Cramon, N.A. Phillips

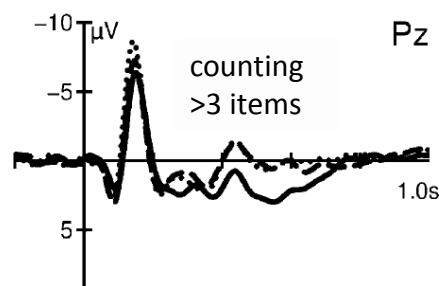
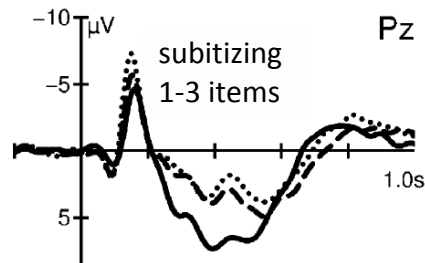
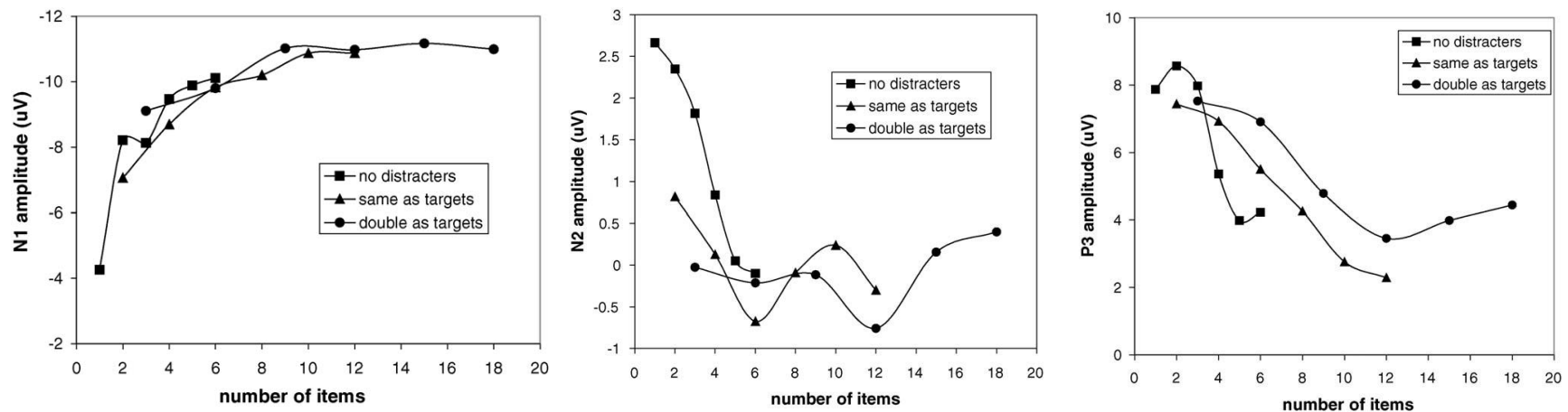
In a cognitive control experiment, we fitted dipoles in fMRI active regions to ERP data. The frontal dipoles contributed to the ERP effect earlier than the parietal one, suggesting that the prefrontal cortex updates general task representations and biases relevant stimulus–response associations in the parietal cortex.



Counting in everyday life: Discrimination and enumeration

Y. Nan, T.R. Knösche, Y.-J. Luo

We study brain activity with a task involving enumeration and discrimination. Although these processes run to some extent in parallel, discrimination happens earlier (< 100 ms). Data suggest a dichotomy between subitizing (< 4 items) and counting. Source estimation suggests distinct processes for subitizing/counting, but similar brain areas.



- No distractors
- Number of distractors equal to targets
- Number of distractors twice as targets

4 Neurocognition

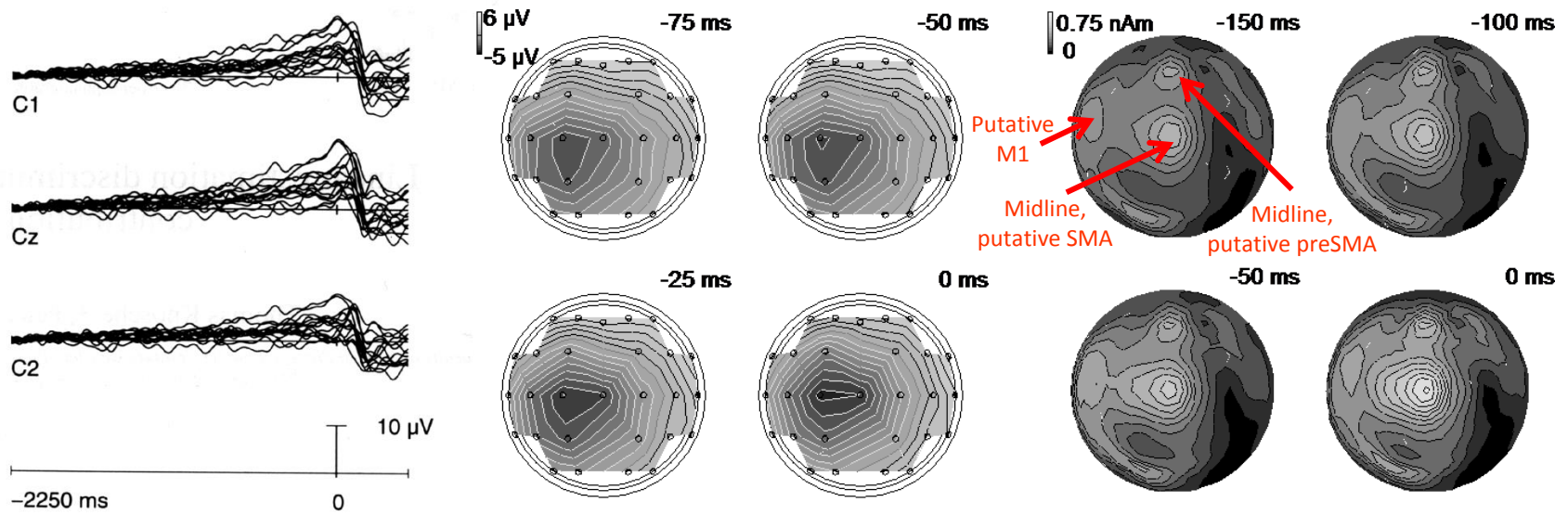
4.4 Motor function

Linear Estimation discriminates midline source and motor cortex contribution to readiness potential

T.R. Knösche, P. Praamstra, D. Stegeman, M.J. Peters

We apply linear estimation to readiness potentials (RP) preceding fixed and freely selected finger movements. We find activity in the midline as well as near the primary motor area.

RP preceding freely selected right hand movements.



Time courses, superimposed for all subjects

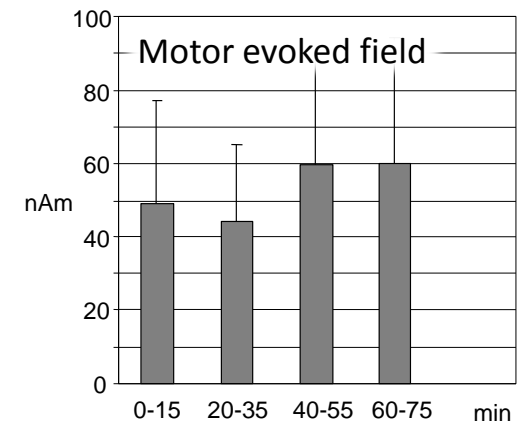
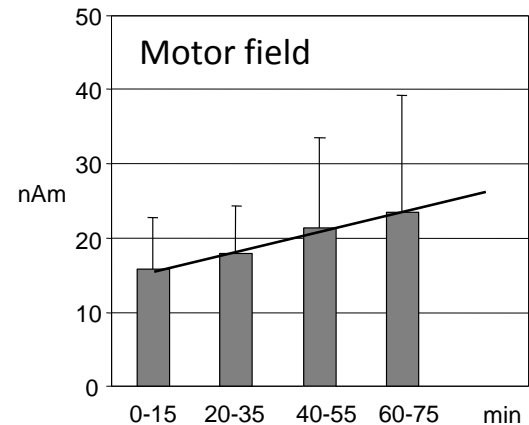
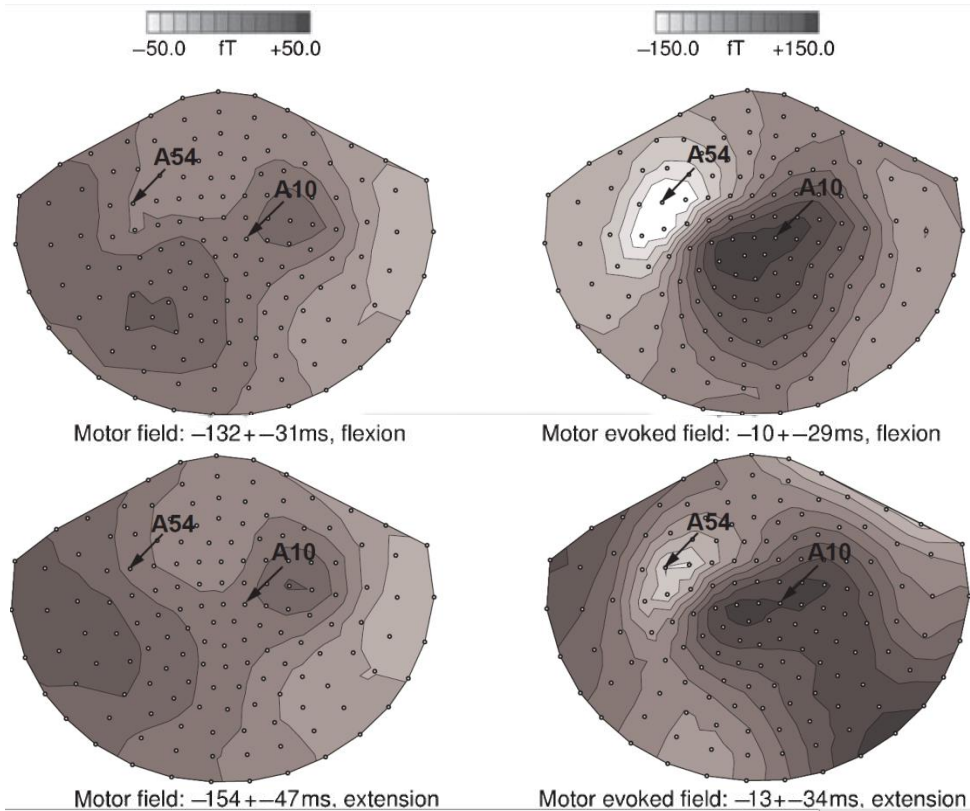
Topographic maps, averaged over all subjects

Current density, estimated by linear estimation.

Rapidly induced changes in neuromagnetic fields following repetitive hand movements

H. Woldag, G. Waldmann, T.R. Knösche, B. Maess, A.D. Friederici, H. Hummelsheim

We analyzed the effect of repeated execution of a simple extension and flexion of the wrist on the sensorimotor cortex using MEG. Spatial filtering based on current dipoles was used to quantify the strength of cortical activation. Results showed an increase of efferent, but not of proprioceptive afferent, cortical activation, suggesting long-term potentiation.



Post-movement beta oscillations studied with linear estimation

M. van Burik, T. Knösche, G. Edlinger, C. Neuper, G. Pfurtscheller, M. Peters

Single trial EEG during self-paced finger movement yielded post-movement beta synchronisation. Surface Laplacian (based on spherical splines) and cortical current density (based on linear estimation) both showed maximal event-related synchronisation over the left sensorimotor area approximately 500–750 ms after termination of movement.

